REPORT NO. FAA-RD-76-223

INSTALLATION AND TEST OF DOPPLER ACOUSTIC SENSOR

R. P. McConville

Avco Corporation
Systems Division
Wilmington MA 01887

OCTOBER 1977

FINAL REPORT

Prepared for

U.S. DEPARTMENT OF TRANSPORTATION
FEDERAL AVIATION ADMINISTRATION
Systems Research and Development Service
Washington DC 20591

NOTICE

This document is disseminated under the sponsorship of the Department of Transportation in the interest of information exchange. The United States Government assumes no liability for its contents or use thereof.

NOTICE

The United States Government does not endorse products or manufacturers. Trade or manufacturers' names appear herein solely because they are considered essential to the object of this report.

Technical Report Documentation Page

1. Report No.	2 Government Accession No.	3 Recipient's Catalog No
FAA-RD-76-223		

4. Title and Subtitle	5 Report Date
INSTALLATION AND TEST OF DOPPLER ACOUSTIC SENSOR	October 1977
	6 Performing Organization Code

7 Author(s)	8. Performing Organization Report No
R. P. McConville*	DOT-TSC-FAA-77-25

9 Performing Organization Name and Address	10 Work Unit No (TRAIS)
Avco Corporation Systems Division 201 Lowell Street Wilmington MA 01887	FA705/R8106
	11 Contract or Grant No DOT-TSC-939
	13 Type of Report and Period Covered Final Report Nov. 1974 - Sep. 1975
12 Sponsoring Agency Name and Address U.S. Department of Transportation Federal Aviation Administration Systems Research and Development Service Washington DC 20591	14 Sponsoring Agency Code

15 Supplementary Notes

* Under contract to: U. S. Department of Transportation
Transportation Systems Center
Kendall Square, Cambridge MA 02142

16 Abstract

This report presents details of the installation of a Doppler acoustic vortex sensing system at JFK Runway 31R, the hardware and software improvements made since installation, vortex diagnostic and tracking data and analysis, and conclusions and recommendations.

17. Key Words	18. Distribution Statement
Doppler Acoustic Vortex Sensor, Wake Vortex, Trailing Vortex Sensing System, Aircraft Vortex Tracking System	DOCUMENT IS AVAILABLE TO THE U.S. PUBLIC THROUGH THE NATIONAL TECHNICAL INFORMATION SERVICE, SPRINGFIELD, VIRGINIA 22161

19. Security Classif. (of this report)	20. Security Classif. (of this page)	21. No. of Pages	22. Price
Unclassified	Unclassified	106	

Form DOT F 1700.7 (8-72) Reproduction of completed page authorized

U. S. GOVERNMENT PRINTING OFFICE 1973 725-534/329

PREFACE

The problems related to aircraft trailing vortices are currently under intensive study for the Federal Aviation Administration (FAA) by the U. S. Department of Transportation (DOT). The Transportation Systems Center (TSC) of DOT has initiated and is carrying out several programs in this area, including programs to develop acoustic systems for detecting, tracking, and measuring the strength of aircraft wake vortices. The system described in this report was designed, built and tested by Avco Corporation's Systems Division (Avco/SD) for DOT/TSC under previous Contract DOT-TSC-710. It was installed and checked out at J. F. Kennedy International Airport and its tracking capability demonstrated under the present Contract DOT-TSC-939 for which this is the final report.

This final report describes the installation of the Doppler Acoustic Vortex Sensing System (DAVSS) at JFK, hardware and software modifications made since installation, the results of data collection and analysis, and conclusions and recommendations offered to DOT/TSC.

The work performed under this contract was significantly enhanced by the close cooperation and contributions of Ralph Kodis, David Burnham, Thomas Sullivan and Edward Spitzer, all of DOT/TSC, as well as Roman Spangler and his NAFEC staff at the JFK vortex field site.

METRIC CONVERSION FACTORS

Approximate Conversions to Metric Measures

Symbol	When You Know	Multiply by	To Find	Symbol
		LENGTH		
in	inches	2.5	centimeters	cm
ft	feet	30	centimeters	cm
yd	yards	0.9	meters	m
mi	miles	1.6	kilometers	km
		AREA		
in^2	square inches	6.5	square centimeters	cm^2
ft^2	square feet	0.09	square meters	m^2
yd^2	square yards	0.8	square meters	m^2
mi^2	square miles	2.5	square kilometers	km^2
	acres	0.4	hectares	ha
		MASS (weight)		
oz	ounces	28	grams	g
lb	pounds	0.45	kilograms	kg
	short tons (2000 lb)	0.9	tonnes	t
		VOLUME		
tsp	teaspoons	5	milliliters	ml
Tbsp	tablespoons	15	milliliters	ml
fl oz	fluid ounces	30	milliliters	ml
c	cups	0.24	liters	l
pt	pints	0.47	liters	l
qt	quarts	0.95	liters	l
gal	gallons	3.8	liters	l
ft^3	cubic feet	0.03	cubic meters	m^3
yd^3	cubic yards	0.76	cubic meters	m^3
		TEMPERATURE (exact)		
°F	Fahrenheit temperature	5/9 (after subtracting 32)	Celsius temperature	°C

Approximate Conversions from Metric Measures

Symbol	When You Know	Multiply by	To Find	Symbol
		LENGTH		
mm	millimeters	0.04	inches	in
cm	centimeters	0.4	inches	in
m	meters	3.3	feet	ft
m	meters	1.1	yards	yd
km	kilometers	0.6	miles	mi
		AREA		
cm^2	square centimeters	0.16	square inches	in^2
m^2	square meters	1.2	square yards	yd^2
km^2	square kilometers	0.4	square miles	mi^2
ha	hectares (10,000 m^2)	2.5	acres	
		MASS (weight)		
g	grams	0.035	ounces	oz
kg	kilograms	2.2	pounds	lb
t	tonnes (1000 kg)	1.1	short tons	
		VOLUME		
ml	milliliters	0.03	fluid ounces	fl oz
l	liters	2.1	pints	pt
l	liters	1.06	quarts	qt
l	liters	0.26	gallons	gal
m^3	cubic meters	35	cubic feet	ft^3
m^3	cubic meters	1.3	cubic yards	yd^3
		TEMPERATURE (exact)		
°C	Celsius temperature	9/5 (then add 32)	Fahrenheit temperature	°F

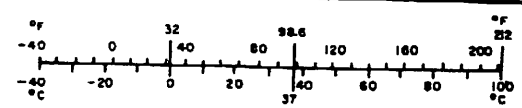

CONTENTS

CONTENTS (Concluded)

ILLUSTRATIONS

ILLUSTRATIONS (Continued)

ILLUSTRATIONS (Continued)

ILLUSTRATIONS (Concluded)

TABLES

ABBREVIATIONS AND SYMBOLS

A, B, C, D, E, F	Any assigned integer from 0 to 225
AC	Alternating current
Avco/SD	Avco Corporation, Systems Division
CRT	Cathode ray tube
cw, CW	Continuous wave
DARS	Doppler acoustic radar subsystem
DAS	Data acquisition subsystem
DAVS	Doppler acoustic vortex sensing
DAVSS	Doppler acoustic vortex sensing system
DDS	Data display subsystem
DEC	Digital Equipment Corporation
deg	Degree, degrees
DOT	Department of Transportation (U.S.)
DOT/TSC	Department of Transportation/Transportation Systems Center (U.S.)
DSS	Data storage subsystem
F	Forward scatter
FAA	Federal Aviation Administration
Fi	Response of comb filter i
ft	Foot, feet
GND	Ground
GT-40	GT-40 graphics display terminal

ABBREVIATIONS AND SYMBOLS (Continued)

GWSS	Ground wind sensing system
Hz	Hertz (cycle per second)
i	Any assigned integer
I	Intensity
IC	Integrated circuit
ID	Inside diameter
in	inch, inches
IN	Input
INT OSC	Internal oscillator
j	Any assigned integer
JFK	John F. Kennedy International Airport
k	1000
kHz	KiloHertz (1000 Hertz)
Ki	Assigned filter output weighting factor, where i is any integer from 1 through 6, inclusive. The weighting factors are as follows: K1, K6 = 1.00 K2, K5 = 0.50 K3, K4 = 0.20
Kn	Assigned filter output weighting factor n (see Ki, above)
LED	Light-emitting diode
Mij	Matrix whose dimensions (i and j) are range and elevation angle
MON	Monitor

ABBREVIATIONS AND SYMBOLS (Continued)

ms	Millisecond (10^{-6} second), milliseconds
n	Any assigned integer
NAFEC	National Aviation Facilities Experimental Center
PAVSS	Pulsed acoustic vortex sensing system
PB	Playback
R	Receive, receiver
RCVR	Receiver
REAL	Real-time
REC	Receive, receiver
Rn	Receiver n
Sk	Skew
Skij	Absolute value of skew response
SOR	Start of run
Sp	Spread
SPKR	Speaker
SWP	Sweep
SYNC	Synchronize, synchronization
T	Transmit, transmitter
Tn	Transmitter n
TP	Test Point
TRANS	Transmit, transmitter
TSC	Transportation Systems Center

ABBREVIATIONS AND SYMBOLS (Concluded)

VOL	Volume
VOM	Volt-ohmmeter
X	Acoustic radar array X
XMIT	Transmit, transmitter
XMTR	Transmitter
Y	Acoustic radar array Y
Z	Acoustic radar array Z
8k	8,000 bits (8 bits x 10^3)
31R	Runway 31R (at JFK)
Ω	ohm, ohms

1. INTRODUCTION

Under a previous contract (DOT-TSC-710), Avco designed and built a DAVSS to detect and track aircraft trailing vortices automatically and in real-time. The purpose of the present program was to install the DAVSS at the JFK runway 31R test site, check out all hardware and software components, bring the system to near optimum performance, and demonstrate its detecting and tracking capabilities against wake vortices generated by landing aircraft. Field installation began on 6 November 1974; the system demonstration was held on 11 February 1975.

In the three months before system demonstration, several hardware and software features were added as part of the installation and checkout process to improve the system's reliability, ease of operation and maintenance, as well as its detecting and tracking performance. After system demonstration, the contract was extended to allow system reconfiguration into an augmented monostatic backscatter mode of operation. Several additional hardware and software improvements were incorporated to make full use of this augmented backscatter array.

This report is organized to reflect the tasks outlined above. A brief outline of the theory and function of the DAVSS is presented in Section 2. For a complete description of the DAVSS design and operating characteristics, see the DAVSS Final Report*. Section 2 also describes the DAVSS as installed at the Vortex Test Site at Runway 31R at JFK.

Section 3 provides an update of the hardware features added between factory acceptance and field demonstration of the unit. Section 4 provides a similar update of the software processing feature development during that period.

Section 5 presents a representative sampling of vortex detection and tracking data. The data is presented both in the diagnostic form and in the DAVS system track form. The performance of the tracking algorithm is analyzed.

Section 6 presents the hardware and software changes incorporated into the DAVSS after system demonstration to realize the augmented monostatic backscatter array. Section 7 describes the significant change in the detection and tracking algorithm, incorporating the features of vortex circulation estimation.

*Final Report, Doppler Acoustic Vortex Sensing System, FAA-RD-76-41.

Section 8 presents the significant conclusions and recommendations for further effort on the program.

Appendix A presents the comb filter calibration and maintenance procedure. Appendix B is the report of inventions.

2. SYSTEM DESCRIPTION AND FIELD INSTALLATION

This section describes the form and function of the DAVSS as installed at the Vortex Test Site at Runway 31R of JFK.

The DAVSS uses the characteristic Doppler signatures of vortex-scattered acoustic energy to detect and track trailing vortices from landing aircraft. Acoustic transmitters, whose beams are shaped into narrow azimuth and large elevation angle fans, are used to insonify regions of suspected vortex activity. Velocity and temperature turbulence eddies entrapped in the organized circulation of the vortices scatter the incident acoustic energy and impart characteristic and recognizable Doppler signatures. The scattered and Doppler-shifted sound patterns are received in arrays of pencil beams which are contiguously arranged in the elevation plane.

Each individual receiver beam is processed to form a time delay versus frequency spectrum pattern. The resultant three-dimensional pattern -- elevation angle, time delay, and Doppler frequency -- from the receiver array is automatically examined within the computer to recognize vortex presence and to estimate the vortex core location. The continuously updated position estimate is displayed in real-time on a CRT and on a page printer to form the vortex track.

2.1 SYSTEM DESCRIPTION

The DAVSS consists of two 4-element acoustic radar antenna arrays and all the hardware, software, and interface items necessary for real-time acquisition, reduction, readout, and display of vortex position data. Analog and digital data is stored on magnetic tape for subsequent offline reduction and evaluation. The system contains a minicomputer which not only performs the required DAVSS functions but also can interface with other external computers or control systems. The system may be considered to consist of the following-listed basic subsystems:

Doppler acoustic radar subsystem

Data acquisition subsystem

Data display subsystem

Data storage subsystem

Software subsystem

Figure 2-1 is a pictorial overview of the DAVSS. Brief descriptions of each of these subsystems follow.

The Doppler acoustic radar subsystem consists of eight acoustic antennas -- four for transmitting, and four for receiving. The antennas are used in two arrays, each consisting of two transmitters and two receivers. The transmitting antennas are all alike as are the receiving antennas. The transmitting antennas are designed to deliver a uniform fan beam of acoustic energy, whose width is 5 deg. in the azimuthal plane and selectable as 37, 45, or 60 deg. in the elevation plane. The beam center is settable in the elevation plane from 15 to 90 deg. above the horizon. Each transmitting antenna consists of a parabolic cylinder reflector activated by center-mounted rectangular aperture feed horns driven by two Altec Lansing 290 E loudspeakers capable of handling 100 watts input each. Their outputs are transmitted from outside of the secondary aperture by acoustic transmission lines and combined using Altec 30170 combiners with two Altec 30546 45-deg. elbows. To reduce the sidelobe response of the transmitting antenna, a 4-ft. long sidelobe suppressing shroud which is flared 30-deg. outward in the vertical plane is attached to the reflector. To avoid line loss and distortion over the long lines between the DAS and the antennas, the transmitter signal is delivered at low power and amplified at the transmitting antenna by a Phase Linear 400 dual-channel amplifier.

The receiving antennas are designed to produce twelve 3 x 3 deg. pencil beams, each separated by 3 deg. in the elevation plane. In addition, this comb of 12 beams is settable in the elevation plane so that the center beam may be positioned from 15 to 90 deg. above the horizon. Thus, horizon-to-horizon coverage is available with both the transmitting and receiving antennas. The resultant comb of 12 beams is formed by placing a linear array of 12 mini-horn-microphone-receiver channels across the focal plane of a 6-ft. parabolic reflecting dish whose focal length is 37 in. The parabolic dish is also shrouded by an 8-ft. long, 6-ft. inside diameter (ID) cylindrical sidelobe suppressor lined with 1-in. thick Coustex™ absorber. The nominal aperture of the 3-in. long primary horns is 2 in. and the set of 12 are spaced 2 in. on center. The microphones are TELectret™ Model 5336C miniature condenser microphones with integral preamplifiers. A 12-channel bandpass and preamplifier stage is provided in the horn-microphone-receiver assembly to reduce susceptibility to noise and interference pickup over the long lines back to the DAS.

The DAS contains all of the elements needed to control system operation (upon receipt of external data either from a central processor or local keyboard), solve for vortex locations, and feed

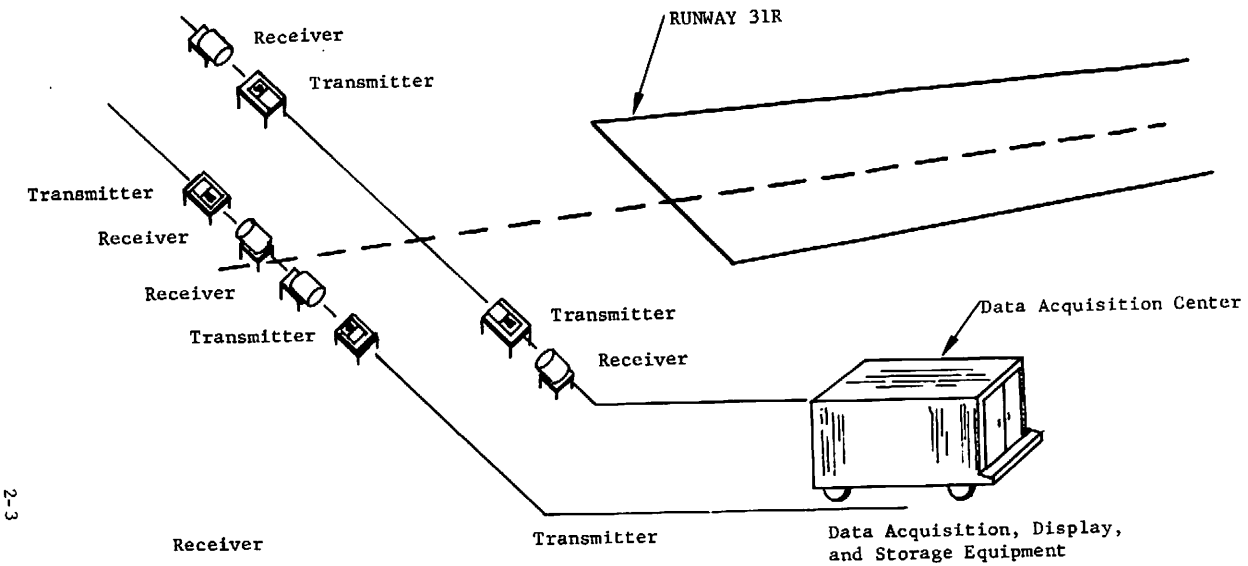

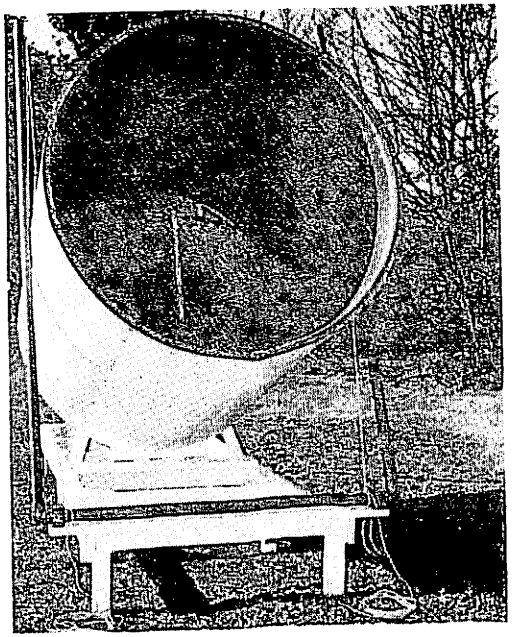

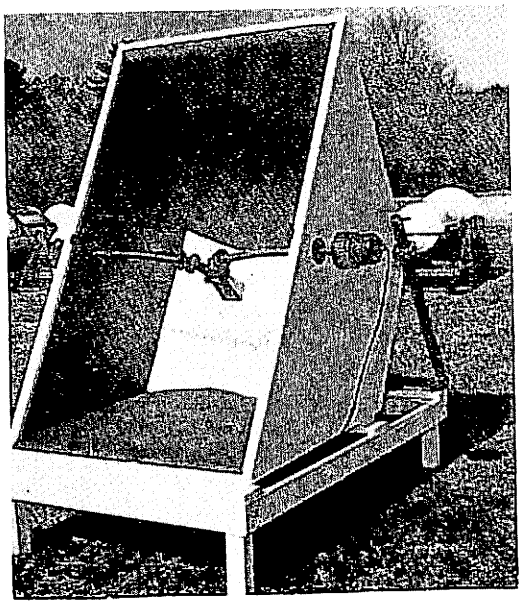

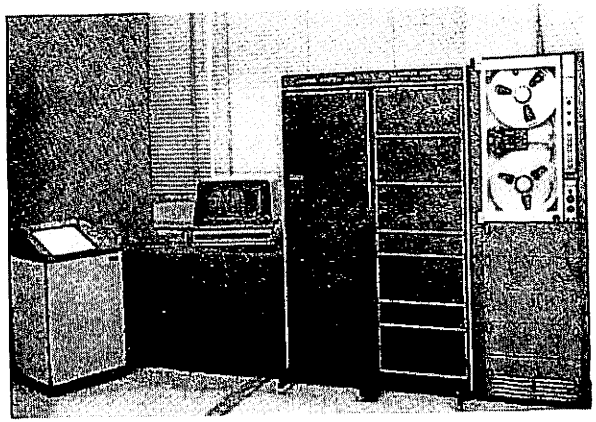

FIGURE 2-1 Pictorial View, DAVSS

2-3

data to the display or storage subsystems. DAS elements include a DEC PDP-11/05 minicomputer with extended arithmetic capability, a bootstrap loader, a core memory (additional to that provided in the minicomputer), a radar subsystem controller, a keyboard unit and associated controller, and an analog signal processor.

The DDS consists of a DEC GT-40 graphics unit that includes a CRT for visual presentation of data. Software is provided to allow use of a Versatec Model 1100A hard-copy display device for presentation of data, including graphics.

The DSS consists of two magnetic tape recorders and their associated controllers. One tape recorder, used for analog data, is a Bell and Howell VR3700B 28-track; the other is a DEC TU-10, 9-track recorder used for digital data.

The combined DAS, DDS, and DSS are housed as shown in Figure 2-2.

The signal in each receiver beam is spectrum-analyzed via a comb of six narrow band filters. The spectral time history of each beam for each frame is further processed to compress the data. Three discriminant algorithms are used to characterize the condition of the six filter outputs. These discriminants are referred to as intensity, spread, and skew.

Each of these three discriminants is designed to combine the outputs of the six comb filters in a manner which emphasizes one of the characteristics of the output spectrum. Intensity, as the name implies, gives an estimate of the average intensity of the spectrum. Spread is intended to give an estimate of the width of the spectrum; while skew is intended to give an estimate of the first moment of the Doppler spectrum. The intensity discriminant is represented by

$$\text{Intensity} = \sum_{i=1} A_i,$$

where A_i is the amplitude of data from filter i, and i is the designation of the filter.

Spread and skew use symmetric and asymmetric weighting of the values of the upper and lower side-band filters in a summing operation. The weighted outputs of filters 1, 2, and 3 on one side of the carrier frequency are summed in one amplifier; the weighted outputs of filters 4, 5, and 6 on the other side of the carrier are summed in the other amplifier.

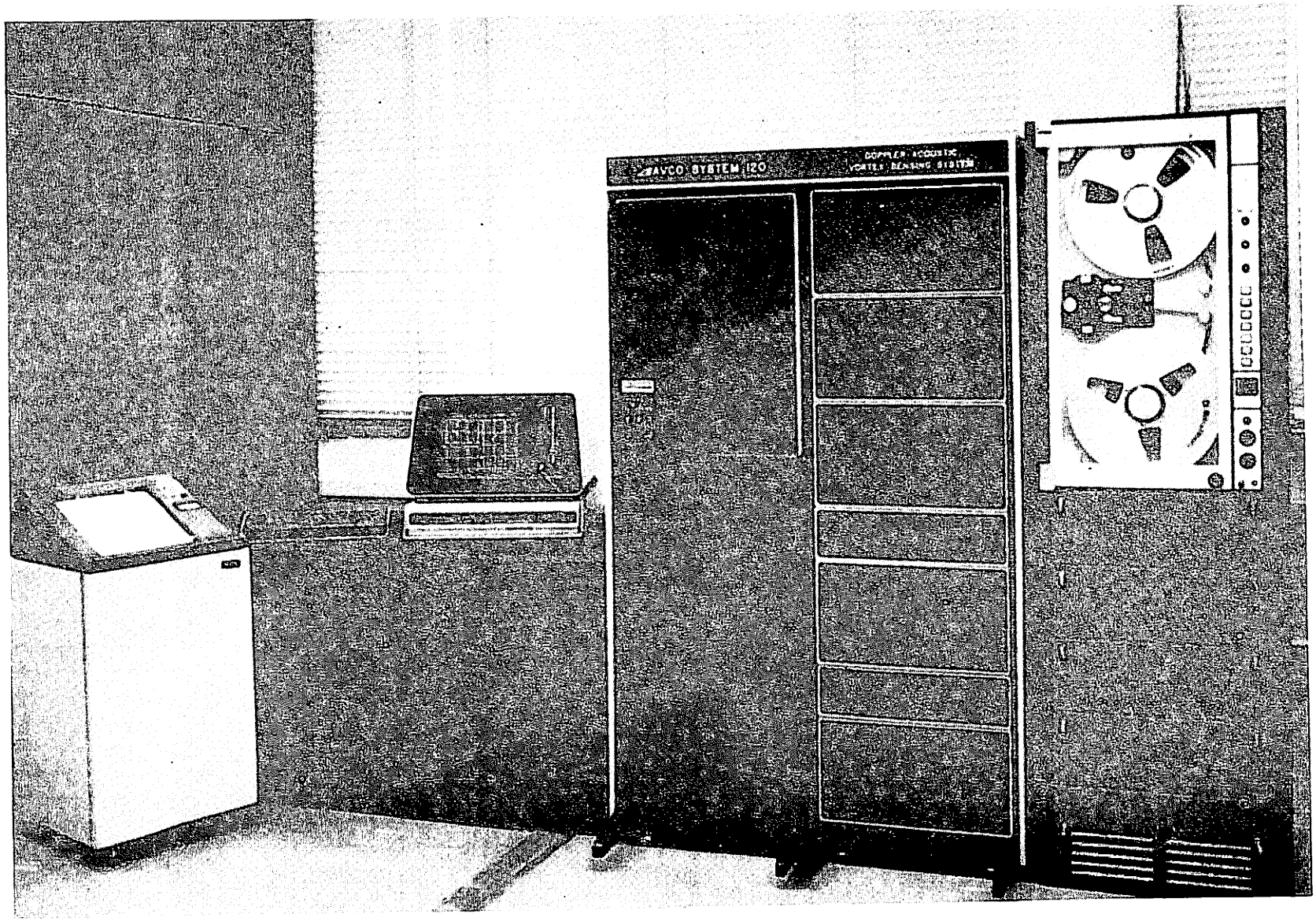

FIGURE 2-2 DAS, DDS, and DSS Hardware

The spread discriminant is then formed by summing the result of these two:

$$\text{Spread} = \sum_{i=1}^{3} K_i A_i + \sum_{i=4}^{6} K_i A_i = \sum_{i=1}^{6} K_i A_i .$$

Skew, on the other hand, is formed by taking the difference of these same two subtotals:

$$\text{Skew} = \sum_{i=1}^{3} K_i A_i - \sum_{i=4}^{6} K_i A_i .$$

In practice, to maintain the symmetric/asymmetric nature of the spread and skew discriminant algorithms, K_1 and K_6, K_2 and K_5, and K_3 and K_4 are chosen to be the same. In addition, they are also so chosen that

$$K_2 = K_1 \leq K_6 = K_5 \leq K_3 = K_4 .$$

A separate matrix is formed for intensity, for spread, and for skew. Each matrix is made up of the N beams (elevation angles) by M range (time delay) values of the discriminant data.

By examination and manipulation of the elements of these three matrices, the computer estimates the positions of any vortices which are detected. The algorithms used in this detection, search, and location process are the principal subject of Sections 5.3 and 7.2.

2.2 INSTALLATION AT JFK

Installation of the DAVSS at the Runway 31R Vortex Test Facility at JFK began on November 6, 1974. Two shipments were made. In the first shipment, three transmitting and three receiving antennas along with the housed electronic subassemblies were shipped in two 45-ft. commercial movings vans from Avco/SD Wilmington to JFK New York.

One transmitting and one receiving antenna were initially retained at Avco/SD Wilmington for further evaluation, testing, and possible validating of any modifications suggested by the JFK installation. These were later shipped to JFK to complete the bistatic Y-array.

Siting and erecting of all the antennas of the initial shipment and the installation and reassembly of all the housed subsystems were completed in one day. Power and signal cabling and distribution constituted the major installation effort. Figure 2-3 shows the siting plan for the monostatic backscatter Z-array and the bistatic Y-array in relation to the other vortex sensors and the equipment trailer. Figure 2-4 is a photograph of the housed equipment installation.

The initial emphasis was concentrated on installation, checkout, and optimization of the Z-array. This choice was made because of: (1) the convenience of providing the prime power to this single site (which was much closer to the equipment trailer), and (2) the greater familiarity with pulsed backscatter operation from the earlier field tests. However, tests were also conducted on the single bistatic path of the Y-array after the installation of the fourth transmitting and receiving antennas part of the Y-array in December.

2.2.1 Y-Array Configuration

The Y-array was configured for either bistatic forward scatter or quasi-monostatic backscatter operation. It was located 800 ft. uprange of the 31R middle marker, as shown in Figure 2-3. The two bistatic paths T1-R2 and T2-R1, were each 950 ft. long and were displaced some 10 ft. from each other so that R1 and R2 were not blocked by T1 and T2, respectively. The receivers were located at the $\pm$500-ft. marks from the runway centerline extension, while the transmitters were at the $\pm$450-ft. marks. The elevation angle of the receiver dishes was set at 22.5 deg. so that coverage extended from 4.5 to 40.5 deg. above the horizon, as shown in Figure 2-5. The resulting beam pointing angles are shown in Table 2-1.

Station 1 of the DAVSS Y-array consists of transmitter assembly 1, receiver assembly 1, the electronics shelter, and the primary power distribution point, as shown in Figure 2-6. Station 2 of the DAVSS Y-array, located on the other side of the runway, consists of transmitter assembly 2, receiver assembly 2, the electronics shelter, and a primary power distribution point.

Figure 2-7 shows the mode configurations possible with the DAVSS.

2.2.2 Z-Array Configuration

The Z-array was configured for quasi-monostatic backscatter operation. It was located 300 ft. uprange of the 31R middle marker,

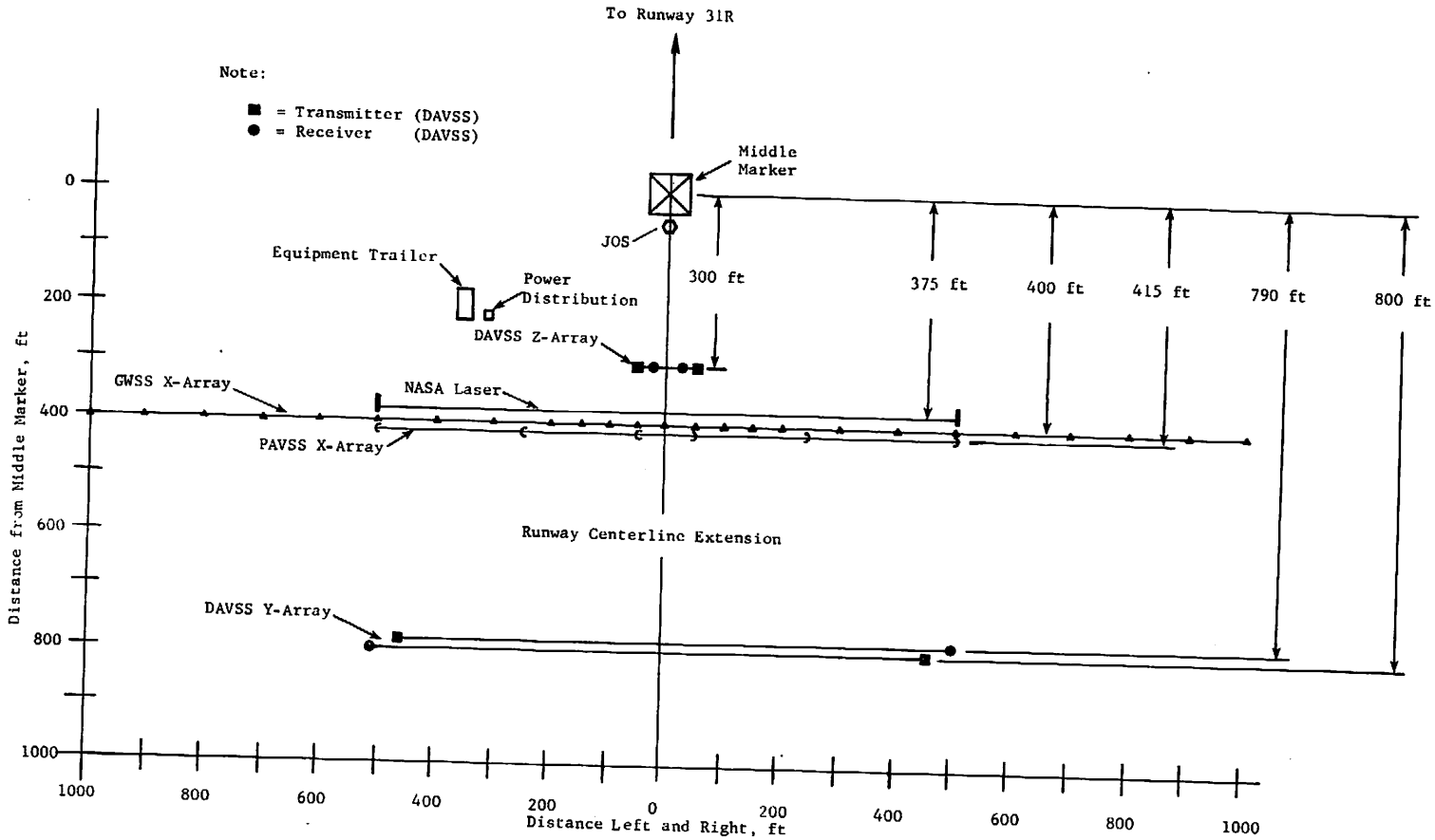

FIGURE 2-3 Siting Plan for DAVSS at JFK Runway 31R

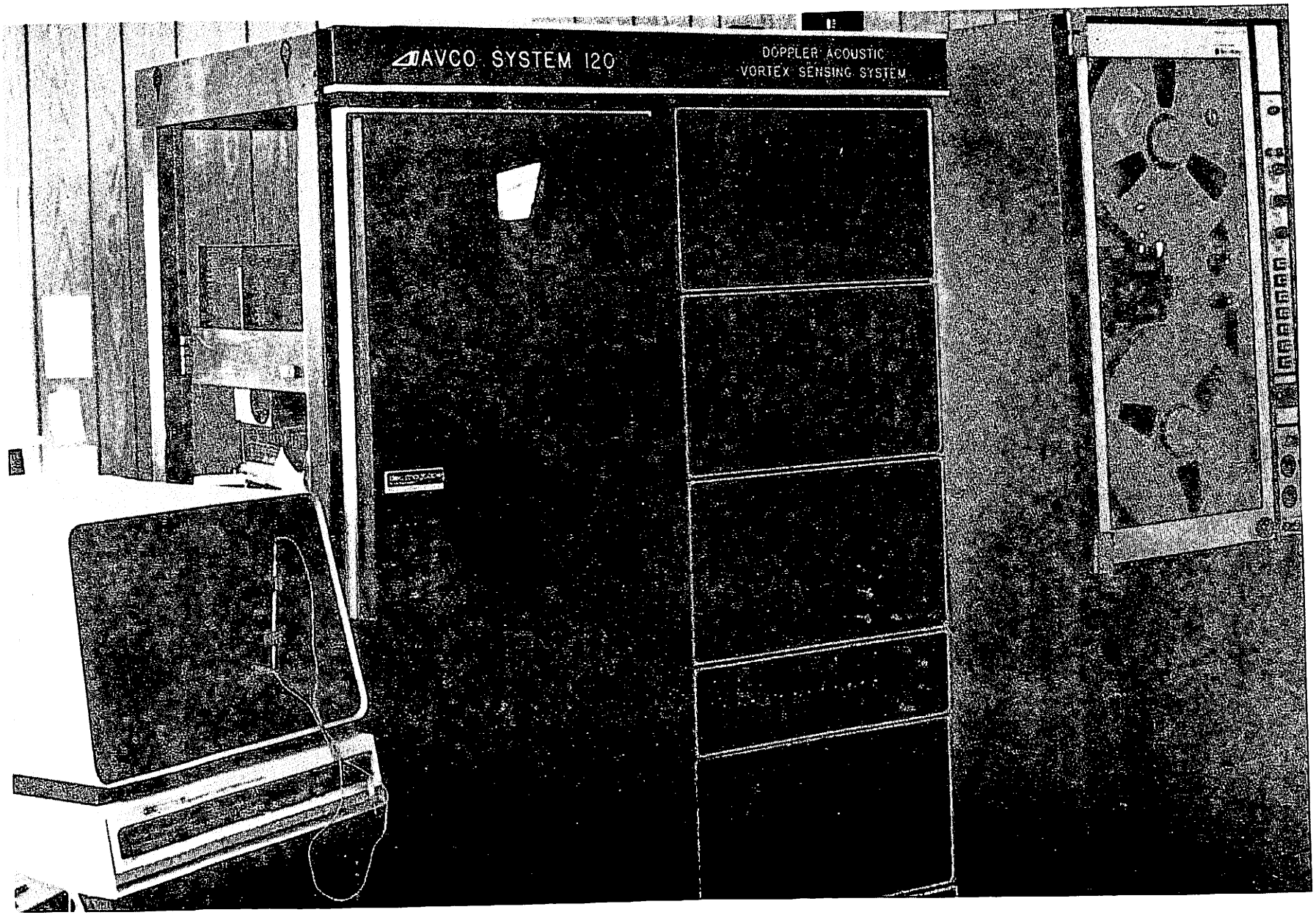

FIGURE 2-4 Housed Electronic Equipment Installation of DAVSS at JFK

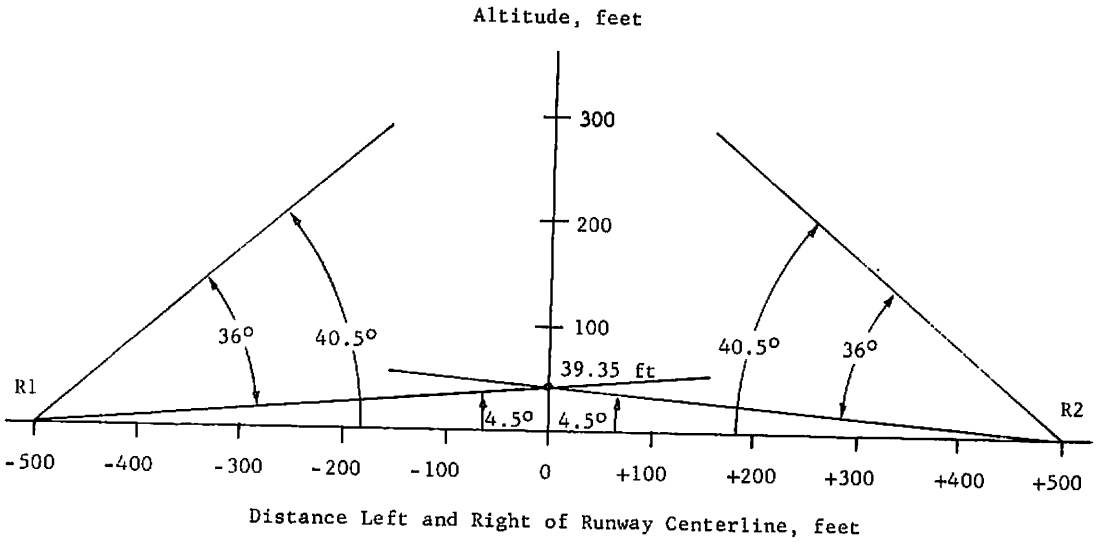

Note: Left and right are as viewed by a pilot landing on the runway. Plus (+) denotes distance to the right; minus (-) denotes distance to the left.

FIGURE 2-5 Elevation-Plane Coverage of the DAVSS Y-Array at JFK

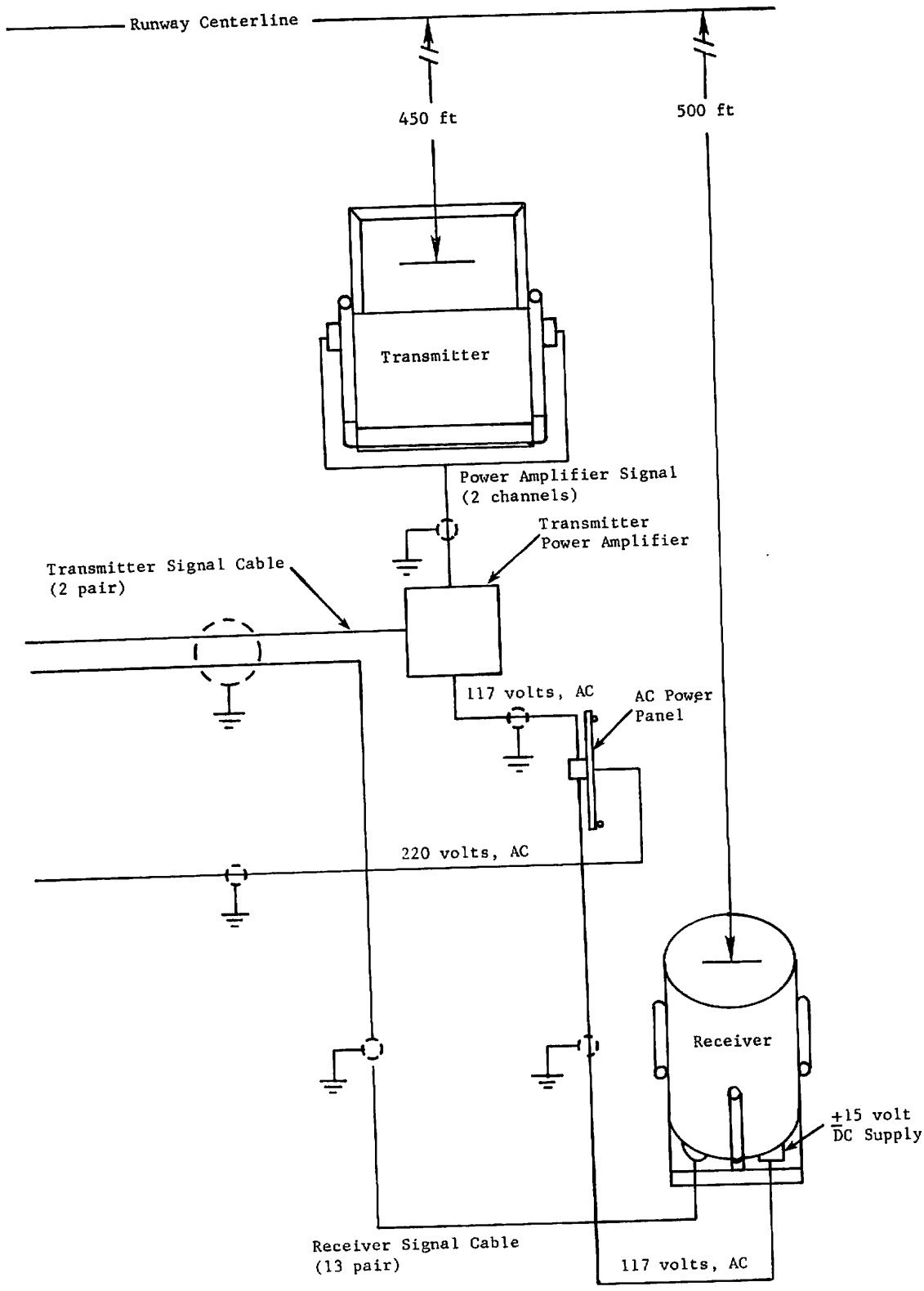

FIGURE 2-6 Detailed Siting Plan of the DAVSS Y-ARRAY -- Station 1

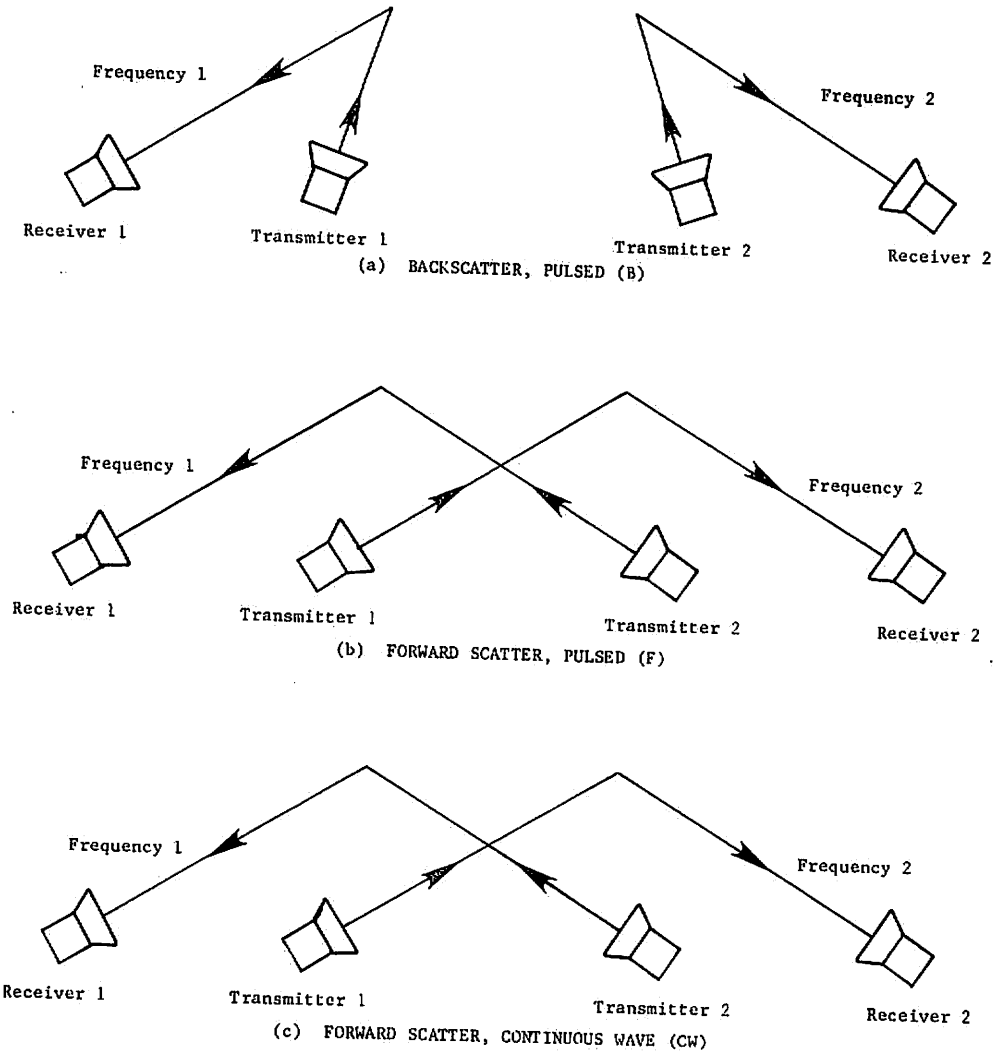

FIGURE 2-7 Possible Mode Configuration of the DAVSS Y-Array

TABLE 2-1

BEAM-POINTING ANGLES -- Y-ARRAY

Beam	Angle	Height at Centerline	Beam	Angle	Height at Centerline
	deg.	ft.		deg.	ft.
12	39	405	6	21	192
11	36	363	5	18	162
10	33	325	4	15	134
9	30	289	3	12	106
8	27	255	2	9	79
7	24	223	1	6	53

as shown in Figure 2-3. For purposes of comparison of vortex data tracks, the DAVSS Z-array may be considered colocated with the PAVSS X-array, the ground wind sensor X-array, and the laser Doppler velocimeter also shown in Figure 2-3. Two sensitive volumes, as shown in Figure 2-8, were illuminated and sensed by the T1-R1 and the T2-R2 paths, respectively. The receivers were located at $\pm$10 ft. from the runway centerline, respectively. The elevation angle of the receiver dishes was set at 54 deg. so that the coverage extended from 36 to 72 deg. above the horizon, as shown in Figure 2-8. The resulting beam-pointing angles are shown in Table 2-2.

TABLE 2-2

BEAM POINTING ANGLES -- Z-ARRAY

Beam	Angle	Beam	Angle
	deg.		deg.
12	70.5	6	52.5
11	67.5	5	49.5
10	64.5	4	46.5
9	61.5	3	43.5
8	58.5	2	40.5
7	55.5	1	37.5

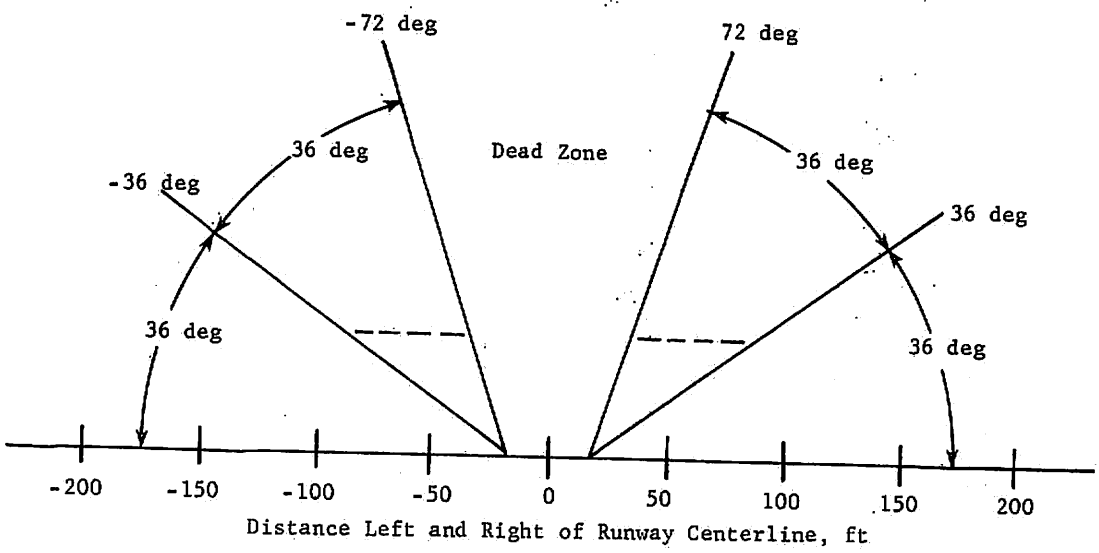

FIGURE 2-8 Elevation Plane Coverage of the DAVSS Z-Array at JFK

All the antenna assemblies of the Z-array were placed in line since the relatively high elevation angles are less susceptible to blockage of the receiver by the transmitter. Since the antenna assembly separations were all $\leq$ 50 ft., only one electronics shelter was required for the transmitter signal power amplifiers which drive the electro-acoustic transducers. Likewise, only one power-distribution point was provided for the Z-array. The actual location of the elements of the Z-array is shown in Figure 2-9.

Figure 2-8 shows both the areas of coverage of the Z-array and the areas of no coverage. The particular angular configuration of the Z-array was chosen to demonstrate the detection and tracking capability of the DAVSS in the quasi-monostatic backscatter mode so that the Y-array operation could be demonstrated concurrently. From these demonstrations, a determination of the most appropriate tracking mode for the DAVSS was to be made. Consequently, although the obvious dead zone directly overhead relative to the Z-array was disconcerting, the presence was not considered detrimental to the aims of the program. The results of the demonstrations revealed the preference for quasi-monostatic backscatter operation over the other modes; and modifications were subsequently made to use elements of the Y-array to fill in the dead zones and raise the Z-array to operational status as a vortex data collection sensor.

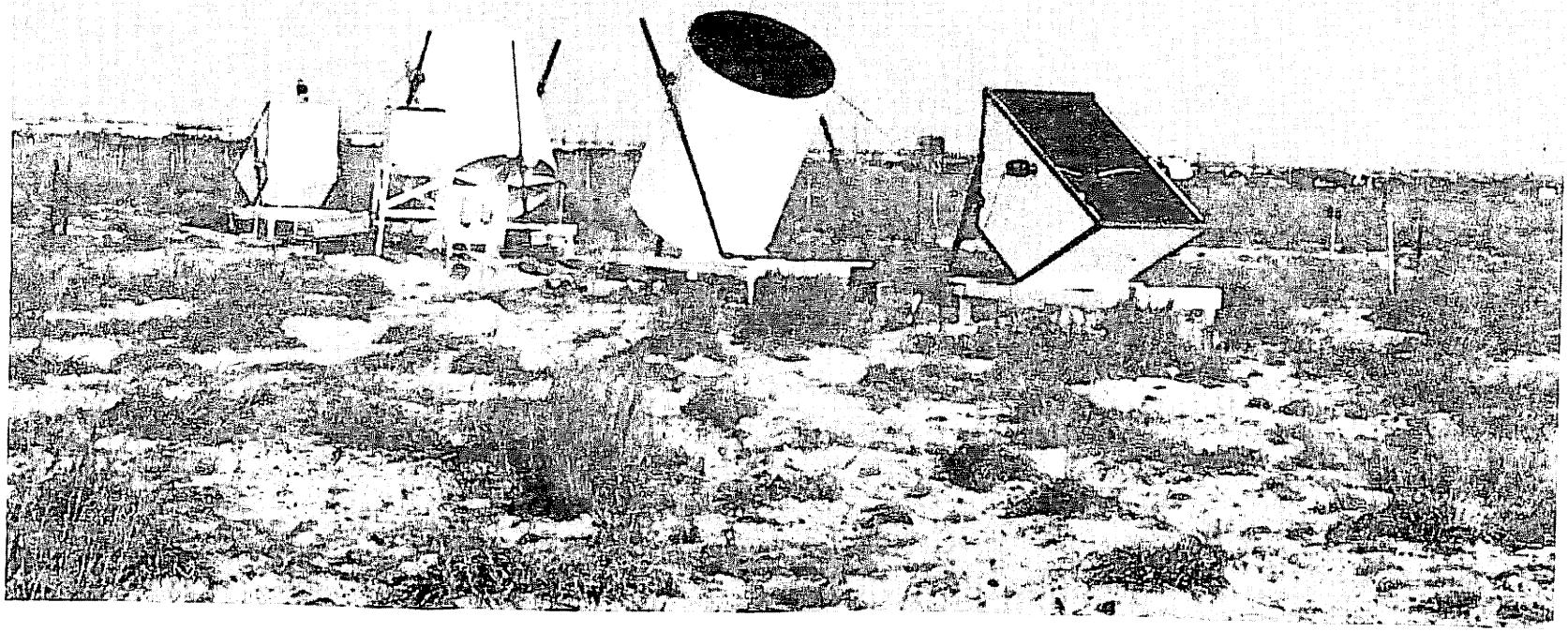

FIGURE 2-9 Z-Array Element Location

3. HARDWARE UPDATING

Several hardware features have been added to the DAVSS during the period between installation at JFK and system demonstration. These features have been designed to make the DAVSS easier to maintain and operate, and more reliable.

They include:

- Front-panel monitor and test circuits
- Front-panel lights for positive indication of remote-transmitter operation
- High-current/low-frequency protection of the electro-acoustical drivers
- High-voltage protection of sensitive integrated circuits (IC's)
- Equalization of record/playback signal levels
- Equalization of intensity, spread, and skew algorithms
- Protection of equipment from rodent damage
- Provision for stabilization of remote microphone-receiver subassemblies.

Some of these items are discussed in the following paragraphs.

3.1 FRONT-PANEL MONITOR-AND-TEST CIRCUITS

Monitor-and-test circuits have been added to the front panel of the DAS. Figure 3-1 is a picture and a line drawing of these front-panel jacks, switches, and controls. The monitor circuits are grouped on the upper panel; the test circuits on the lower panel.

The monitor circuits allow audio-and-visual monitoring of the active receiver and transmitter channels. The test circuits allow insertion of known audio signals into the receiver signal-processor channels.

The receiver channels are monitored at the input to the analog tape record amplifiers. The combination of a 3-position toggle switch and a 12-position rotary switch allows any receiver channel in either receiver in the active array to be heard individually on a speaker and/or viewed on an oscilloscope. The choice of the

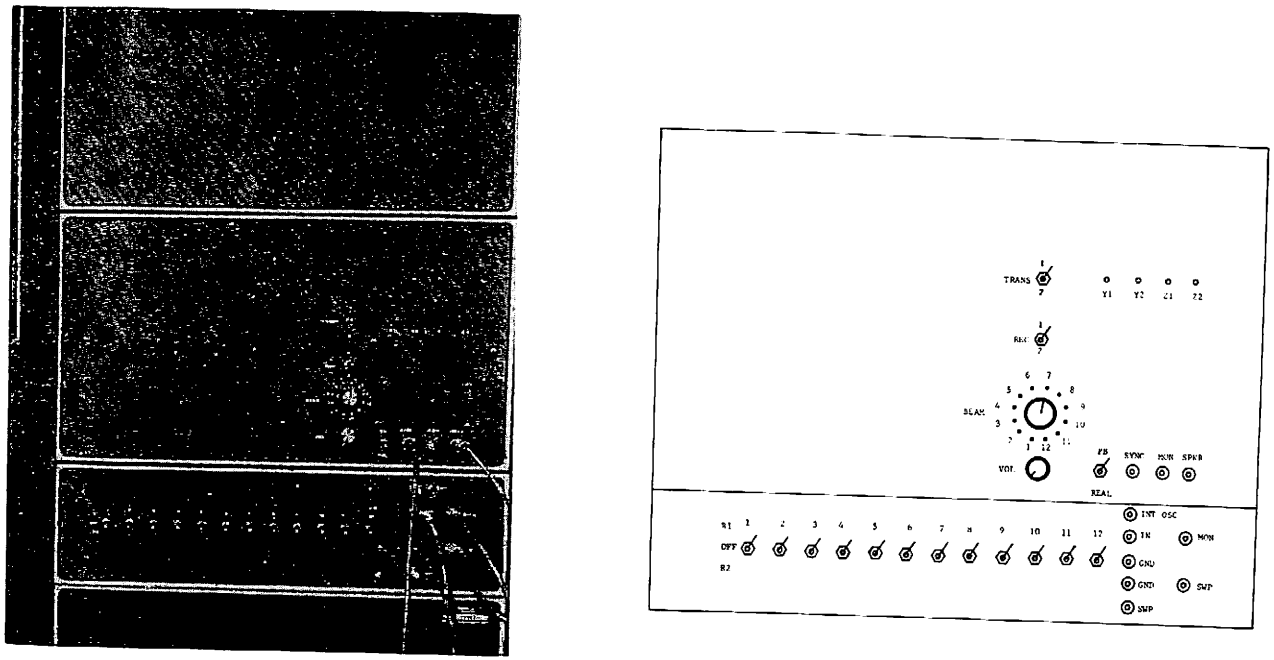

FIGURE 3-1 Picture and Line Drawing of the Front Panel Monitor and Test Jacks, Switches, and Controls

monitor position at the input to the analog tape recorder includes the effects of the receiver-microphone-preamplifier, cable run, isolation, and configuration modules, as well as the gain ramp in the individual signal-processing board for that channel.

The transmitter exciter signals from either transmitter are selected by means of another 3-position toggle switch. The exciter signals are monitored after the line driver module thus sampling the actual shaped pulses which are delivered to the remote transmitters. Four light-emitting diodes (LED's) indicate the operation of each of the remote transmitters. They are further explained in paragraph 3.2.

The combination of audio-and-visual monitoring of the transmitter and receiver signals constitutes a powerful diagnostic and maintenance tool to aid the operator in assessing the current functioning of the circuits monitored. The 12-position selection switch allows the operator, by listening to all receiver channels in rapid succession, to distinguish abnormal from normal operation and to determine whether excessive noise is environment- or system-caused.

To aid the operator to assess the functioning of the rest of the signal-processing chain, signal insertion capability has been added. This allows DAVSS internally generated swept-audio-signals or fixed externally generated signals to be inserted at the front end of any one or simultaneously in up to 12 of the 24 analog signal-processor boards. By this method, the response of the processor system to known signals can be monitored on the DAVSS, CRT, and Versatec hard-copy displays.

Figure 3-1 shows this signal-insertion panel (the lower panel). There are 12 three-position toggle switches which allow insertion of the oscillator signal into either or neither receiver for each of the 12 channels. The various connectors allow monitoring of the internal signal sweep and synchronization signals, and also allow input of external signals to the circuit.

3.2 TRANSMITTER DRIVER CIRCUIT PROTECTION AND MONITORING

Several failures in the electrical/acoustical drivers had been experienced at the remote transmitter stations during the installation and checkout period. Indication of when such a failure has occurred and, therefore, has degraded the system, and protection against such failures are the purposes of the transmitter driver circuit protection and monitoring circuits. Each of the four transmit indicators on the front panel (shown in Figure 3-1) lights only when both drivers in that transmitter assembly are operating.

Thus, the lighted lamp is a positive indicator that both drivers in that remote transmitter are functioning. The lights also show which transmitters of which array are energized, thus confirming the DAVSS mode of operation.

Driver operation is remotely sensed by using the spare pair in each transmitter signal cable. Two transistors are placed in series, and each is energized by a toroidal current transformer which senses the current flow in its electro-acoustic driver circuit. If current flows through the driver voice coil, the secondary current developed in the toroid causes transistor conduction. Since the transistors sensing each driver are in series, both drivers must be operating for the sensing circuit driving the indicator LED to be completed. Each sensing circuit drives one LED on the front panel.

The voice coil failures have been both mechanical and electrical. The mechanical failures are most probably a result of a weakness in the voice coil itself. The weak ones fail within the first few hours of operation. The electrical failures have been caused by excess current in the drive circuit. Although the origin of this excessive current has not been positively determined, it is thought to be the result of low magnetic flux in the driver magnet and/or low-frequency, high-amplitude drive signals for which the voice coil is effectively unloaded. A highpass filter, whose cutoff frequency is 1 kHz, and a current-limiting fuse have been added to each driver circuit to prevent further electrical failures in the voice coils. These additional circuits, shown in Figure 3-2, are mounted on the transmitter power amplifier in the remote equipment shelters.

3.3 OTHER HARDWARE MODIFICATIONS

Other minor hardware modifications and precautions such as may be expected in any field installation and in checkout of a new and complex system, such as the DAVSS, have been performed as needed.

Special precautions have to be taken to prevent rodent damage both to the field and the housed equipment. Adjustment of gains in the record and playback amplifiers, as well as in the discriminant-processing amplifiers to match more closely the actual data experienced, is a standard checkout activity. Component failure and replacement during the first hundred hours or so of burn-in is also a standard experience for integrated circuitry. DAVSS reliability after the initial burn-in has been quite satisfactory.

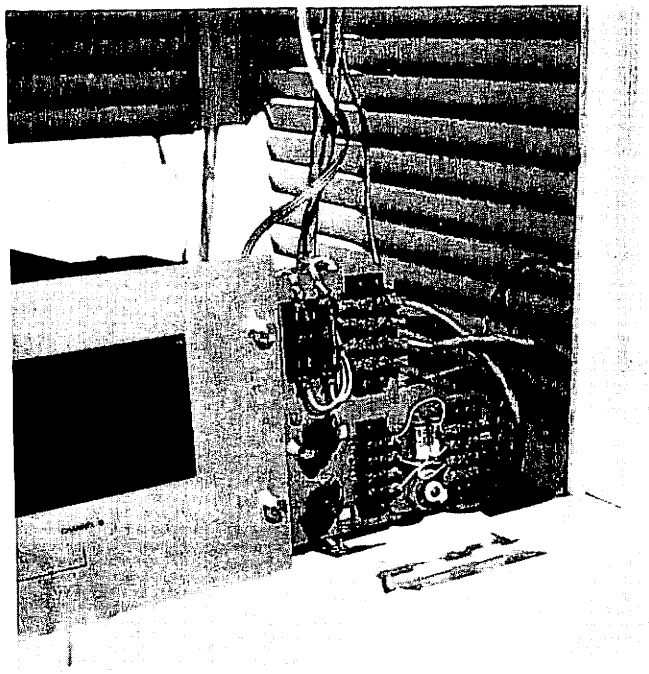

FIGURE 3-2 Transmitter Drive-Circuit, Protection and Monitor Circuits as Mounted on the Transmit-Power Amplifier in the Remote-Equipment Shelter

4. SOFTWARE/PROCESSING CHANGES

During the installation and checkout period, many hours of online experience in monostatic backscatter operation were acquired. Many changes to improve the detection-and-tracking algorithms were tested and when they proved useful, were integrated into the DAVSS operating system. These changes included:

a. altering the weighting of intensity in hardware to be normalized more nearly to the spread and skew

b. converting skew to an absolute value for display and for use in the search routines

c. providing capability for arbitrarily weighting intensity, skew, and spread individually in the search routine

d. averaging spatially before the search routine

e. adding a temporal averaging and frame-to-frame vortex movement criterion

f. adding noise rejection criteria

g. homing-in on those processing parameter values most effective for vortex detecting and tracking

h. assessing their dependence on system configuration and meteorological conditions.

4.1 NORMALIZATION OF WEIGHTS OF THE DISCRIMINANTS

In the original search routine, only intensity and spread have been summed to form the composite matrix in which the highest peak represents the vortex position estimate. Since the form of the algorithm is

$$I = \sum_{i=1}^{6} F_i,$$

and spread is

$$Sp = \sum_{i=1}^{6} K_i F_i,$$

where I is intensity, Sp is spread, Fi is the individual comb filter response, and the nominal values of Ki are:

$$K_1, K_6 = 1.00$$

$$K_2, K_5 = 0.50$$

$$K_3, K_4 = 0.20,$$

the total weighting of I is 6 times the average value of the filter amplitude, while Sp is 3.4. The Ki weights are used for spread and skew, so that skew's influence is deweighted by approximately one-half also. The relative influence of these discriminants is made more nearly equal in the hardware by reducing the intensity gain by one-half.

4.2 CONVERTING SKEW TO ABSOLUTE VALUE

The use of the real-time CRT diagnostic discriminant display was limited by the attempt to retain the signed value of skew. The skew value, as displayed using print characters to represent intensity in Z-axis modulation, had meaning only when the display limits were symmetrically placed about 50 percent of full-scale i.e., 10 - 90 percent or 33 - 67 percent, etc. This limitation on selecting the display scale severely hampered its effectiveness for displaying intensity and spread. Consequently, it was decided to convert skew to an absolute value for display purposes. Now no restrictions are placed on the display scale selection, and with the reduction in the weighting of intensity, the importance of all three discriminants in visually determing the vortex location was made manifest.

4.3 ARBITRARY WEIGHTING OF ALL THREE DISCRIMINANTS IN SEARCH ROUTINE

The fact that all three discriminants contributed to visual vortex location suggests the use of summing all three discriminants in the search routine with arbitrary weighting factors. Thus the new matrix, M_{ij}, on which the vortex search is performed consists of elements of the following form

$$M_{ij} = (A/B)\ I_{ij} + (C/D)\ Sp_{ij} + (E/F)\ Sk_{ij}$$

where S_{kij} is the absolute value of the skew response; and A, B, C, D, E, and F are any integers from 0 to 255.

The proportional effect of each of the three discriminants toward good tracking results has been evaluated. Good tracking results seem to be obtained most consistently with approximately equal proportions of intensity, spread, and skew. The proportions of intensity, spread, and skew actually used in the search are a software, toggle-in selection option (not an operator keyboard option).

4.4 SPATIAL-AVERAGING

The tacit assumption made in designing the search routine is that vortices manifest themselves as singularities in the discriminant field of the matrix. Although this assumption may hold for some vortices, it certainly does not hold for all. For many vortices, significant scattering returns exist in several beams and range gates which correspond to the spatial extent of the vortex itself. Therefore, spatial averaging has been introduced in the processing software.

The purpose of the spatial-averaging algorithm is to replace each range-beam element in the intensity, spread, and skew matrices with a new element which represents a weighted average of itself and its neighbors. The weighted spatial-averaging is accomplished in two passes over the data, first in the beam dimension and second in the range dimension. The spatial average is formed over 1, 3, or 5 range gates and over 1 or 3 beams. The center element is weighted as 1, immediate neighbors by 1/2, and next neighbors by 1/4, as shown in Table 4-1.

TABLE 4-1

SPATIAL-AVERAGING

Range	Beam Weighting			Normalization
	1/2	1	1/2	
1/4	1/8	1/4	1/8	4 x 1/8 = 1/2
1/2	1/4	1/2	1/4	6 x 1/4 = 1-1/2
1	1/2	1	1/2	4 x 1/2 = 2
1/2	1/4	1/2	1/4	1 x 1 = 1
1/4	1/8	1/4	1/8	15 ÷ 3 = 5

The 1/2, 1, and 1/2 sliding beam filter is first applied to all the data in each range gate moving across the beams. Next, the 1/4, 1/2, 1, 1/2, 1/4 sliding range filter is applied to all the data in each beam from range gate to range gate. The resultant product is the matrix shown in Table 4-1. For the 3 x 5 matrix, the data points are renormalized by dividing by 5. Thus, the center point contributes 1/5 of the total weight of the spatial average by which it is replaced in the new intensity, spread, and skew matrices. The filtering is done on the individual discriminant matrices rather than on the search matrix so that the spatially averaged discriminants may be displayed on the CRT in diagnostic discriminant display.

Selection of the vortex range-beam position within the search matrix is then carried out as previously. The three highest-valued peaks in the matrix are selected. However, the second and third highest valued peaks cannot be picked within an exclusion zone drawn around the highest value. This limitation is designed to prevent selecting two position estimates from the same vortex. The size of the exclusion zone is a keyboard entry and is given in terms of beam widths and range gates. If, for example, the exclusion zone is set at 5 beams and 7 range gates, a secondary peak 4 beams and 6 range gates away from the highest peak will be excluded. A peak 4 beams and 8 range gates away will be accepted. Three peaks are always chosen. However, a maximum of two can be used to compute vortex position in rectangular coordinate space. The thresholding criteria used are discussed in the following paragraphs on noise, false alarms, and frame-to-frame integration.

4.5 NOISE, FALSE ALARMS, AND FRAME-TO-FRAME INTEGRATION

Not only during aircraft passage but also for several frames thereafter, aircraft noise typically saturates the receivers. No valid detection or tracking can be accomplished during this time. This condition is sensed by averaging the values of intensity and spread for all beams in the last sampled range gate of each frame. If this average is greater than an operator-specified fraction of the maximum scale value, the system is assumed to be dominated by aircraft noise, and no detection or tracking is attempted for that frame. The same average value of intensity and spread in the last range gate is used as the basis for a vortex-detection threshold. Candidate range-beam estimates from the vortex-search routine are compared with the average value of intensity and spread in the last range gate. Only position estimates whose combined spread, skew, and intensity value exceeds the threshold by some operator-selected factor, such as 2.5 or 3.0, etc., are considered as valid vortex detections. If no position estimate exceeds the factored threshold, no vortex position is calculated for that frame.

The first two thresholding techniques outlined above are designed to deal with the prolonged aircraft noise from the aircraft passage and to set a signal-to-noise threshold for acceptance of vortex detection data. Two other types of noise are potential sources of system false alarm. These noise sources are impulsive in nature, and, therefore, when convoluted with the data-scan period, tend to have the appearance of a range-gated signal. One type of such noise appears in all beams simultaneously; the other type appears to be beam-dependent. To eliminate the first type of noise appearing in all beams for one or more range gates, the amplitude of the elements in beam 2 and 11 is compared with the noise threshold level. The sum and difference of beams 2 and 11 are calculated. If the sum exceeds twice the selection threshold and if the difference is less than a preset fraction of the threshold, the noise is assumed to be across all beams for that range gate and the entire range gate is ignored for that frame.

To deal with angle-dependent noise bursts, a frame-to-frame comparison can be used. In this mode, the fact that three candidate vortex positions per receiver are selected is used to select the best two for final vortex position selection. This selection criterion requires that the vortex position estimate for two successive frames lie within a preset number of beams and range gates. One or two such position estimates may be selected from the three available.

5. DAVSS DATA ANALYSIS

This section is intended to provide the reader with an exposure to Doppler acoustic vortex data in several stages of processing and representation to convey an appreciation of the character and complexity of the vortex detection and tracking problem. The several types of data illustration presented include:

a. "before and after" comparisons of the DAVSS detection and tracking performance on vortices from several aircraft flybys

b. examples of the diagnostic discriminant display as printed on the Versatec printer-plotter

c. examples of the digital vortex position display as printed on the Versatec printer-plotter

d. examples of several frames from the same vortex of the offline digital diagnostic discriminant display

e. construction of the vortex location algorithm for one frame

f. summary of the Doppler time history of the vortex passage through the twelve receiver beams

g. examples of the use of the line integral for vortex circulation and position estimate and comparison with the position estimates from the present tracking algorithm.

5.1 "BEFORE AND AFTER" COMPARISONS

During the course of the field test optimization and the evaluation activities leading to the demonstration, the processing algorithms changes and additions described in Section 4 were evolved. At the same time, experience and theory were combined to empirically focus on the optimum choice of selectable processing parameters. However, to assess the effect of the processing algorithms as opposed to the selectable parameters, the DAVSS operating system was reset to the original processing configuration. The analog recorded data for the same set of aircraft flybys was then processed with the identical set of selectable parameters using both the original and the final processing algorithms. The results of the side-by-side comparison for three aircraft flybys are shown in Figure 5-1. The most significant difference between the two results is the substantial reduction in the number of false alarms with the new processing algorithms. The new track is for the most part a subset of the old track with the false alarms removed. This lends confidence that the

AFTER

BEFORE

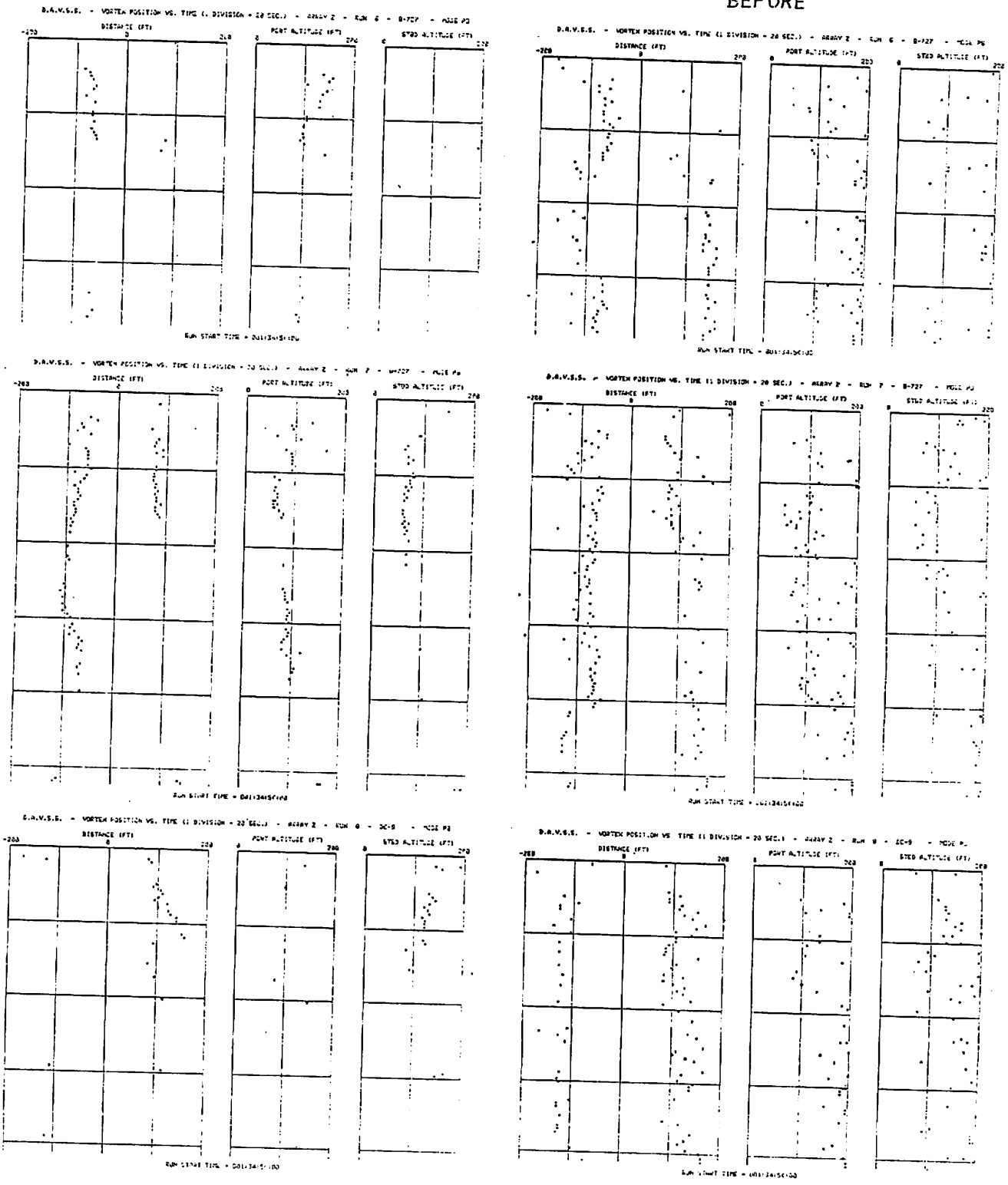

FIGURE 5-1 Side-by-Side Comparison of Tracking Results of Three Aircraft Flybys with Original and Final Processing Algorithms

essential data quality has not been altered by the new processing algorithms. The vortex detection discrimination process was improved by the changes in the processing algorithms.

5.2 VERSATEC PRINTER-PLOTTER USE

Figure 5-1 is an example of the primary intended use of the Versatec printer-plotter to provide a hardcopy record of the vortex position time histories. However, the experience gained during this phase of the program has shown the power of utilizing the Versatec printer-plotter as a diagnostic tool in data quality control as well. The primary usage is for quality assurance of the digital-tape-recorded output of the DAVSS. Figure 5-2 is an example of the digital dump of the digitally recorded position tracks of an aircraft flyby. Inspection of such tape recordings by the Versatec digital dump during and/or after a vortex data collection effort assures the quality of the digital tapes which are returned to TSC for further analysis. The secondary use is for checking the processing fidelity. By comparing the diagnostic discriminant output on the Versatec as shown in Figure 5-3 for several frames during an aircraft flyby with the corresponding frames in the digital dump, one can spot-check the validity of the processing algorithm operation.

5.3 FURTHER ANALYSIS OF DAVSS DETECTING AND TRACKING

At the present time, no objective calibration of vortex position or strength is available. No standard exists against which to assess the fidelity of the DAVSS detection and tracking algorithms. Such assessment can be accomplished, however, by careful analysis of the DAVSS data itself. Several methods for monitoring the operation of the hardware portions of the signal processing chain from exciter and transmitter through receiver and comb filter operation have been developed and implemented during the current phase of the DAVSS program. These are described in Section 3. The diagnostic discriminant matrix, or array, is the raw data for the computer detection and tracking algorithms. While the Versatec and the GT-40 displays of this diagnostic discriminant array give continuous and qualitative visibility of the raw data, a digital diagnostic discriminant array is necessary to really analyze the effects of current and/or alternative methods of detection and tracking. For this purpose, capability was provided to dump the digital diagnostic discriminant data on digital tape from which offline display and processing can proceed.

Figure 5-4 shows two digital discriminant data frames of the same aircraft flyby, approximately 8 seconds apart. The period of each frame is 900 ms. The digital discriminant data shows the intensity, spread, and skew matrices. The elements of each are arranged by

FILE 4 ERROR? N

HEADER

RUN 4
AIRPORT K

TIME 34:5<:00
AIRCRAFT B-727

TAPE 1

SYSTEM CONFIGURATION PBS

ARRAY Z

ACTIVE RECEIVER(S) B

FRAME LENGTH 900

PULSE RISE TIME	20	20
FREQUENCY	4006	4006
TRANSMITTER POSITION	-35.0	37.0
RECEIVER POSITION	-10.0	12.0
RECEIVER ANGLE	-54.0	54.0
SONIC VELOCITIES	1094.2	1094.2

CROSS WIND .0

AIR TEMPERATURE 38.00
RELATIVE HUMIDITY 50.0

FILE 4 RUN 4

FRM	RECEIVER 1 PORT VORTEX DIST	HT	STBD VORTEX DIST	HT		RECEIVER 2 PORT VORTEX DIST	HT	STBD VORTEX DIST	HT
1	.0	.0	.0	.0	N	.0	.0	.0	.0
2	.0	.0	.0	.0	N	.0	.0	.0	.0
3	.0	.0	.0	.0	N	.0	.0	.0	.0
4	.0	.0	.0	.0	N	.0	.0	.0	.0
5	.0	.0	.0	.0	N	.0	.0	.0	.0
6	-61.4	57.2	.0	.0	N	.0	.0	.0	.0
7	-60.6	53.4	.0	.0	N	.0	.0	.0	.0
8	-78.8	61.9	.0	.0	N	.0	.0	.0	.0
9	-77.0	48.6	.0	.0	N	.0	.0	.0	.0
10	-64.1	46.2	.0	.0	N	.0	.0	.0	.0
11	.0	.0	.0	.0	N	.0	.0	.0	.0
12	-76.7	54.0	.0	.0	N	.0	.0	.0	.0
13	-85.7	55.0	.0	.0	N	.0	.0	.0	.0
14	-77.0	48.6	.0	.0	N	.0	.0	.0	.0
15	-91.5	59.2	.0	.0	N	.0	.0	.0	.0
16	-97.3	63.4	.0	.0	N	.0	.0	.0	.0
17	-97.3	63.4	.0	.0	N	.0	.0	79.8	57.9
18	-96.3	69.9	.0	.0	N	.0	.0	.0	.0
19	.0	.0	.0	.0	N	.0	.0	.0	.0
20	-78.8	61.9	.0	.0	N	.0	.0	.0	.0
21	-94.4	61.3	.0	.0	N	.0	.0	83.2	54.6
22	-79.5	56.3	.0	.0	N	.0	.0	79.8	57.9
23	-79.5	56.3	.0	.0	N	.0	.0	.0	.0
24	.0	.0	.0	.0	N	.0	.0	.0	.0
25	-65.7	58.6	.0	.0	N	.0	.0	.0	.0

FIGURE 5-2 Digital Dump on Versatec Printer/Plotter of Vortex Position Output

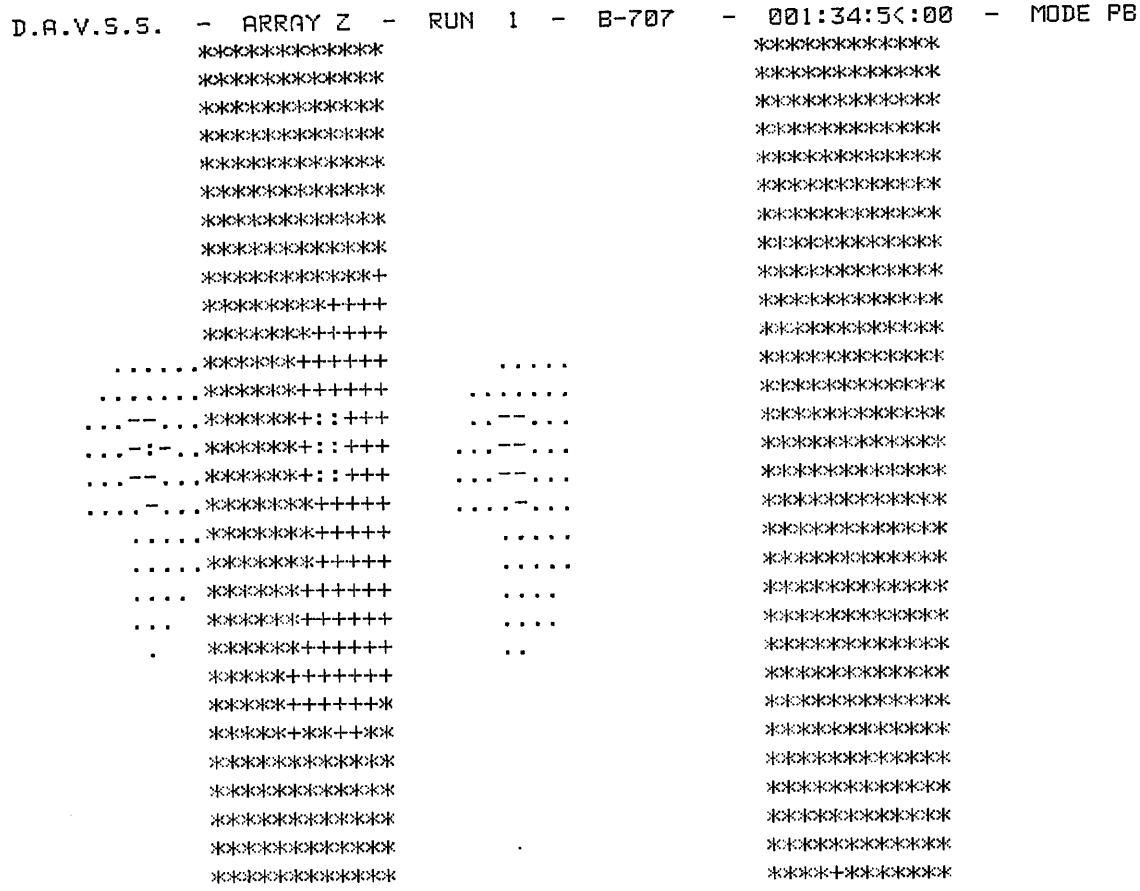

FIGURE 5-3 Versatec Diagnostic Discriminant Output -- One Frame

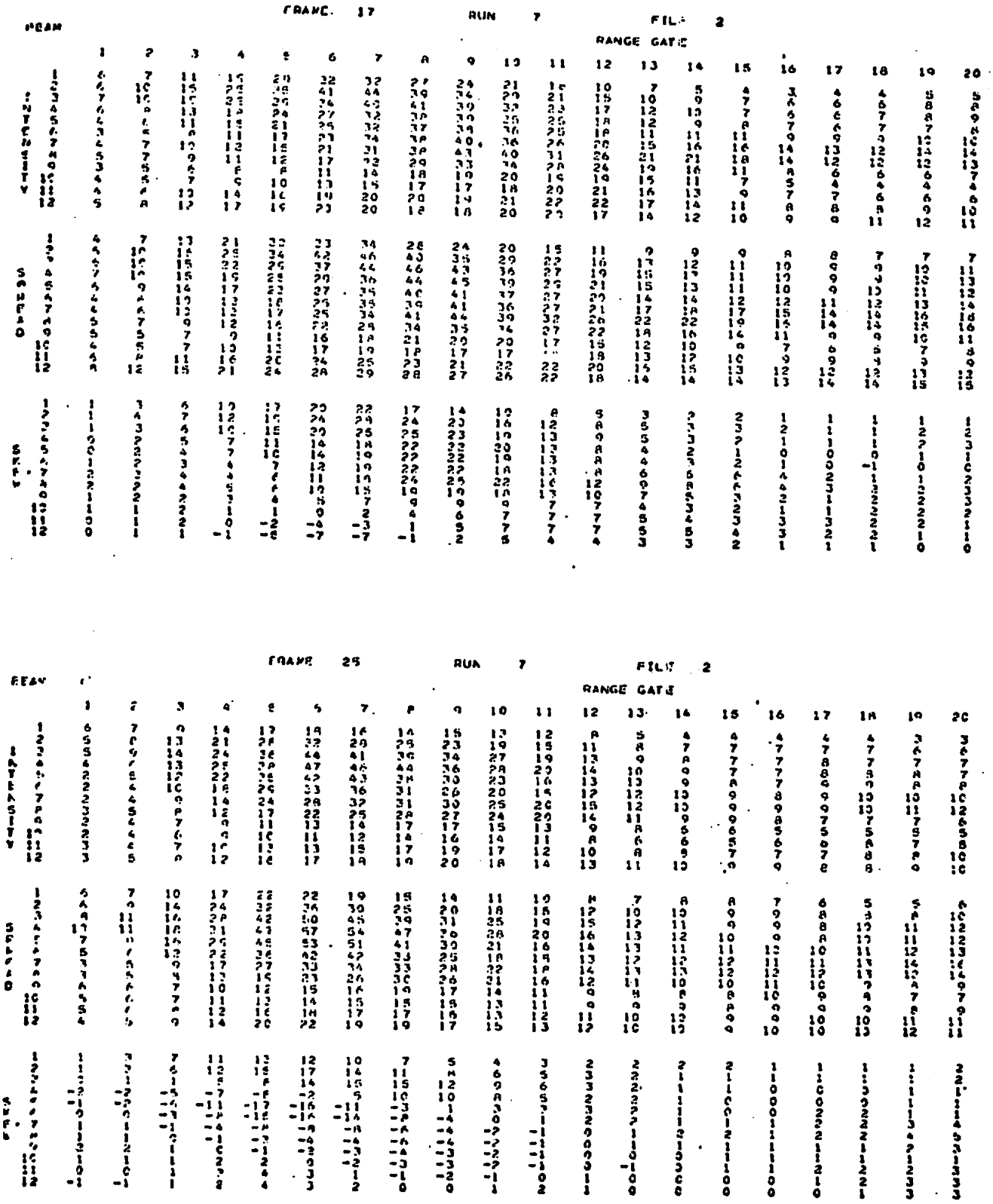

FIGURE 5-4 Two Digital Discriminant-Data Frames Offline-Computer Output

beams versus range gate. Beam 1 is the lowest elevation angle at 37.5 deg. and angles increase with beam number at 3 deg. increments. Range gate 1 is the closest time delay, and range gate time delays increase in increments of 13 ms. However, range gate 1 may start at any selected delay from the beginning of the frame period. In this case, it is 90 ms. By inspection, one can see that the region of the greatest magnitude of the intensity, spread, and skew discriminants is centered approximately in beam 2, range gate 7 for frame 17; and beam 4, range gate 6 for frame 25. Using skew to estimate the vortex core location, since skew is most sensitive to Doppler offset, one would place the center of the vortex in beam 8, range gate 6 for frame 17; and in beam 4, range gate 6 for frame 25. The presence of the vortex circulation, especially in frame 25, is quite convincing. It is evidenced by the general symmetry of the intensity and spread discriminants about beam 4 and the anti-symmetry of skew about beam 4. This indicates that beams below beam 4 sense the flow is toward the radar and beams above beam 4 sense flow away from the radar with beam 4 seeing the vortex core.

Perhaps an even more convincing and revealing picture of the temporal movement of the core of the vortex circulation across the twelve beams of the receiving antenna is presented in Figure 5-5. This illustration represents the first moment of the Doppler frequency versus time for each of the twelve beams in two range gates. The Doppler time history for each beam can be characterized as a gradual buildup to a positive Doppler peak followed by a rapid traversal to a negative Doppler peak and a gradual relaxation toward zero Doppler. The aggregate of the twelve beam time-histories clearly shows the movement of the vortex core (the zero Doppler between the positive and negative Doppler maxima) successively through each beam from beam 12 to beam 1. This Doppler time-history was calculated by computing the ratios of skew divided by intensity in a particular range gate for each beam for each successive frame. The picture shows the tracking advantage of the time sequence. Without recourse to the context of the time sequence, the precise moment of zero crossing may not be apparent due to the rather slow sampling period (900 ms) caused by the frame time.

Use of the time sequence is rather cumbersome for the real-time detecting and tracking requirement; but, since the vortex is usually travelling across beams, time and space are transformable. Two methods of spatial integration have been utilized for detecting and tracking on a single frame basis.

The first method is the one previously used in the DAVSS real-time tracking algorithm. The method is illustrated in the sequence of Figures 5-4b, 5-6, 5-7, and 5-8 for frame 25. This sequence shows the raw digital discriminant array, the summation of intensity,

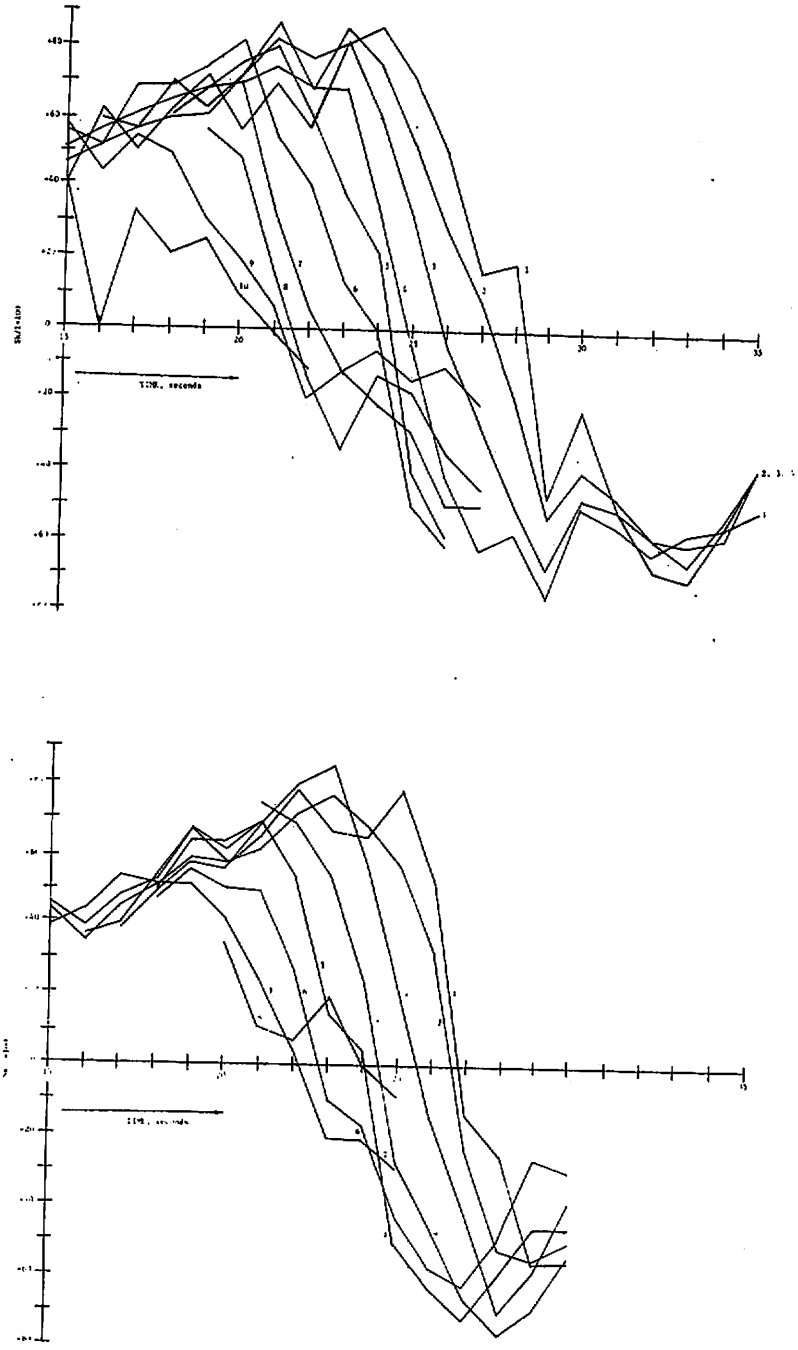

FIGURE 5-5 Pseudo Doppler Time Histories of Vortex Passage for Each of 12 Beams in 2 Different Range Gates

Beam	Range Gate								
	3	4	5	6	7	8	9	10	11
1	26	42	52	52	45	36	34	28	25
2	33	57	75	85	72	61	51	43	59
3	31	57	76	108	101	93	77	61	44
4	36	63	95	106	105	101	82	64	45
5	34	62	97	111	105	82	61	47	35
6	25	48	80	91	92	72	55	38	31
7	19	35	59	69	74	70	62	49	39
8	16	26	39	49	55	64	57	47	37
9	15	19	24	30	33	40	37	31	25
10	14	22	25	25	29	32	34	29	23
11	16	25	33	34	33	35	37	31	24
12	18	29	40	42	30	38	37	34	29

FIGURE 5-6 Summation of Intensity, Spread & Skew into Single-Search Array for Frame 25

Beam	Range Gate								
	3	4	5	6	7	8	9	10	11
1	28	46	58	60	52	42	38	32	28
2	31	53	70	83	73	63	53	44	35
3	33	59	81	102	95	87	72	57	42
4	34	61	91	108	104	94	76	59	42
5	32	59	92	105	102	84	65	49	37
6	26	48	79	91	91	74	58	43	34
7	20	36	59	70	74	69	59	46	37
8	17	27	40	49	54	60	53	44	35
9	15	22	28	34	38	44	41	35	28
10	15	22	27	29	31	35	36	30	24
11	16	25	33	34	34	35	36	31	25
12	18	28	38	40	38	37	37	33	28

FIGURE 5-7 Vortex Search Array after Beam Integration

Beam	Range Gate								
	3	4	5	6	7	8	9	10	11
1	32	44	52	54.8	51	44	38	33	27
2	36	53	62	73	70	63	53	45	35
3	39	60	77	90	91	84	71	59	44
4	42	64	84	98	99	90	75	61	45
5	40	62	83	95	94	82	66	52	38
6	33	52	71	82	83	73	59	46	35
7	25	39	54	65	69	66	58	48	37
8	19	29	38	47	53	55	51	44	35
9	16	22	27	33	37	40	39	35	28
10	16	21	25	29	31	33	33	30	24
11	18	25	30	33	34	34	34	31	25
12	20	28	34	38	38	37	35	33	27

FIGURE 5-8 Vortex Search Array after 3-5 Spatial Averaging

spread, and skew; and the 1/2, 1, 1/2 beam integration; followed, in Figure 5-8, by the result of the 1/4, 1/2, 1, 1/2, 1/4 range gate integration. The highest-valued element in beam 4, range gate 7 is the estimated location of the vortex in range-angle space. This range-angle space location is then transformed to altitude-displacement space by using the antenna configuration geometry. A secondary peak also appears in beam 12, range gate 7. If this secondary peak were not excluded by the range-beam exclusion zone selection or the threshold level, it would be used as the second vortex location.

A second method for vortex location and tracking after the suggestion of D. Burnham of TSC was investigated in offline data analysis. This method utilizes the definition of vortex circulation as the line integral of the vortex flow field velocity around the closed path encompassing the vortex. Again the ratio of skew divided by intensity is taken as the measure of the vortex flow velocity in computing the line integral. The elements of a new matrix of skew/intensity are added in each beam for all range gates, as shown in Figure 5-9 for frame 25. The resulting signal sums are examined to identify the beam in which zero crossing occurs. This beam is taken as the angular location of the vortex core. The absolute value of the elements in each range gate are summed for all twelve beams and the highest valued range gate sum becomes the estimate of the vortex range. For this frame -- in which the vortex core is near the middle of the receiver sensitive volume -- these two methods yield similar results. However, Figure 5-10, which covers frame 17, shows a vortex location estimate for the line integral method, an estimate quite different from the result obtained by the first method.

One general conclusion emerges from the analysis of the two single-frame methods. The first method, which was implemented in the DAVSS operating system at the time of system demonstration, performs adequately when the vortex is wholly within the sensitive volume. It tends to misestimate the vortex position as being within the sensitive volume when, in fact, the vortex core has passed just outside. This characteristic may be acceptable for a vortex detection and warning system. For tracking and especially for data gathering for vortex behavior studies, it is not.

This unsatisfactory situation, however, was unduly aggravated by the incomplete tracking coverage applied in the JFK demonstration. This coverage had been chosen as a compromise to accomplish other objectives concurrently. The original tracking coverage, shown in Figure 5-11a, uses two transmitting and two receiving antennas with three ~36 deg gaps and four edges which cause tracking difficulties. By using all four transmitting and receiving antennas in the monostatic back-scatter Z-array, as shown in

Beam	Range Gate									Sum
	3	4	5	6	7	8	9	10	11	
1	78	79	76	67	63	50	33	31	25	502
2	46	57	54	53	50	44	35	32	33	404
3	7	21	22	32	37	38	35	33	32	257
4	-38	-28	-21	- 4	11	23	28	29	25	25
5	-50	-50	-49	-38	-26	- 8	3	13	19	-186
6	-30	-44	-51	-48	-39	-26	-15	0	7	-246
7	-11	-29	-33	-29	-25	-19	-13	- 8	- 5	-172
8	0	- 8	-18	-18	-16	-21	-15	- 8	- 5	-109
9	14	0	- 9	-15	-21	-24	-18	-13	- 8	- 94
10	17	22	20	0	-17	-21	-19	-14	- 9	- 21
11	14	30	31	23	7	- 6	-11	- 6	0	82
12	13	17	25	18	11	0	0	6	14	104
Sum	318	385	409	345	323	280	225	193	182	

FIGURE 5-9 Pseudo Doppler Array (Skew/Intensity) for Frame 25

Beam	Range Gate									Sum
	3	4	5	6	7	8	9	10	11	
1	55	53	59	63	69	63	58	48	50	518
2	47	48	54	59	64	62	59	55	57	505
3	40	45	52	59	63	61	59	59	57	495
4	38	39	46	52	56	58	56	57	52	454
5	36	47	48	56	59	59	58	53	52	468
6	38	36	41	52	56	58	55	50	50	436
7	40	33	40	52	58	63	58	55	52	451
8	44	45	50	59	68	66	58	53	46	489
9	33	38	50	45	50	50	47	45	37	395
10	29	11	10	0	13	24	35	39	35	196
11	20	0	-13	-21	-15	5	26	33	32	67
12	8	- 6	-26	-35	-35	6	11	25	20	- 32
Sum	428	401	489	553	606	575	580	572	540	

FIGURE 5-10 Pseudo Doppler Array (Skew/Intensity) for Frame 17

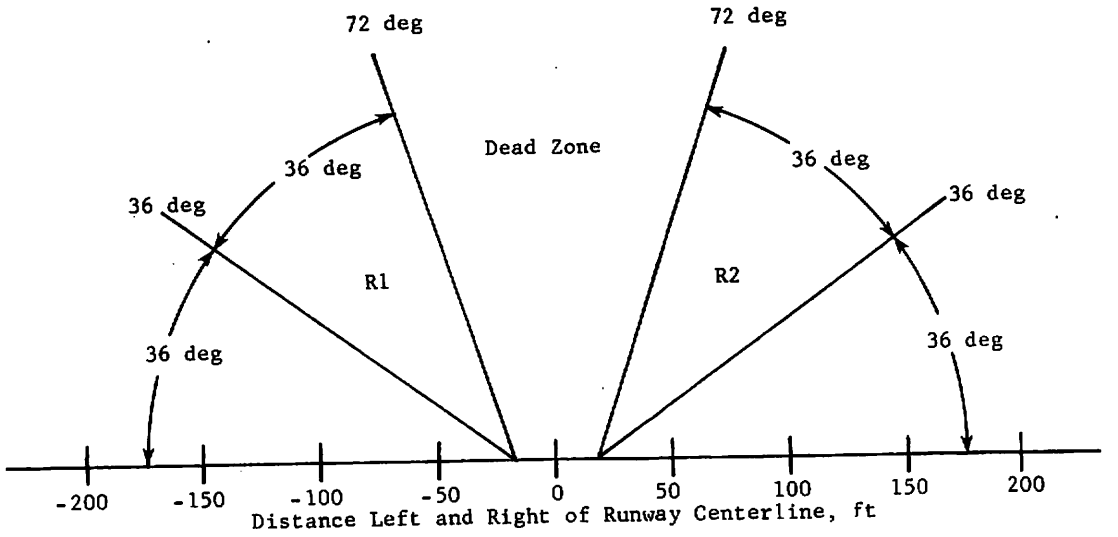

(a) Present Z-Array Coverage

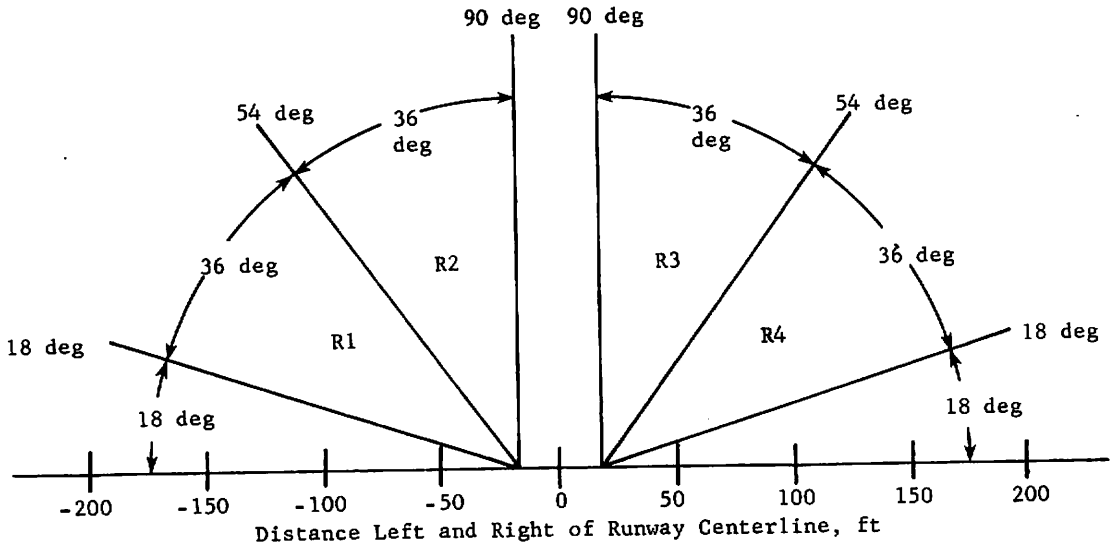

(b) Recommended Z-Array Coverage

FIGURE 5-11 Present and Recommended Monostatic Array Coverage

Figure 5-11b, continuous elevation coverage from -18 to +18 deg. could be achieved, thus leaving only two edges at low altitude.

Following the demonstration and data analysis this full coverage configuration was recommended to TSC as a system modification. Its implementation alone was sufficient to substantially improve the real time tracking accuracy of the DAVSS operating system. Left/right identification was improved as well and for the same reason. Since both vortex cores remain in the single sensitive volume for almost all tracking situations, left/right identification can be made by the relative position of the two vortices. These results are further discussed in Section 6 which outlines these post-demonstration modifications.

The offline application of the line integral method of vortex detection and tracking through estimating its total circulation was promising enough to justify modification of the DAVSS detection and tracking algorithms to incorporate some features of this method. The description and results of this algorithm modification are presented in Section 7.

6. CHANGES AFTER FIELD DEMONSTRATION

As a result of the field demonstration of the DAVSS detecting and tracking performance, a contract extension was granted to use the elements of the bistatic forward scatter Y-array to augment the monostatic backscatter Z-array and to perform the hardware and software modifications required to fully utilize this full-coverage centerline array. The following paragraphs detail these changes and the resulting improvement in tracking performance.

6.1 HARDWARE CHANGES

As part of this effort the following logistical and hardware changes have been performed:

a. Relocate the transmitter, receiver, and amplifier elements of the bistatic array in an augmented monostatic backscatter array configuration.

b. Relocate two AC power distribution points from stations 1 and 2 of the bistatic array to the monostatic array location.

c. Install and checkout a patch panel to accommodate the forty-eight (48) beam augmented monostatic array in the twenty-four (24) analog signal processor channels.

d. Install additional Coustex^{TM} acoustical absorbing material at the back of the receiving antenna reflectors to provide additional rear-lobe noise suppression for the two low-angle receiver assemblies.

6.1.1 Relocation of Transmitters, Receivers, and Amplifiers

The initial monostatic backscatter array consisted of two transmitting antenna assemblies, two receiving antenna assemblies, and the associated amplifiers, power source and cabling, and signal cabling required to provide the coverage shown in Figure 6-1(a). This coverage had been selected to make use of the available hardware and to prove the feasibility of the centerline monostatic backscatter array while yet allowing the other array to be used for demonstration of bistatic forward scatter operation. Monostatic backscatter feasibility had been demonstrated in the initial field operation of the DAVSS at JFK. Thereafter, more extensive coverage was desired by making use of all the DAVSS hardware to form an augmented monostatic backscatter array. Its coverage is shown in Figure 6-1(b).

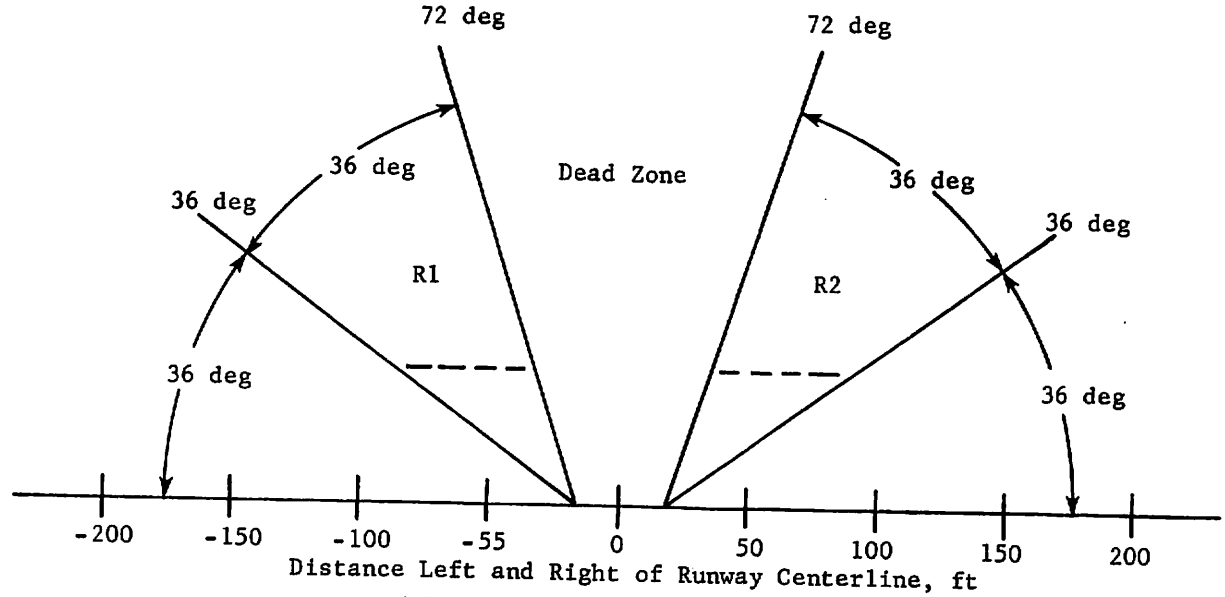

(a) Initial Z-Array Coverage

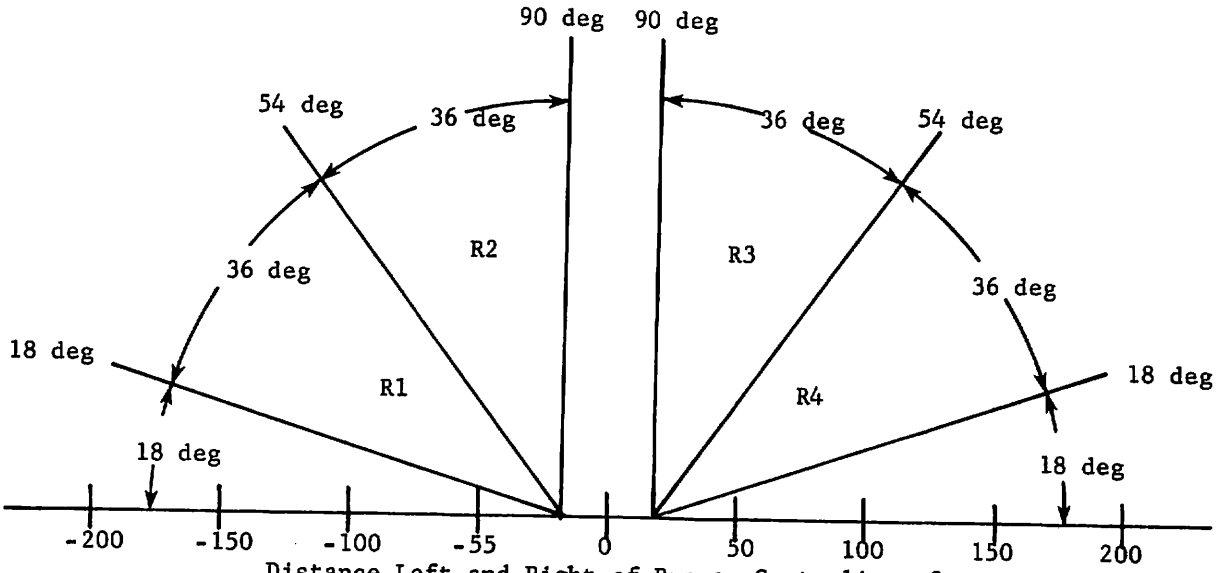

(b) Augmented Z-Array Coverage

FIGURE 6-1 Initial and Augmented Monostatic Backscatter-Array Coverages

Consequently, the two transmitting antenna assemblies, the two receiving antenna assemblies, the two field equipment shelters, and associated cabling which formerly comprised the bistatic array were relocated in a line alongside the original monostatic backscatter array. The elevation angles of the original antenna assemblies were raised to 72 deg. above the horizon and the elevation angles of the new antenna assemblies were set at 36 deg. as shown in Figure 6-1(b). Figure 6-2 is a photograph of the augmented monostatic backscatter array.

6.1.2 Relocation of Two AC Power Distribution Points

Two AC power distribution points were previously located at station 1 and station 2 of the bistatic array. As part of the formation of the augmented monostatic backscatter array, the two AC power distribution points were relocated within the monostatic backscatter array to provide AC power to the transmitter power amplifiers. The receiver power supplies are all powered by the third AC power distribution point which remains in the center of the monostatic backscatter array.

6.1.3 Installation and Checkout of the Beam/Processor Patch Panel (48/24)

The augmented monostatic backscatter array contains four (4) receiving antenna assemblies, each of which contains 12 pencil beams. Hence, forty-eight (48) 3-deg. pencil beams which cover elevation angles from 18 deg. above one horizon to 18 deg. above the other horizon are available to be processed in the twenty-four (24) analog signal processor boards. A patch panel which allows a choice of three normal mode configuration options by use of simple jumpers was designed, fabricated, installed, and checked out. These three options are: the selection of odd alternate beams, the selection of even alternate beams, or the selection of 24 pairs of summed adjacent beams which form 6-deg. beams. In any case, the beam spacing is 6 deg. but the beam width is either 3 deg. or 6 deg.

Figure 6-3 is a schematic diagram of the beam/processor patch panel inserted between the isolation module and the configuration control module.

Table 6-1 lists the microphone elevation angles and processor beam numbers for each of the three configuration modes.

6.1.4 Installation of Additional Acoustical Absorbing Material

Two of the receiving antenna assemblies in the augmented monostatic backscatter array are positioned with elevation angles of

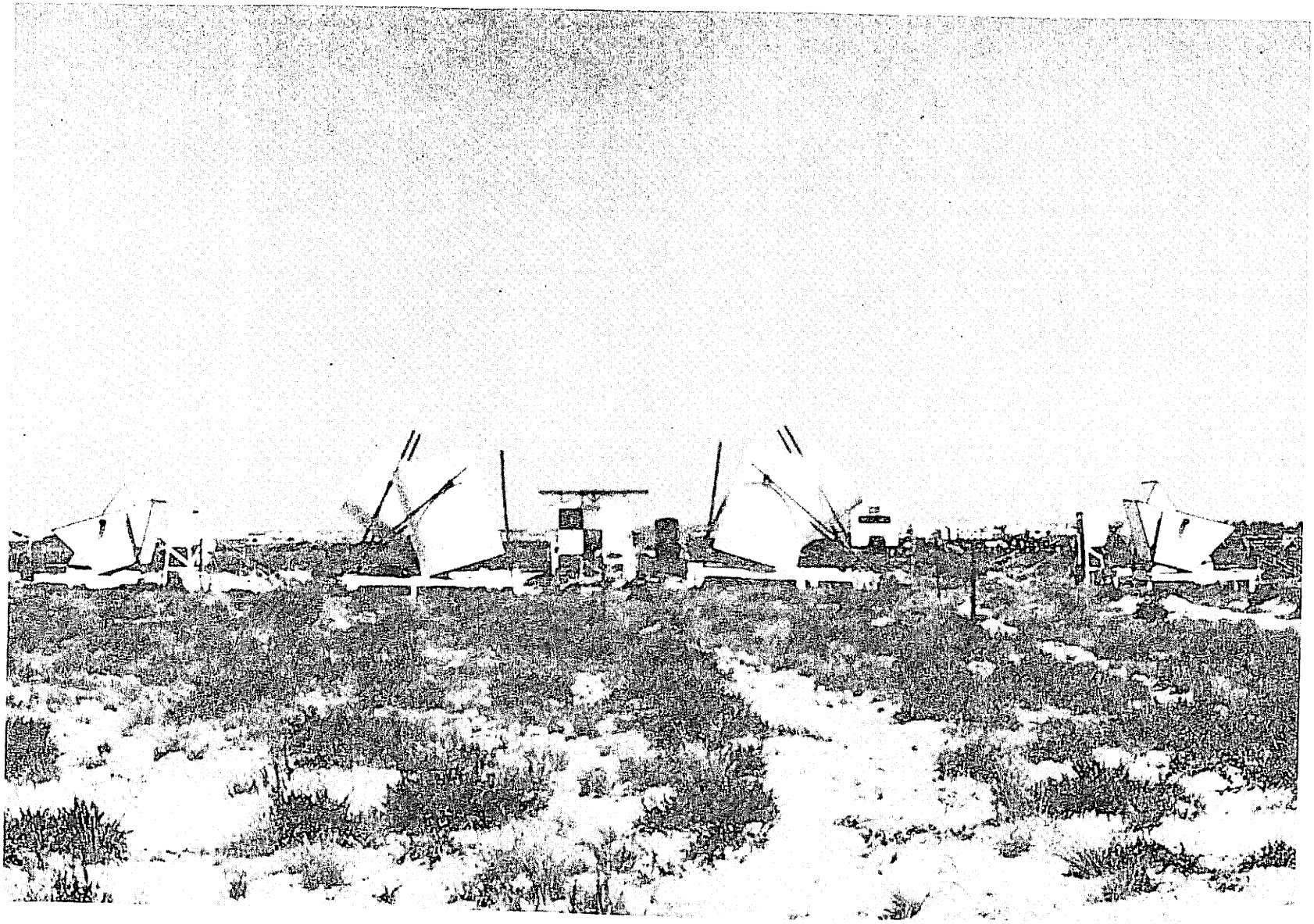

FIGURE 6-2 Augmented Monostatic Backscatter Array

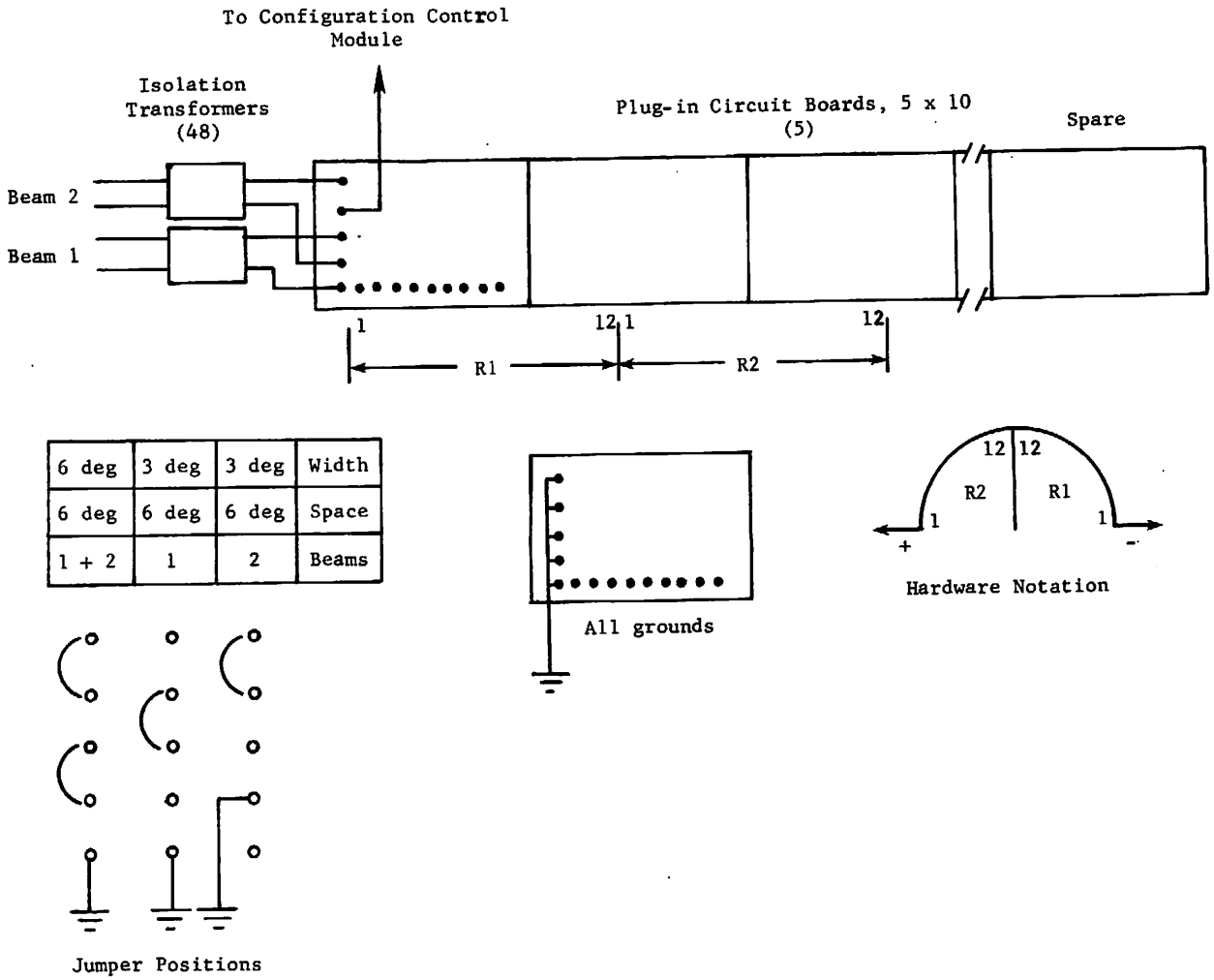

FIGURE 6-3 Schematic Diagram, 48/24 Beam/Processor Patch Panel

TABLE 6-1

PROCESSOR -- BEAM CONFIGURATIONS

Channel	Combined		Odd Beams		Even Beams	
	Beam No.	Elevation Angle	Beam No.	Elevation Angle	Beam No.	Elevation Angle
		deg.		deg.		deg.
1	LL 1,2	21	LL 1	19.5	LL 2	22.5
2	LL 3,4	27	LL 3	25.5	LL 4	28.5
3	LL 5,6	33	LL 5	31.5	LL 6	34.5
4	LL 7,8	39	LL 7	37.5	LL 8	40.5
5	LL 9,10	45	LL 9	43.5	LL 10	46.5
6	LL 11,12	51	LL 11	49.5	LL 12	52.5
7	LH 1,2	57	LH 1	55.5	LH 2	58.5
8	LH 3,4	63	LH 3	61.5	LH 4	64.5
9	LH 5,6	69	LH 5	67.5	LH 6	70.5
10	LH 7,8	75	LH 7	73.5	LH 8	76.5
11	LH 9,10	81	LH 9	79.5	LH 10	82.5
12	LH 11,12	87	LH 11	85.5	LH 12	88.5
13	RH 11,12	87	RH 11	85.5	RH 12	88.5
14	RH 9,10	81	RH 9	79.5	RH 10	82.5
15	RH 7,8	75	RH 7	73.5	RH 8	76.5
16	RH 5,6	69	RH 5	67.5	RH 6	70.5
17	RH 3,4	63	RH 3	61.5	RH 4	64.5
18	RH 1,2	57	RH 1	55.5	RH 2	58.5
19	RL 11,12	51	RL 11	49.5	RL 12	52.5
20	RL 9,10	45	RL 9	43.5	RL 10	46.5
21	RL 7,8	39	RL 7	37.5	RL 8	40.5
22	RL 5,6	33	RL 5	31.5	RL 6	34.5
23	RL 3,4	27	RL 3	25.5	RL 4	28.5
24	RL 1,2	21	RL 1	19.5	RL 2	22.5

36 deg. above the horizon. To further reduce the rear lobe response of these antennas to the relatively large noise sources on the horizon, Coustex™ acoustical absorbing material was mounted on the back (outside) of the parabolic reflector dishes of these two antenna assemblies. Although no meaningful comparative measurements could be made in the field, it seemed that this reduced the background noise in these lower beams while making good use of the left-over material.

6.2 SOFTWARE CHANGES

The major software changes implemented herein were designed to enable processing of the augmented monostatic backscatter array data as if it were from one continuous array. They consisted of changes to the matrix formation, the ordering of the antenna beams within the matrix, the tracking geometry, and the display formats.

In the previously developed DAVSS operating modes, each receiving antenna assembly (12 beams) constituted one detection space; and a separate range/angle matrix was formed for each set of twelve beams. To achieve best use of the augmented array coverage and to eliminate unnecessary edge effects, it was most desirable to combine the processed outputs of all 24 beams into a single range/angle matrix.

In addition, since the previous beam numbering was from low angle to high angle, the order in which the beams from R2 are read into the matrix had to be reversed i.e., R2-12 becomes R13, R2-11 becomes R-14, etc., until R2-1 becomes R-24. This was necessary to make the matrix continuous in angle.

The tracking geometry was altered to use angle estimates from 18 to 162 deg. rather than two separate calculations from 18 to 90 deg. for each side of the runway.

The diagnostic discriminant displays had to be modified to present the three 24-beam arrays of intensity, spread, and skew, respectively, rather than the two sets of 3 to 12 beam arrays of intensity, spread, and skew as before.

With these changes accomplished, the augmented monostatic backscatter array was ready for evaluation using the same detection and tracking algorithm reported in the initial contract.

6.3 AUGMENTED MONOSTATIC BACKSCATTER DATA

Limited data was acquired in the augmented monostatic backscatter mode under relatively good meteorological conditions in June 1975. The winds were gentle and the crosswind component was variable

throughout the data sample. The data was taken using combined 6 deg. beams at 6 deg. increments from 21 to 159 deg.

Figures 6-4 through 6-8 show Versatec printer-plotter displays of the processing parameters and the resulting vortex detecting and tracking data using the previously developed detecting and tracking algorithms.

Although the data looks promising, it still suffers from tracking algorithm difficulties -- notably the left/right identification problem and what appears to be consistent but non-optimum vortex location choices or biases.

The following section deals with further algorithm development, a development which successfully handles these difficulties.

D.A.V.S.S. PROCESSING PARAMETERS - RUN 2 - PAGE 1

A = MODE (M,P) - PLOT TIME (1,2,3 MIN)	D	2
B = AUTO START - AUTO STOP (E,D)	D	D
C = DISPLAY MODE (GT-40) (VERS)	P	ff Line
D = RANGE MIN - MAX (NSEC)	90	500
E = R. GRAN. (MS) - S. AV. B-R (1,3-1,3,5)	13	3-5
F = CENTER FILTER OFFSET (HZ)	75	75
G = MIDDLE FILTER OFFSET (HZ)	150	150
H = OUTER FILTER OFFSET (HZ)	225	225
I = CENTER FILTER WIDTH (-20 HZ)	2	2
J = MIDDLE FILTER WIDTH (-20 HZ)	3	3
K = OUTER FILTER WIDTH (-20 HZ)	4	4
L = NOTCH FILTER WIDTH (50 HZ)	2	2
M = CENTER DISC. GAIN (%)	20	20
N = MIDDLE DISC. GAIN (%)	50	50
O = OUTER DISC. GAIN (%)	100	100
P = DIAG. DISPLAY LIMITS - LOWER, UPPER (%)	10	90
Q = EXCLUSION ZONE - RANGE, BEAM	7	4
R = THRESHOLDS - NOISE MULTIPLIER, A/C NOISE	2.3	0.8
S = MIN. AND MAX. ALTITUDE (ELEMENT 1)	40.0	150
T = MIN. AND MAX. ALTITUDE (ELEMENT 2)	40.0	150

D.A.V.S.S. PROCESSING PARAMETERS - RUN 2 - PAGE 2

A = ACTIVE ARRAY - PROCESSING MODE	Z	BA
B = ACTIVE STATIONS - FRAME LENGTH (MSEC)	B	900
C = AIRPORT CODE - TAPE NUMBER	K	1
D = WIND (FT/SEC) - REL HUM (%)	0.	50.
E = TEMP (DEG F) - DAY OF YEAR	34.0	001:09:05:42
F = RAMP MIN GAIN (%)	1	1
G = RAMP MAX GAIN (%)	100	100
H = RAMP START (MSEC)	90	90
I = RAMP STOP (MSEC)	600	600
J = PULSE RISE TIME (10 MSEC)	2	2
K = PULSE DURATION (MSEC)	15	15
L = RECEIVED FREQUENCY (HZ)	3333	3333
M = ARRAY Y TRANS. POSITION (FT)	-450.0	450.0
N = ARRAY Y RECV. POSITION (FT)	-500.0	500.0
O = ARRAY Y RECV. ANGLE (DEG)	22.5	-22.5
P = ARRAY Z TRANS. POSITION (FT)	-35.0	37.0
Q = ARRAY Z RECV. POSITION (FT)	-10.0	12.0
R = ARRAY Z RECV. ANGLE (DEG)	-54.0	54.0

FIGURE 6-4 DAVSS Processing Parameters, Run 2, Pages 1 and 2

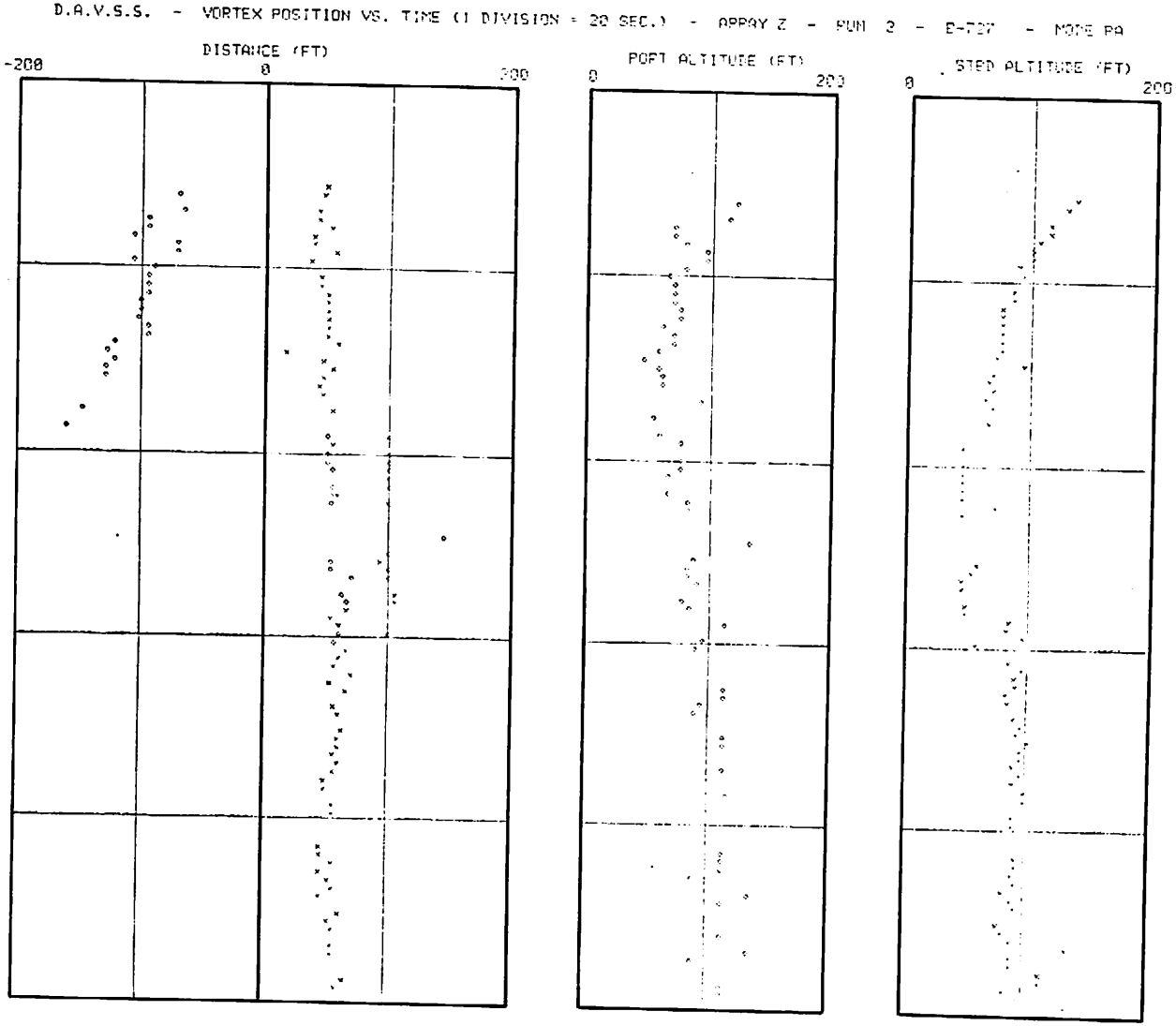

FIGURE 6-5 DAVSS, Vortex Position versus Time, Array Z, Run 2, B-727

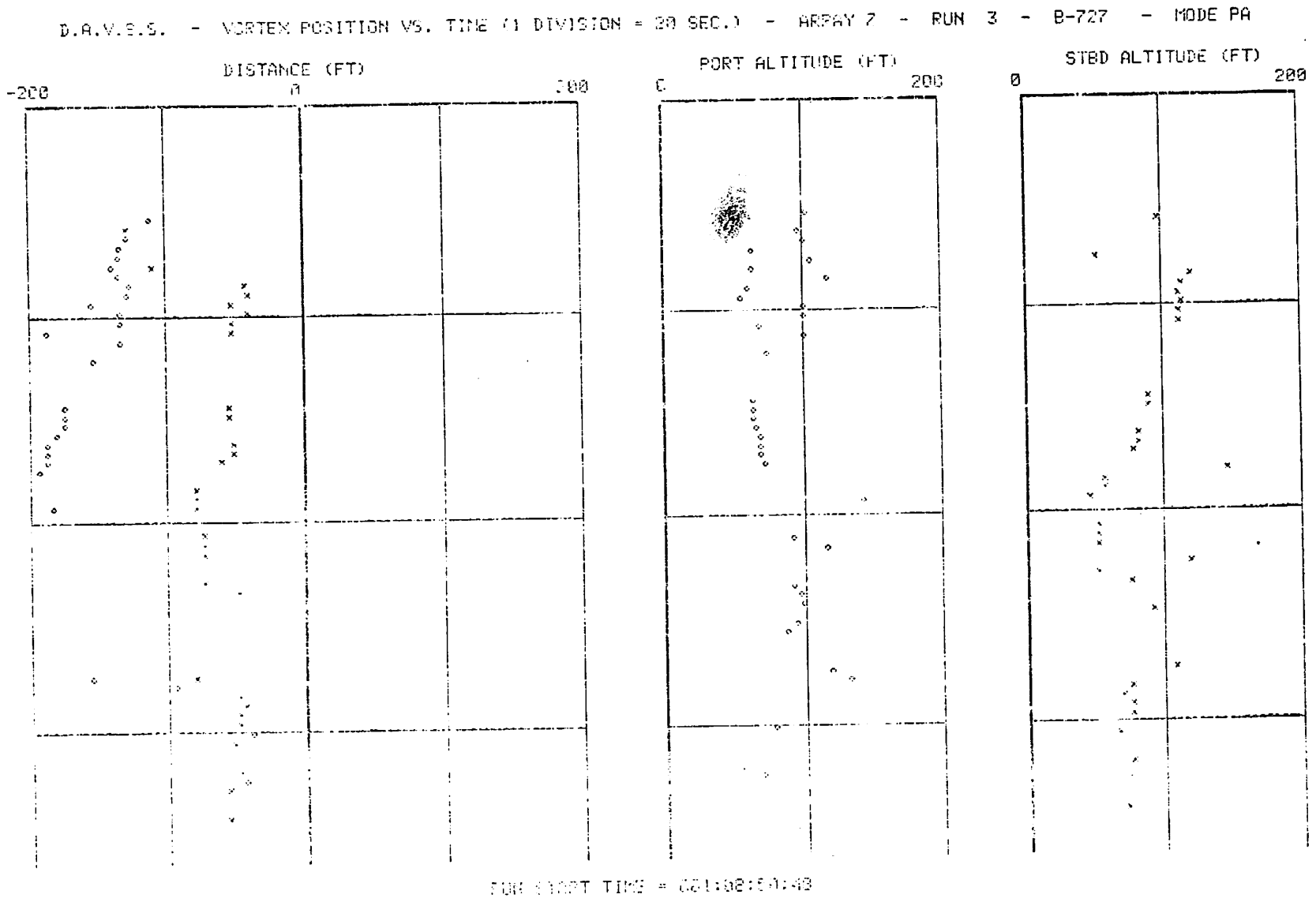

FIGURE 6-6 DAVSS, Vortex Position versus Time, Array Z, Run 3, B-727

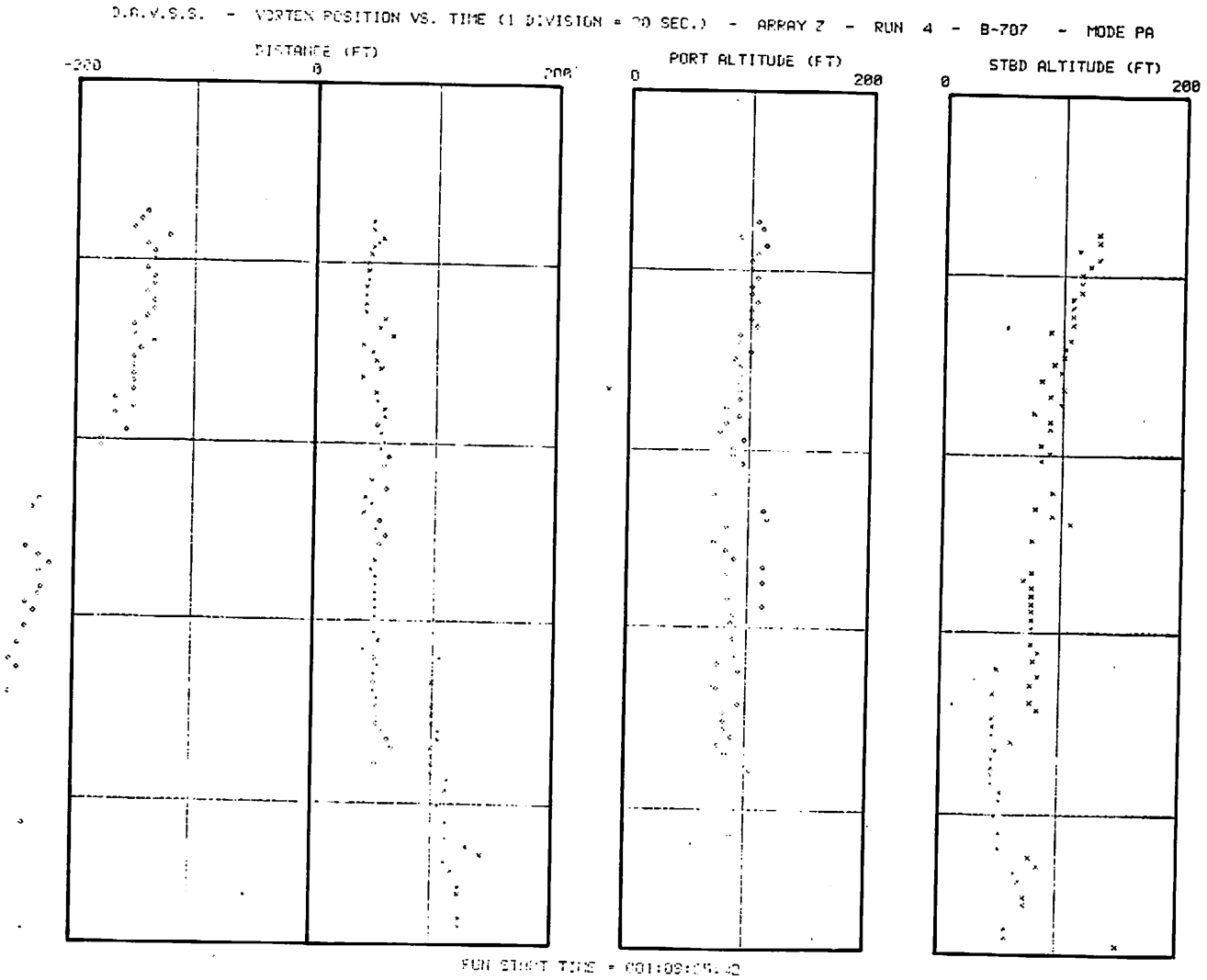

FIGURE 6-7 DAVSS, Vortex Position versus Time, Array Z, Run 4, B-707

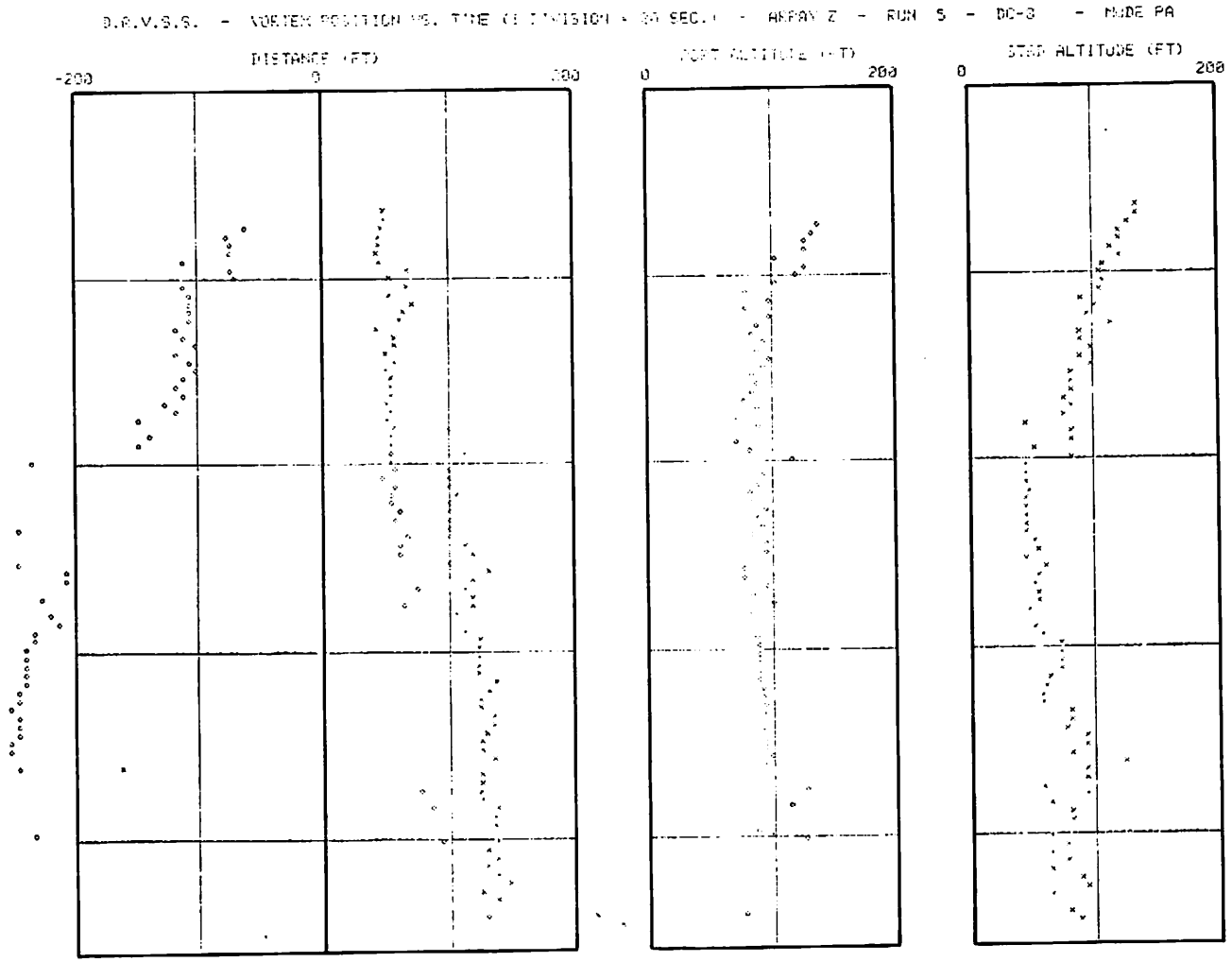

FIGURE 6-8 DAVSS, Vortex Position versus Time, Array Z, Run 5, DC-8

7. IMPROVED DETECTING AND TRACKING ALGORITHMS

7.1 BACKGROUND

Evaluation of the previous DAVSS data and the experience of TSC with its monostatic backscatter system have led to methods for improving the detecting and tracking performance of the DAVSS. This was accomplished by introducing a pseudo-circulation calculation into the tracking algorithm. The major change to the operating system has been to form a new discriminant which is the ratio of skew divided by intensity for each range-angle element in the matrix. This ratio is approximately proportional to the Doppler shift and is relatively insensitive to amplitude variations in the backscattered signals. This new discriminant, together with the data correlation used, is responsive to the principal characteristic of the vortex target -- its circulating air mass.

The remainder of this section describes the major software changes (Paragraph 7.2) and the resulting vortex tracking data (Paragraph 7.3).

7.2 SOFTWARE MODIFICATIONS

To implement the desired change in the DAVSS detecting and tracking algorithm, the following software tasks were performed.

a. Provide an option for reading digital diagnostic discriminant tapes as program input.

b. Provide a plotting program to display the scaled ratio of skew/intensity in each range gate for any beam.

c. Incorporate an improved vortex tracking algorithm in the DAVSS operating system.

These items are described in Paragraph 7.2.1 through 7.2.3.

7.2.1 Digital Diagnostic Discriminant Tape Program Input

An option had previously been provided which allowed digital diagnostic discriminant tape output to be written from real-time vortex detector data. This option was designed for offline data analysis and for digital data display on the Versatec printer/plotter. As part of the modification task, a subroutine was written to allow use of the same digital diagnostic discriminant tape as input to the vortex data processing routines. In this way, modifications to the data processing and algorithm operations can be evaluated and compared with other processing schemes and algorithms while using exactly the same source data.

7.2.2 Display of Skew/Intensity versus Range along Any Ray

As part of any evaluation of the feasibility of computing the vortex circulation, it is necessary to assess the capability of the DAVSS signal processor to yield reliable estimates of Doppler shifts to enable wind velocities to be computed. Consequently, an operating program was written for the DAVSS which provides a Versatec display of the scaled skew/intensity ratio for each range gate along any single beam. With this program the sensitivity of the processed skew/intensity ratio to signal amplitude and noise, and its linearity with respect to Doppler shift may be investigated.

The linearity over the range set by the frequency position of the innermost and outermost filters was checked. A known frequency was inserted into the processor and the output plot was compared with the input frequency curves. The result was linear within the limits of the frequency precision of the reference signal.

The sensitivity of the processor to acoustic noise in the airport environment has been investigated. A trace has been provided on the Versatec display of the signal intensity in the longest range gate (assumed to be noise). By comparing the relationship between this "noise" trace and the backscattered signal traces from the ambient wind, the level at which significant distortion of the skew/intensity ratio occurs -- a level that might be used as a noise rejection threshold -- has been noted.

Tests were also conducted with single frequency tones to determine the effect of signal amplitude on the linearity of the skew/intensity ratio. The linearity does not seem to be visibly altered for signal amplitudes within the non-saturating range of the processor.

To date, no tests have been conducted which compare the Doppler estimate from the skew/intensity ratio with actual spectra derived from high resolution spectral analysis of the complex signals that might be expected as a result of scattering from distributed wind velocities.

7.2.3 Improvement of the Vortex-tracking Algorithms

Problems encountered with the earlier detecting and tracking routine included left/right identification and the tendency of the algorithms to place a vortex within the sensitive volume when the vortex core was just outside and only part of the vortex could be sensed. This last problem was further complicated by the earlier monostatic backscatter configuration in which there were four edges to the two sensitive volumes. This difficulty was partly alleviated by forming the augmented monostatic backscatter array

with its single effective sensitive volume extending from 18 deg. above one horizon to 18 deg. above the other.

The formation of the one continuous volume instead of two volumes also partly alleviated the left/right identification problem since the relative positions of the two vortices (if there are two) uniquely identify them.

However, in consultation with TSC, it was concluded that further improvements in the tracking algorithm could be obtained by making use of the skew/intensity ratio as a measure of wind speed, and that wind speed could be used to sense vortex circulation. Further, by performing relatively simple correlations on the skew/intensity data, both the circulation center and sense (left or right) could be more reliably and accurately determined. The following is a brief description of the improved detecting and tracking algorithm which has been incorporated into the DAVSS operating system.

The three discriminant matrices (24 beams by 32 range gates) for intensity, spread, and skew are formed in range-angle space. Spatial averaging is performed on all three of these matrices. This is a keyboard option of 1, 3, or 5 range gates and 1 or 3 beams. The combination currently used for vortex processing is 1 and 5,that is, one beam and five range gates. The ratio skew/intensity is then formed for each spatially averaged range-beam element and the resulting skew/intensity matrix replaces the skew matrix as it is formed. (Elements in the skew/intensity matrix whose corresponding intensity is below a threshold value are set to zero.) Next a correlation is performed on all the elements of the matrix by moving a -1, 0, 1 slider across all beams in each range gate. The greatest negative result of this correlation are found from all the matrix elements. These two peaks -- one positive and one negative -- correspond to the center of the left and the center of the right circulating vortex respectively. These estimates are accepted as vortex locations if the absolute values of their correlation functions exceed a keyboard selectable value. Further resolution of the vortex position between beams is attained by making use of the slopes of the two line segments which make up the three correlation elements. The larger of the two slopes is chosen and the equivalent beam value of the zero crossing calculated. This non-integer beam value is that which is used as the final elevation angle for the vortex position calculations.

Paragraph 7.3 describes the detecting and tracking results of the application of this tracking algorithm to the June 1975 data.

7.3 DETECTING AND TRACKING RESULTS

The data of June 1975 presented in section 6 were written in real-time on a digital diagnostic discriminant tape. Using the subroutine described in Paragraph 7.2.1, this source tape was used for developing the improved detecting and tracking algorithm described in Paragraph 7.2.3. The following detecting and tracking results represent the final form of the detecting algorithm which has been incorporated in the DAVSS operating system.

Figure 7-1 presents the operating parameters for the DAVSS during data collection and data processing. These parameters represent the current recommendation for optimum data selections. The data presented in Figures 7-2 to 7-12 shows favorable results for all the types of aircraft seen in the data set (B727, B707, B747, and DC-8).

7.4 VORTEX CIRCULATION DETERMINATION ESTIMATION

As part of this task, the possibility of determine and recording the circulation of each vortex in real-time was studied. The work described in Paragraph 7.2.2 in which the skew/intensity ratio was displayed along a single ray versus time gave confidence to the possibility of calibrating the skew/intensity ratio as a Doppler shift for single tones. The work described in Paragraph 7.2.3, in which the skew/intensity ratio was used as the principal data element in the vortex detecting and tracking algorithm, furthered that confidence.

However, several items would have to be investigated further before real time implementation of a quantitative circulation determination in the DAVSS operating system. These include:

a. Investigation of the DAVSS processor skew/intensity ratio calibration for distributed spectral signals.

b. Investigation of the effect of spectral averaging prior to taking the ratio of skew/intensity.

c. Determination of the optimum method of taking the line integral around the vortex to compute the circulation.

d. Defining methods of calibration and display of the calculated circulation for each vortex.

Avco/SD is confident that a relative circulation determination can be computed and that an empirical determination of useful threshold values of this relative quantity could be used to key the vortex track symbols shown on the displays. There is less confidence at

D.A.V.S.S. PROCESSING PARAMETERS - RUN 1 - PAGE 1

A = MODE (R,P) - PLOT TIME (1,2,3 MIN)	D	2
B = AUTO START - AUTO STOP (E,D)	E	E
C = DISPLAY MODE (GT-40) (VERS)	P	P
D = RANGE MIN - MAX (MSEC)	90	500
E = R. GRAN. (MS) - S. AV. B-R (1,3-1,3,5)	13	1-5
F = CENTER FILTER OFFSET (HZ)	75	75
G = MIDDLE FILTER OFFSET (HZ)	150	150
H = OUTER FILTER OFFSET (HZ)	225	225
I = CENTER FILTER WIDTH (-20 HZ)	2	2
J = MIDDLE FILTER WIDTH (-20 HZ)	3	3
K = OUTER FILTER WIDTH (-20 HZ)	4	4
L = NOTCH FILTER WIDTH (50 HZ)	2	2
M = CENTER DISC. GAIN (%)	20	20
N = MIDDLE DISC. GAIN (%)	50	50
O = OUTER DISC. GAIN (%)	100	100
P = DIAG. DISPLAY LIMITS - LOWER, UPPER (%)	10	90
Q = SLOPE THRESHOLDS STAT. - DYN.	40	4.0
R = MIN. INTENSITY - A/C NOISE	16	0.5
S = MIN. AND MAX. ALTITUDE (ELEMENT 1)	40.0	200.0
T = MIN. AND MAX. ALTITUDE (ELEMENT 2)	40.0	200.0

D.A.V.S.S. PROCESSING PARAMETERS - RUN 1 - PAGE 2

A = ACTIVE ARRAY - PROCESSING MODE	Z	BA
B = ACTIVE STATIONS - FRAME LENGTH (MSEC)	B	900
C = AIRPORT CODE - TAPE NUMBER	K	1
D = WIND (FT/SEC) - REL HUM (%)	0.	50.
E = TEMP (DEG F) - DAY OF YEAR	34.0	001
F = RAMP MIN GAIN (%)	1	1
G = RAMP MAX GAIN (%)	100	100
H = RAMP START (MSEC)	90	90
I = RAMP STOP (MSEC)	600	600
J = PULSE RISE TIME (10 MSEC)	2	2
K = PULSE DURATION (MSEC)	15	15
L = RECEIVED FREQUENCY (HZ)	3333	3333
M = ARRAY Y TRANS. POSITION (FT)	-450.0	450.0
N = ARRAY Y RECV. POSITION (FT)	-500.0	500.0
O = ARRAY Y RECV. ANGLE (DEG)	22.5	-22.5
P = ARRAY Z TRANS. POSITION (FT)	-35.0	37.0
Q = ARRAY Z RECV. POSITION (FT)	-10.0	12.0
R = ARRAY Z RECV. ANGLE (DEG)	-54.0	54.0

FIGURE 7-1 DAVSS Processing Parameters, Run 1, Pages 1 and 2

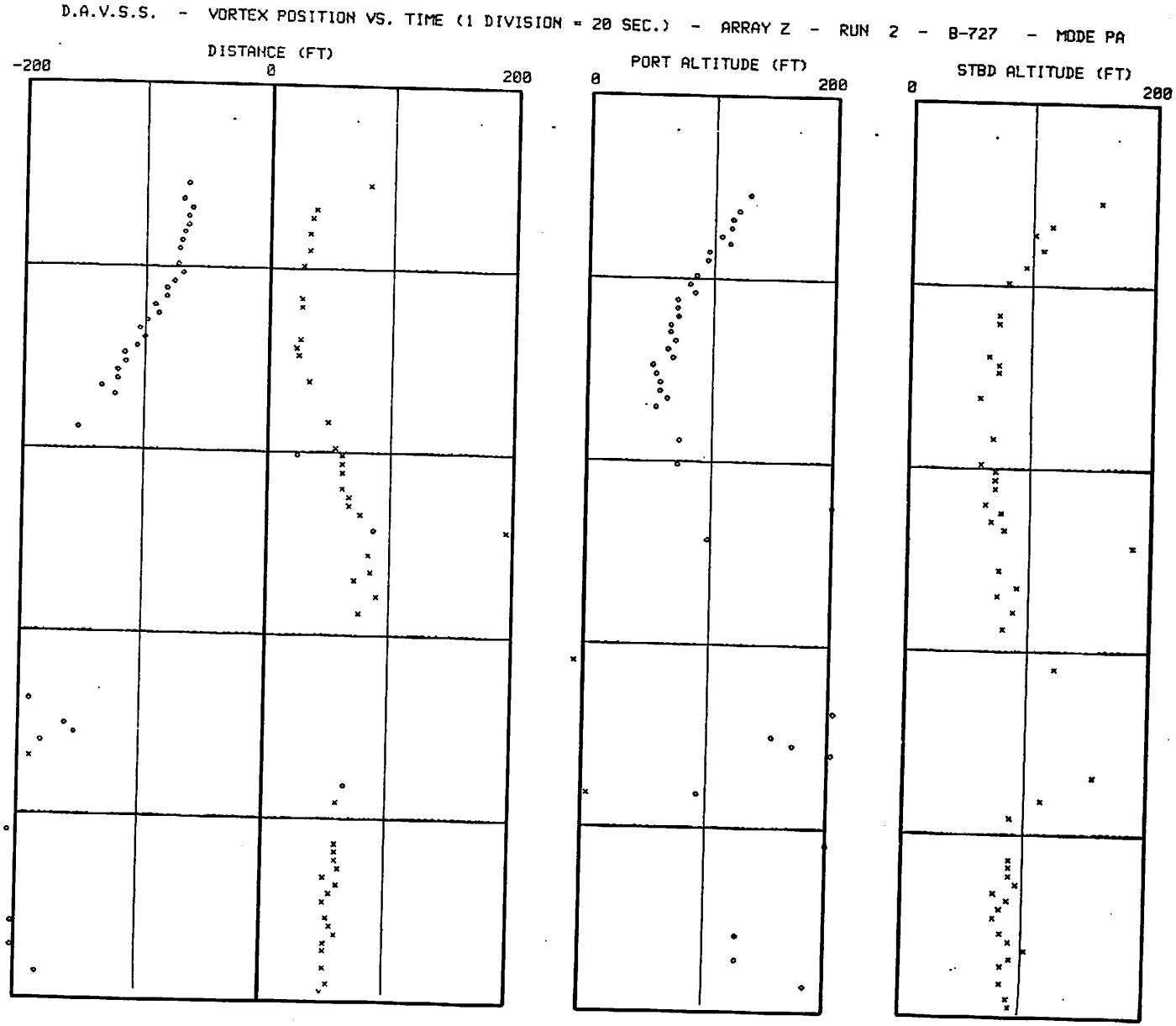

FIGURE 7-2 DAVSS, Vortex Position versus Time, Array Z, Run 2, B-727

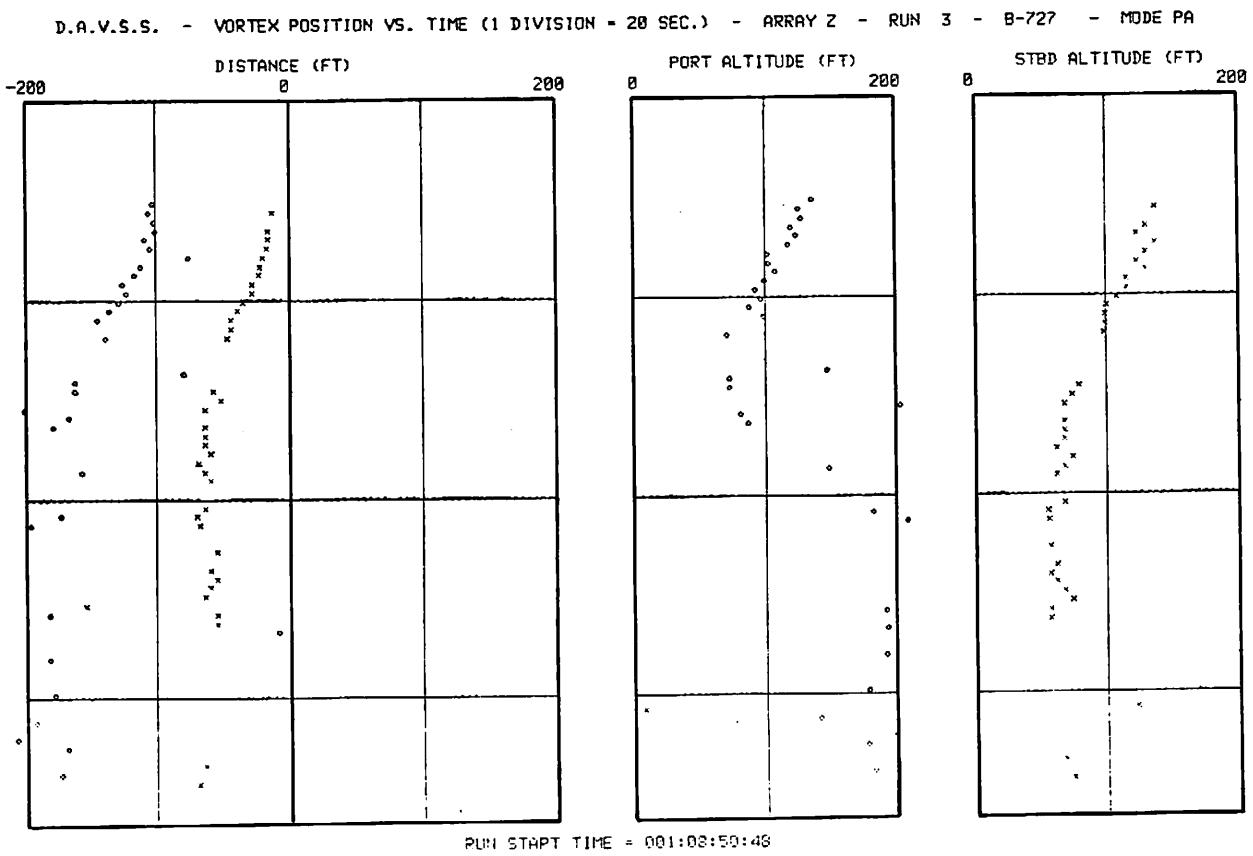

FIGURE 7-3 DAVSS, Vortex Position versus Time, Array Z, Run 3, B-727

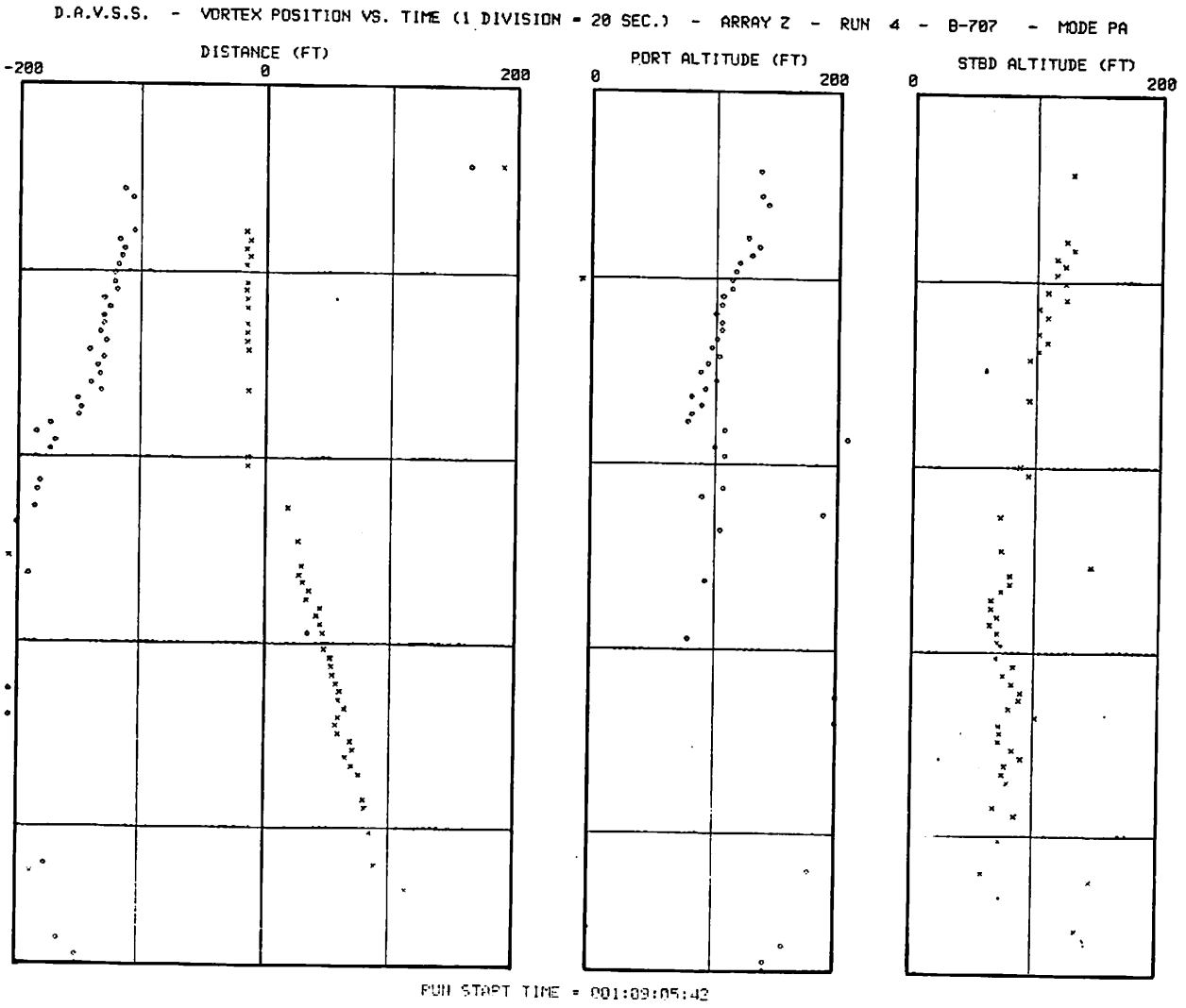

FIGURE 7-4 DAVSS, Vortex Position versus Time, Array Z, Run 4, B-707

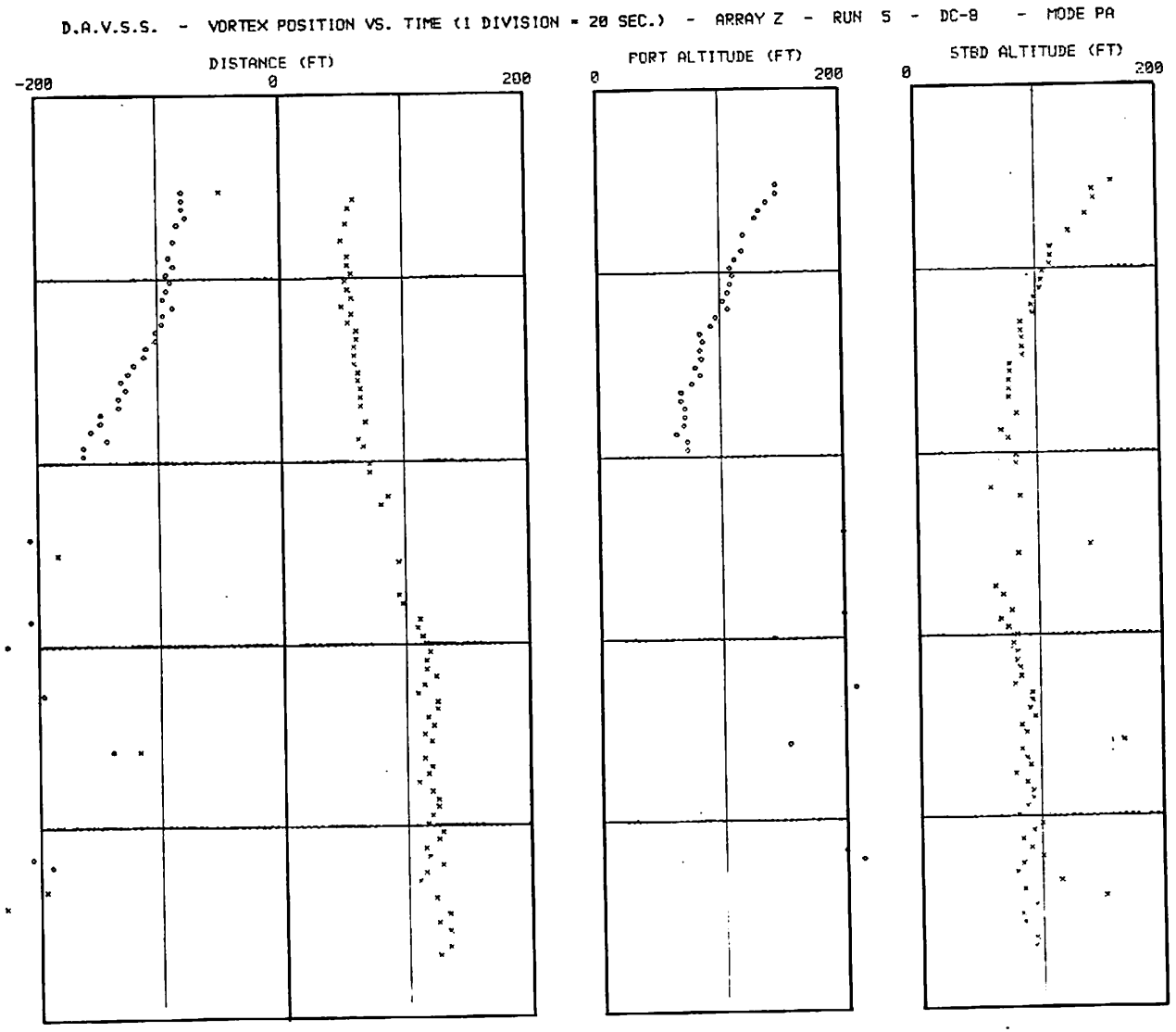

FIGURE 7-5 DAVSS, Vortex Position versus Time, Array Z, Run 5, DC-8

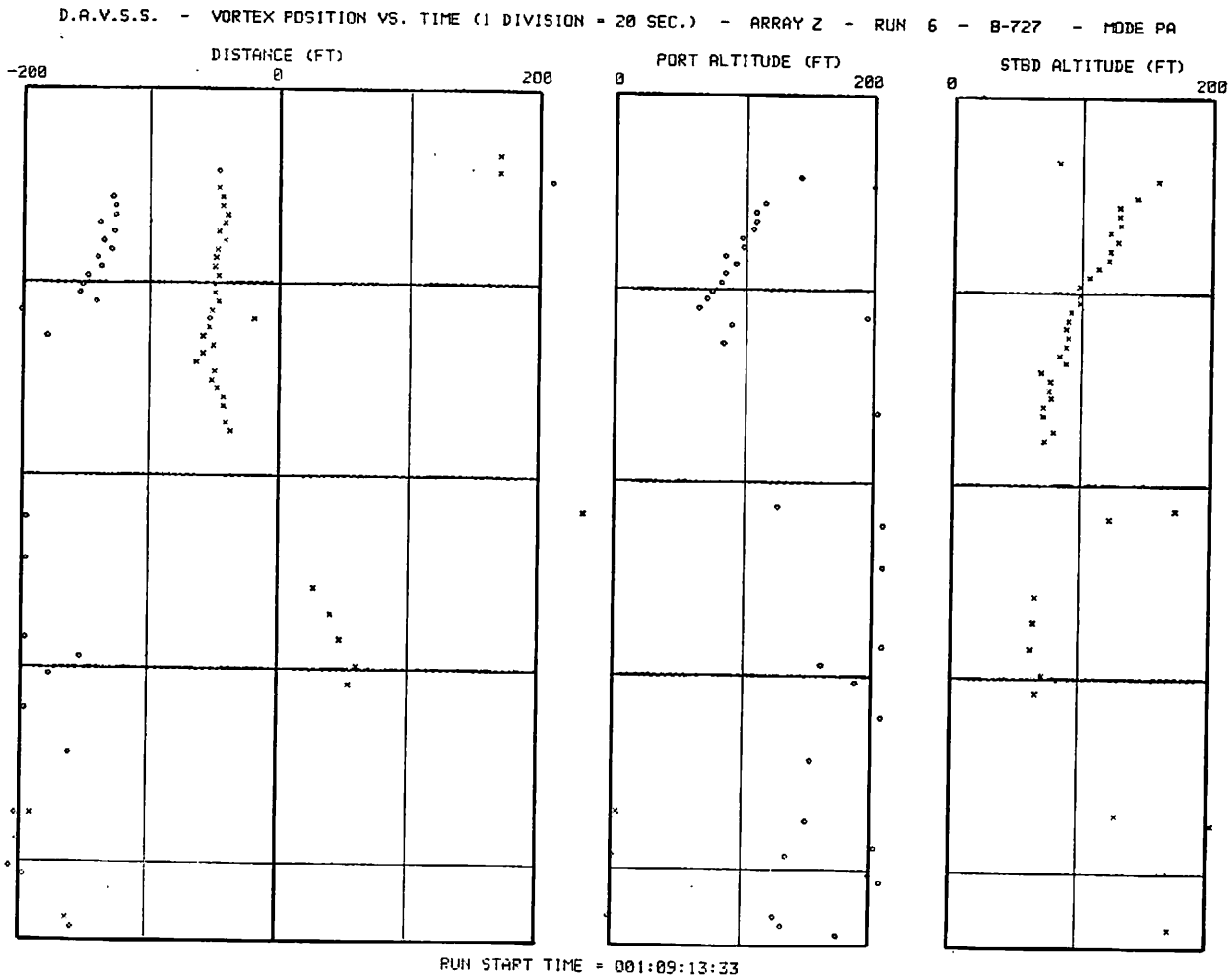

FIGURE 7-6 DAVSS, Vortex Position versus Time, Array Z, Run 6, B-727

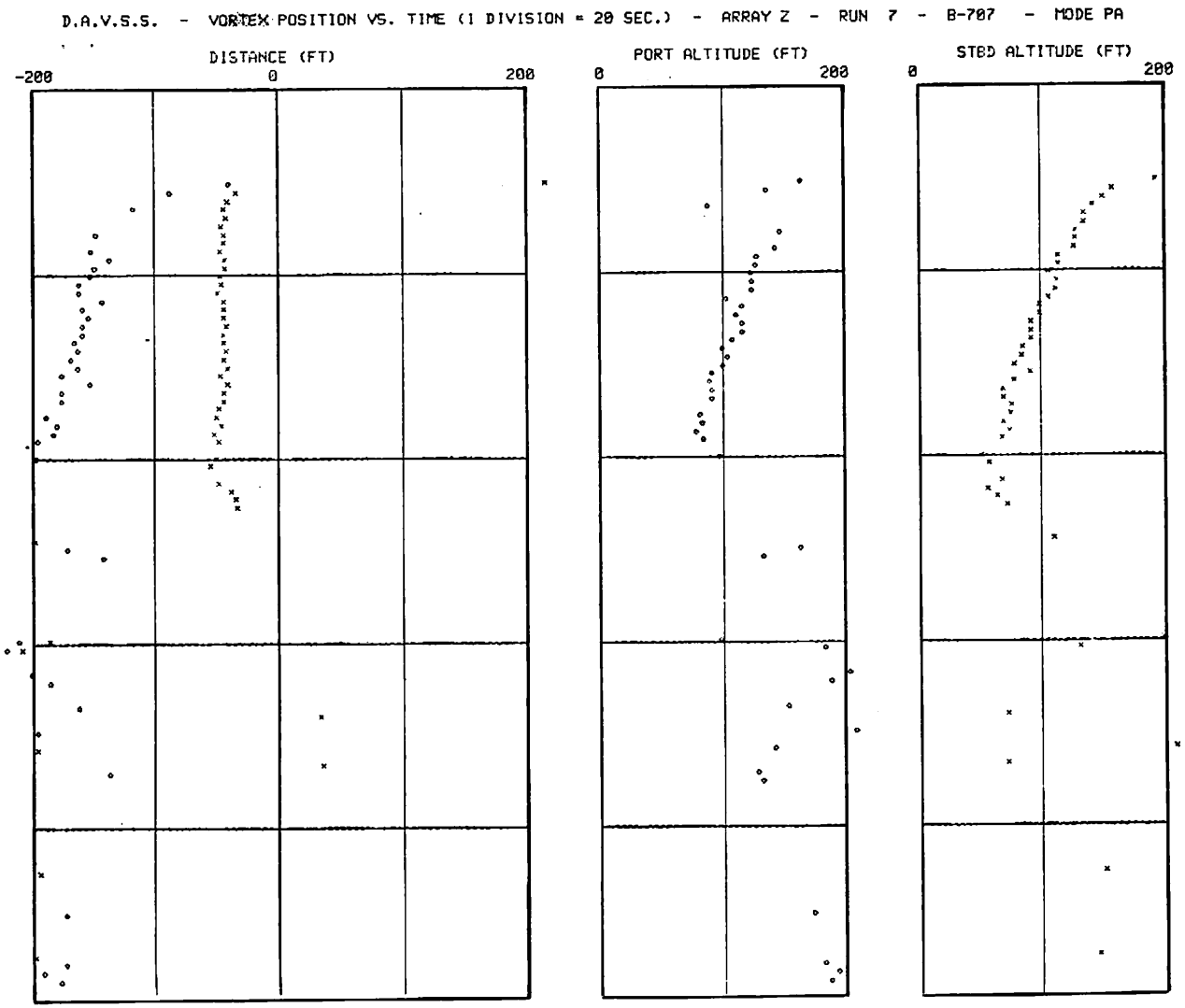

FIGURE 7-7 DAVSS, Vortex Position versus Time, Array Z, Run 7, B-707

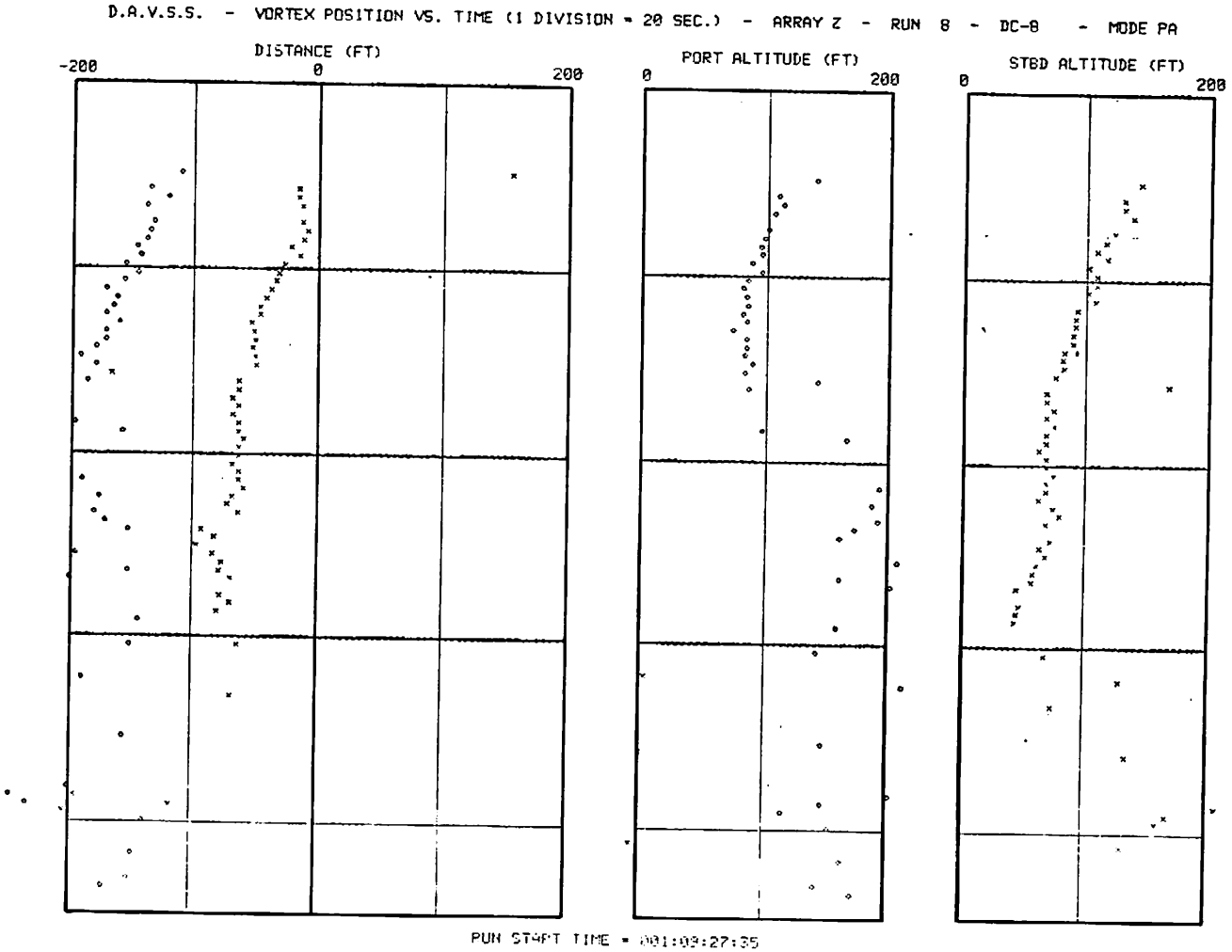

FIGURE 7-8 DAVSS, Vortex Position versus Time, Array Z, Run 8, DC-8

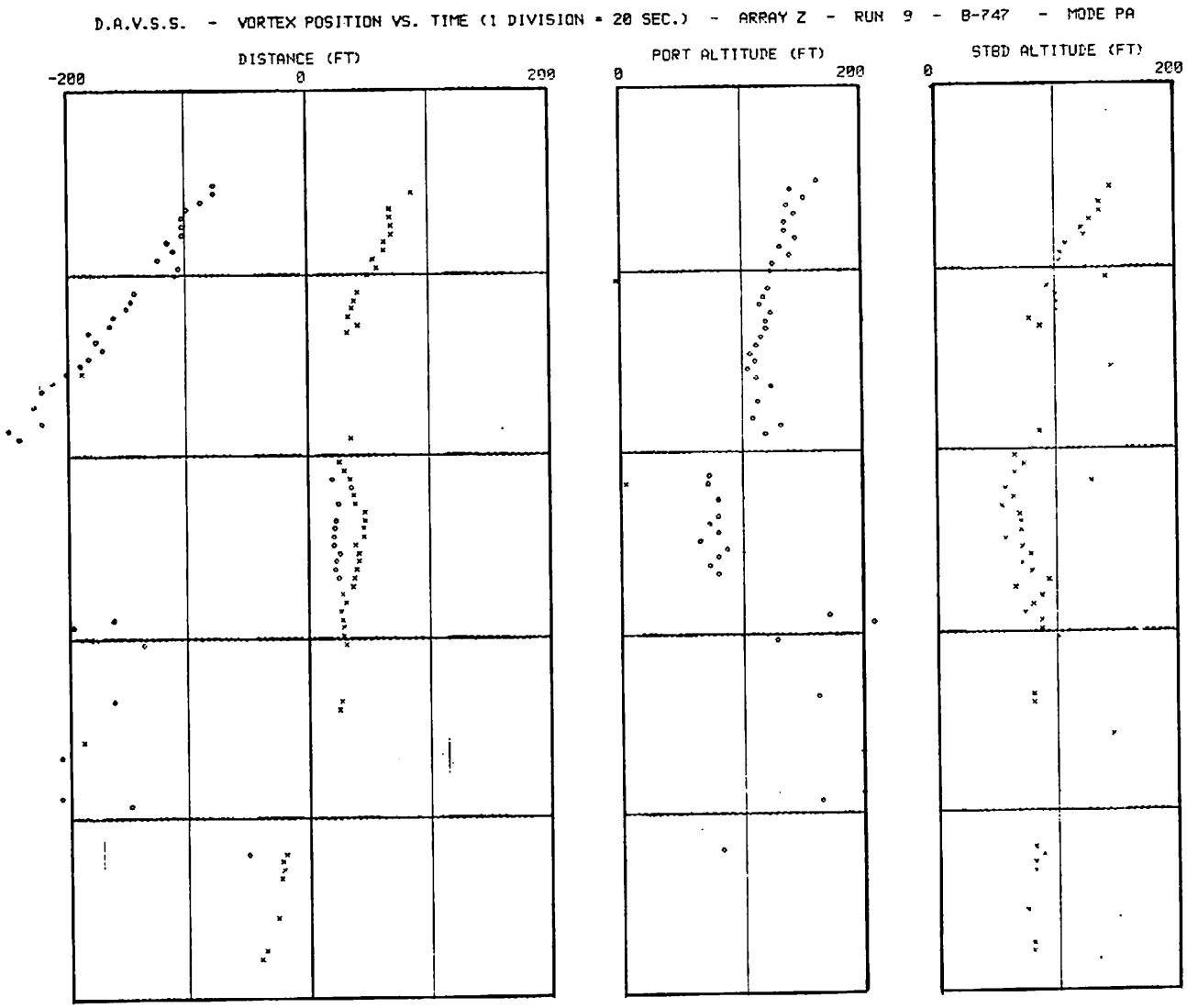

FIGURE 7-9 DAVSS, Vortex Position versus Time, Array Z, Run 9, B-747

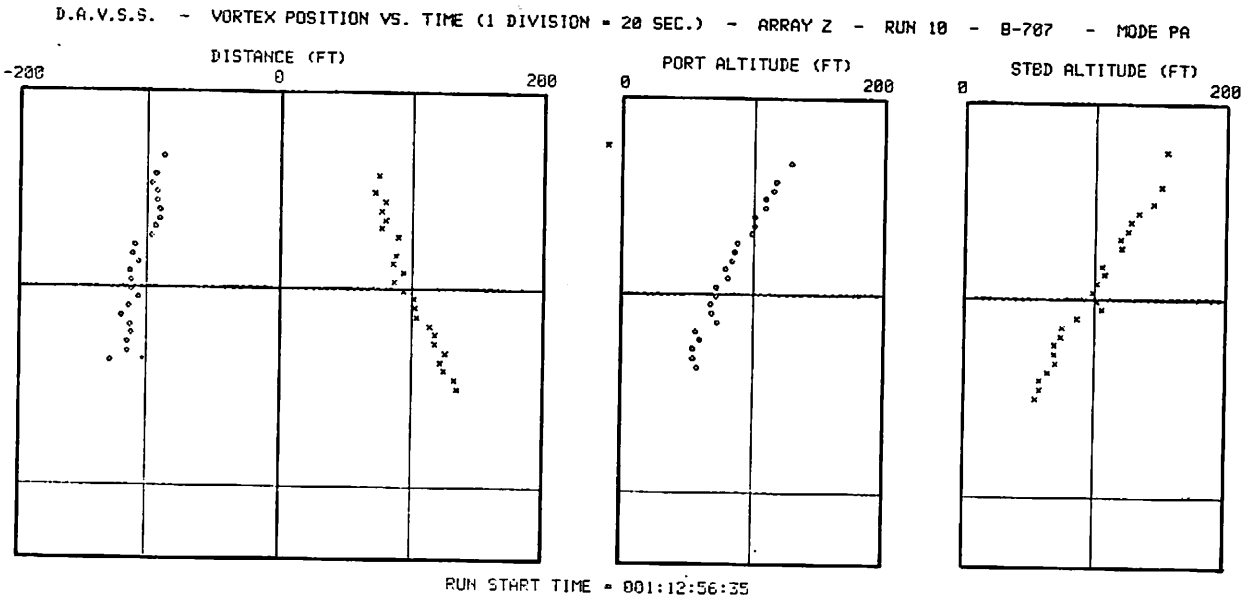

FIGURE 7-10 DAVSS, Vortex Position versus Time, Array Z, Run 10, B-707

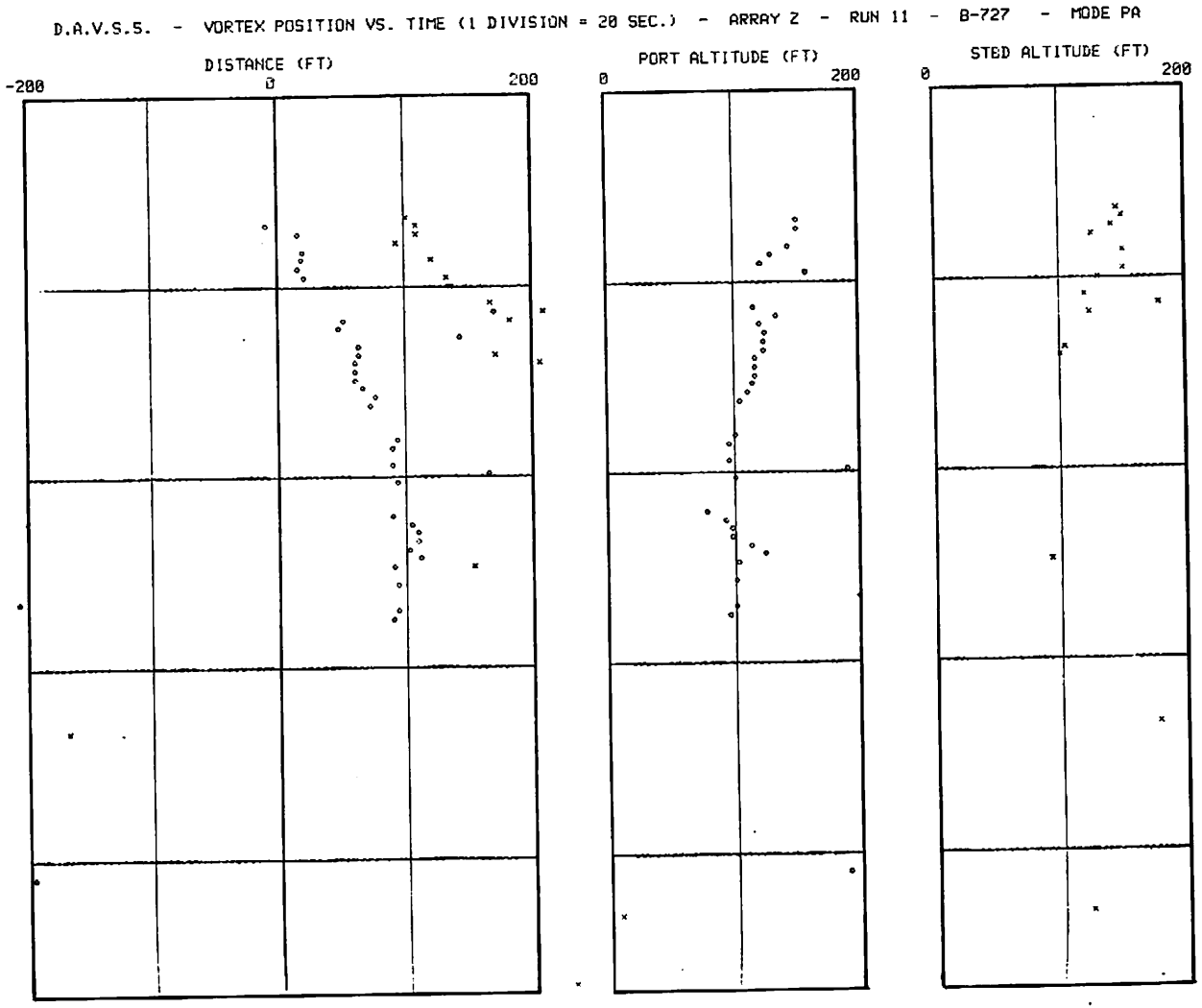

FIGURE 7-11 DAVSS, Vortex Position versus Time, Array Z, Run 11, B-727

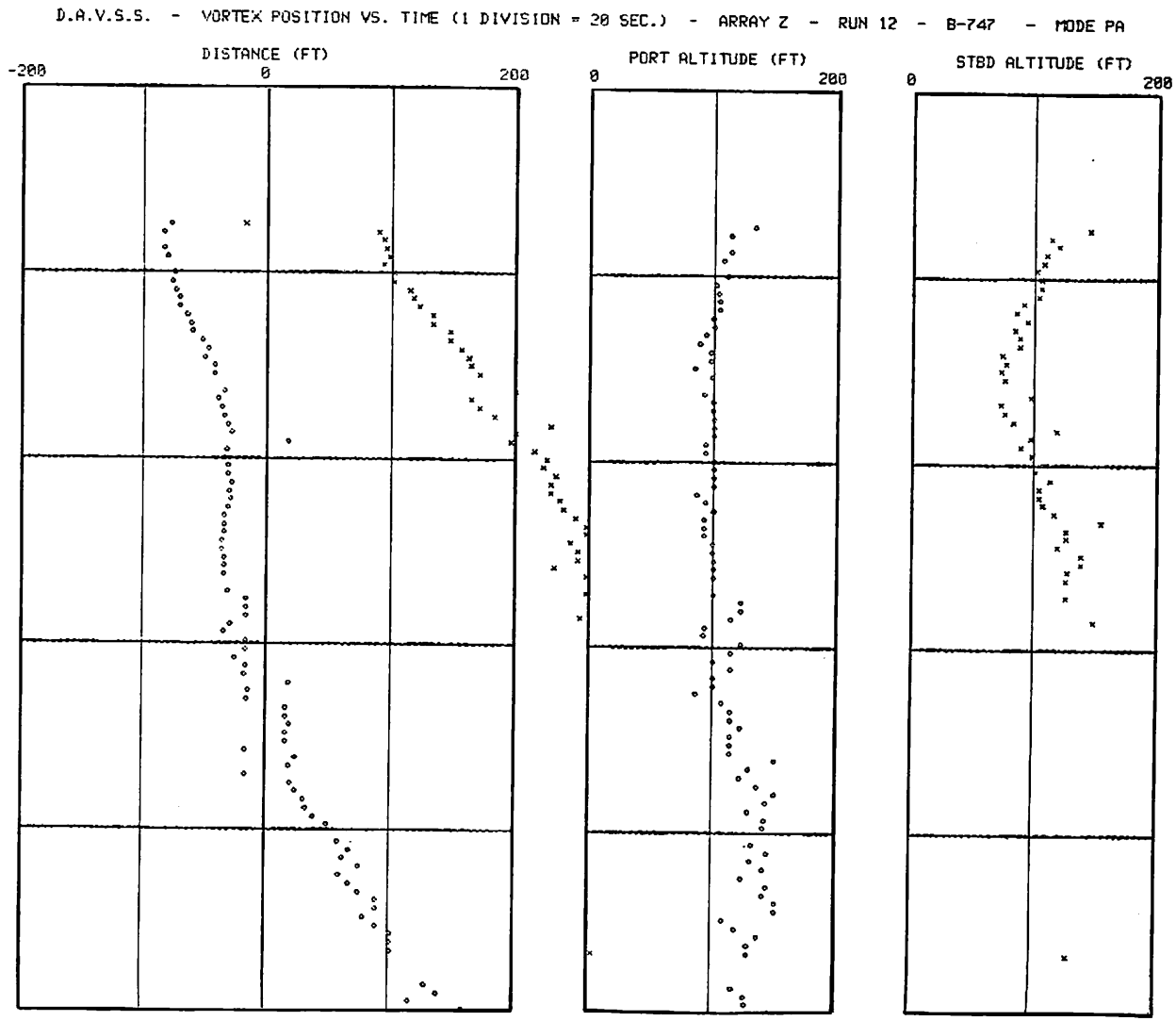

FIGURE 7-12 DAVSS, Vortex Position versus Time, Array Z, Run 12, B-747

this time that absolute determination of vortex circulation can be made reliably and accurately in real-time for all vortices.

Avco/SD recommends that the investigations outlined above be undertaken by TSC or Avco, and that the results of these investigations be used in defining further modifications to the DAVSS operating system to provide quantitative estimates of vortex circulation.

8. CONCLUSIONS AND RECOMMENDATIONS

The DAVSS was designed to be a flexible tool for the study and investigation of vortex behavior using Doppler acoustic scattering radar principles. The flexibility designed into the hardware and software paid off in its ability to accommodate the modifications suggested by specific operating experience at JFK. These suggested changes were quickly breadboarded and tested, and those which proved effective were easily integrated into the DAVSS operating system.

Considerably more capability in the latitude and ease of selection of operating and processing parameters and displays was built into the system than would now be necessary in an operational DAVSS. However, that capability in the demonstration DAVSS proved invaluable in efficiently converging on a satisfactory operating system.

Monostatic backscatter operation at the runway centerline extension proved to be the most satisfactory configuration and mode for tracking vortices from landing aircraft. Bistatic forward scatter was satisfactory for tracking vortices behind landing aircraft principally because of the low elevation angles and small scattering angles involved. However, this mode may prove effective for vortex detecting and tracking during aircraft takeoff.

The second-generation detecting and tracking algorithms using vortex circulation criteria have been successfully integrated into the DAVSS operating system. The resulting tracking performance on the augmented monostatic backscatter array is believed to be quite satisfactory. The tracks are most dramatic, especially under those meteorological conditions in which vortices persist within the flight path and present the most significant potential hazard to following aircraft.

The potential exists to quantitatively estimate vortex strength by means of an online calculation of vortex circulation. This capability should be implemented and evaluated.

APPENDIX A

COMB FILTER CALIBRATION & MAINTENANCE PROCEDURE

This appendix describes hardware and software changes made to the DAVSS and presents a procedure written to allow the DAVSS operator to monitor continually the gain and frequency accuracy of the 144 comb filters which form the heart of the Doppler processing function. With this capability, the operator can adjust the filters to compensate for any non-uniform drift in the filter characteristics as may become necessary.

A.1 INTRODUCTION

The detecting and tracking algorithms used by the DAVSS depend on the characterization of the spectra in each of 24 beam processing channels by six comb filters. Non-uniform performance of the filters in the 24 analog signal processing channels will degrade the DAVSS detecting and tracking performance.

Each of the 144 individual comb filters is under digital control for selection of its bandwidth and center frequency. Aging of the individual components of the filters can create non-uniform alteration of the filter characteristics from those designed and initially set. An operator maintenance procedure is required to monitor the filter performance on a routine basis and to adjust for out-of-tolerance performance when necessary.

The hardware and software modifications made to the DAVSS and the procedures devised and described herein allow for this operator maintenance function.

Paragraph A.2 describes the hardware modifications, Paragraph A.3 describes the software modifications, and Paragraph A-4 describes the procedures used by the operator to monitor the filters and make the necessary adjustments.

A.2 HARDWARE MODIFICATIONS

Hardware modifications were made to each of the 24 analog signal processor boards to provide for trim potentiometer adjustment of each of the individual 144 comb filter fine frequency selections and sensitivity adjustments.

Fixed resistors used in the fine frequency selection circuits and gain sensitivity circuits were replaced with resistor and trim potentiometer circuits in which the trim potentiometers are

installed on a front panel in the case of the gain adjustments, and on the back of the individual analog signal processor boards in the case of the fine frequency selection trim potentiometers.

Figure A-1 shows the filter sensitivity-calibration circuits; Figure A-2 shows the configuration of the analog processor sensitivity adjust panel.

Figure A-3 shows the filter frequency-calibration circuit, while Figure A-4 shows the location of the associated trim potentiometers on the rear edge of the analog signal processor boards.

A. 3 SOFTWARE MODIFICATIONS

A software subroutine was written as part of the DAVSS operating program which is available for use upon loading the program tape but which is wiped out upon use of the DAVSS in its detecting and tracking operation. Thus this subroutine is available for use upon program start-up.

The subroutine displays the digital output of each of the six comb filters of analog signal processor channels 1-12 or 13-24 on either the GT-40, the Versatec, or both. Thus, when the analog signal processor channels are stimulated in parallel by a known input the digitized output from the 72 comb filters is displayed in real-time and can be used to determine if the filter sensitivities are equalized. If they are not, the trim potentiometers for each of the filters may be used as described in Paragraph A. 4 to bring the individual outputs within the desired tolerance.

A.4 DAVSS FILTER CALIBRATION PROCEDURE

The following filter calibration procedure may be used upon loading the DAVSS operating program tape. It is designed to make use of the hardware and software modifications described above to permit operator verification or adjustment of the comb filter frequency positioning and sensitivity. This calibration subroutine is only available upon loading the DAVSS operating program tape since it makes use of core storage, storage which is written over during operation of the DAVSS in its primary role of vortex detecting and and tracking.

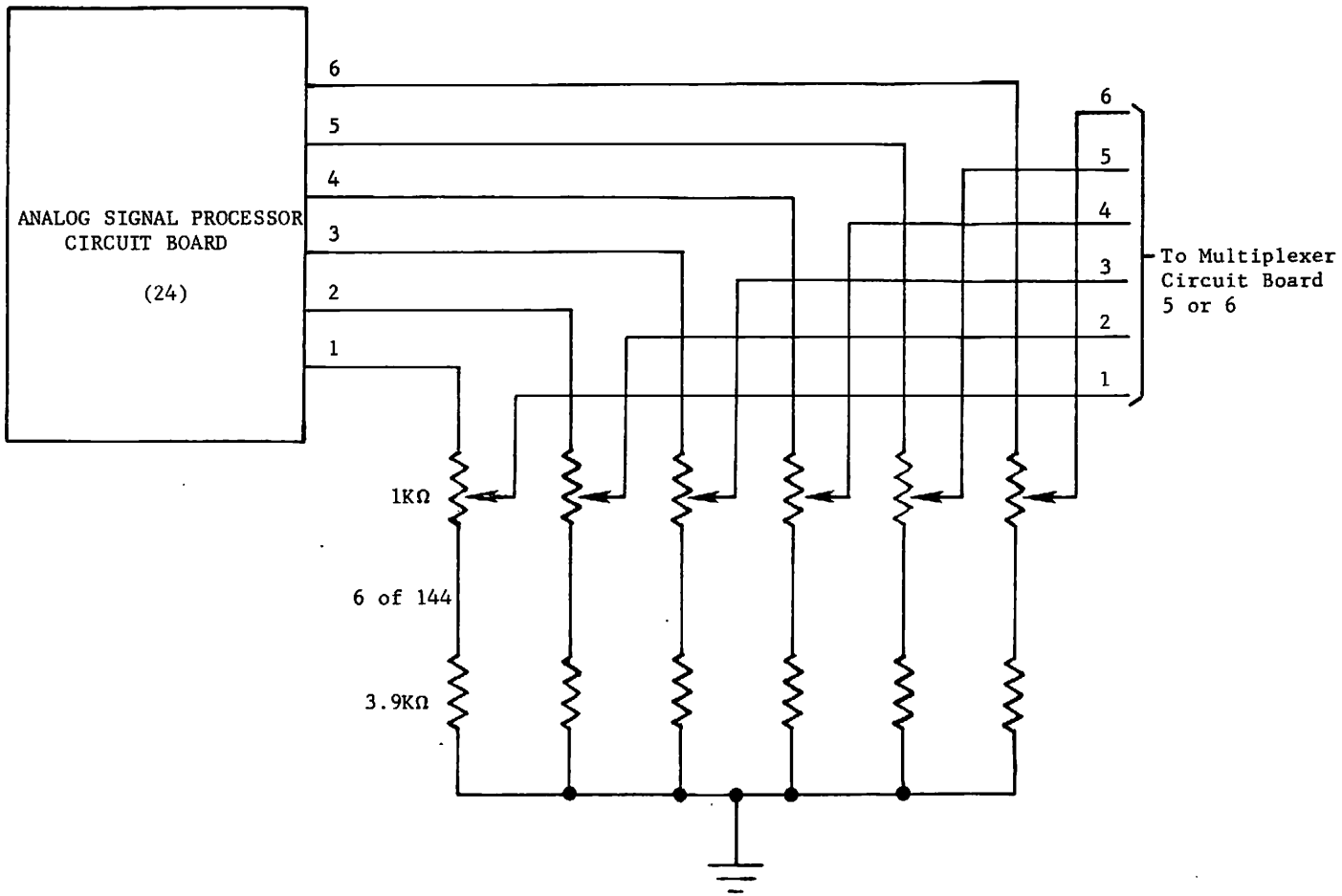

FIGURE A-1 Filter Calibration -- Sensitivity Circuit

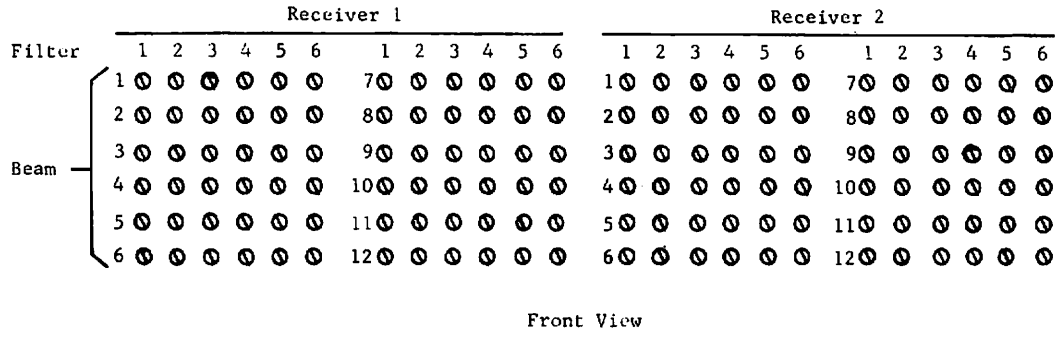

FIGURE A-2 Analog Processor - Sensitivity Adjust Panel

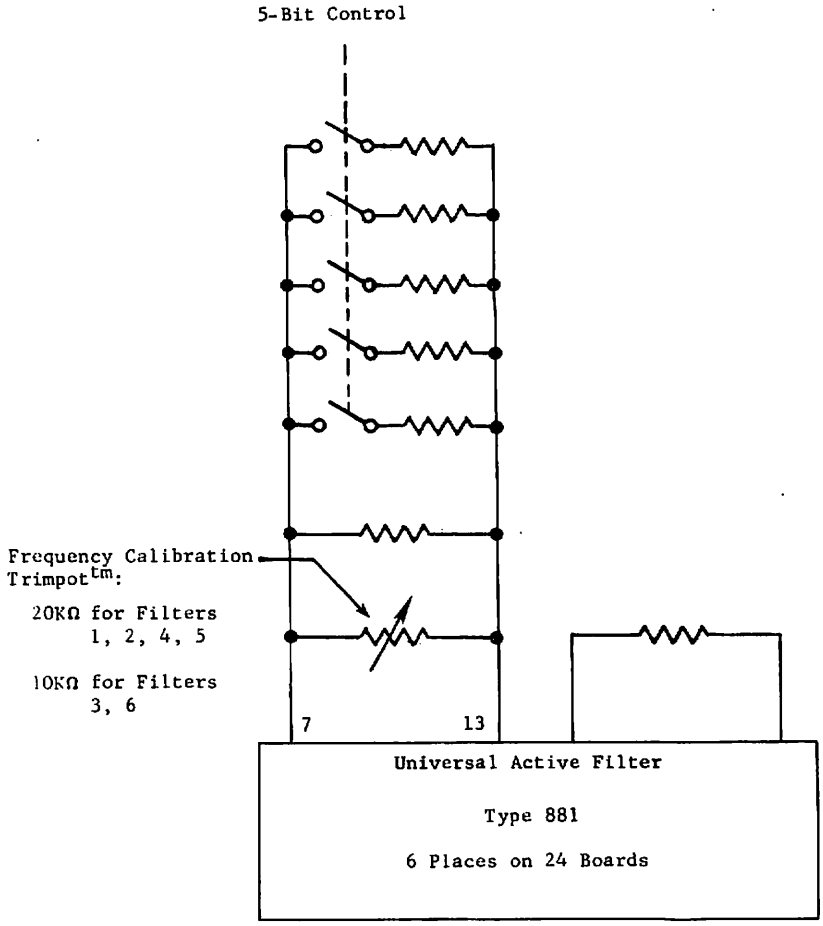

FIGURE A-3 Filter Calibration -- Frequency Circuit

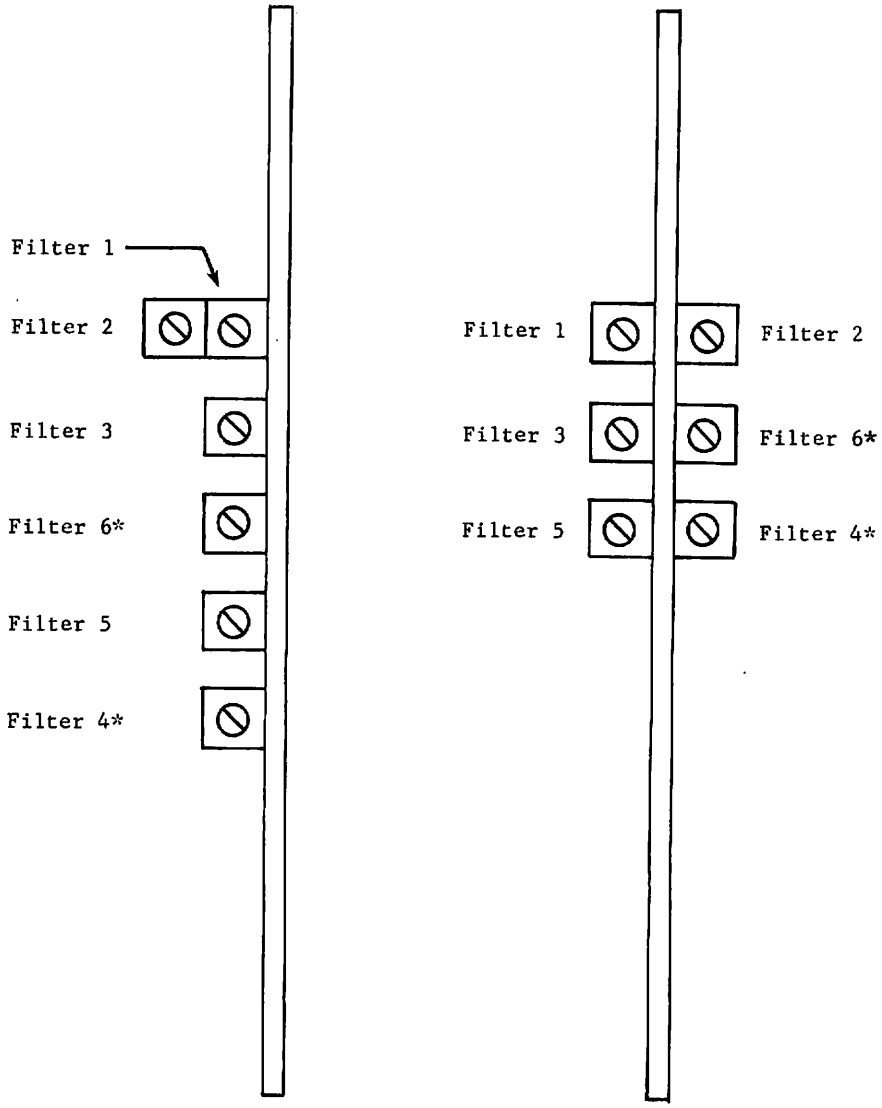

* Hardware drawings show Filters 4 and 6 reversed.

FIGURE A-4 Analog Processor - Frequency Calibrate Locations

1. Determine the desired system operating frequency and filter offsets and enter this data in appropriate places on page 2, line L and page 1, lines F, G, and H of the processing parameters.

2. Calculate the six filter frequencies as follows:

Filter 1 = carrier minus outer filter offset
Filter 2 = carrier minus center filter offset
Filter 3 = carrier minus inner filter offset
Filter 4 = carrier plus inner filter offset
Filter 5 = carrier plus center filter offset
Filter 6 = carrier plus outer filter offset

(For example, for a carrier of 3333 Hz, the offsets are 75, 150 and 225 Hz. Then filter 1 = 3108 Hz, filter 2 = 3183 Hz, filter 3 = 3258 Hz, Filter 4 = 3408 Hz, filter 5 = 3483 Hz and filter 6 = 3558 Hz).

3. Calibrate receiver 1: set filter 1 frequency in accordance with the information on page 2 column 2, line L. Do a ready and start of run. (SOR) Using test points as shown in Figure A-5 with a 0-10 volt VOM, adjust the filter 1 Trimpot™ (Figure A-4) on each of the 12 boards in cage 1 (upper) for maximum.

4. Use the GT-40 display (Figure A-6) and adjust the Trimpots™ (Figure A-2) in column 1 for an average reading on each beam of 75.

5. Repeat steps 3 and 4 for all receiver 1 filters (column 2 of GT-40 display is for filter 2 etc.) except that in step 4, filters 3 and 4 are set to a reading of 65 (filters 1, 2, 5 and 6 are set to 75).

6. Check the notch filters of receiver 1: enter the carrier frequency given on page 2, column 2, line L. After a ready and start of run, the GT-40 display should show all filters in all beams less than 5. If a filter is above this value, the notch for that filter is inoperative.

7. Calibrate filters in receiver 2: change the information on page 1 column 1, from R1 to R2. Set page 2, column 2 to the desired carrier frequency and enter the appropriate filter frequencies in line 1. Repeat steps 3, 4, and 5 to complete filter calibration.

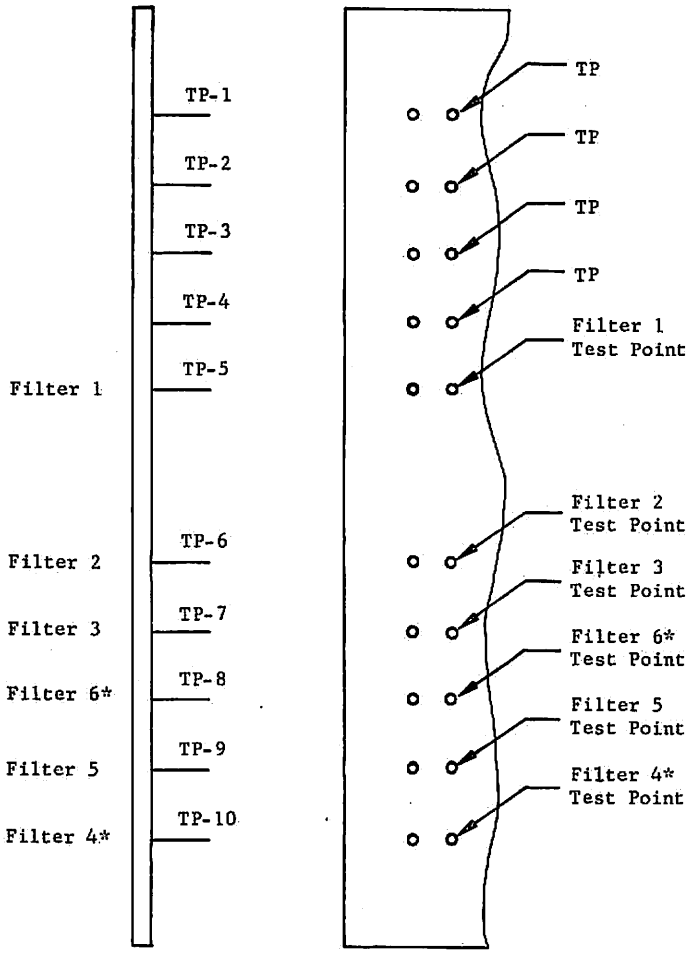

TP = Test Point

* Hardware drawings show Filters 4 and 6 reversed.

FIGURE A-5 Analog Filter-Test Points

CALIBRATION OF D.A.V.S.S. RECEIVER 1

	1	2	3	4	5	6
BEAM 1	101	32	11	9	5	10
BEAM 2	97	32	13	10	5	8
BEAM 3	96	31	13	13	5	9
BEAM 4	88	32	13	8	5	10
BEAM 5	98	32	14	8	3	8
BEAM 6	95	32	12	8	5	9
BEAM 7	91	32	14	10	6	8
BEAM 8	96	33	12	11	4	9
BEAM 9	94	34	13	10	5	10
BEAM 10	91	24	12	8	5	7
BEAM 11	84	32	13	7	5	7
BEAM 12	98	34	11	9	5	9

FIGURE A-6 GT-40 Display

APPENDIX B

REPORT OF INVENTIONS

This program resulted in the installation, checkout, and hardware and software modifications of the Doppler acoustic vortex sensing system built by Avco/SD under previous contract to the U. S. Department of Transportation. The hardware and software modifications included a number of clever and innovative changes in the DAVSS. These are described below.

Monitor and test circuits were added for audio and visual signal monitoring. For fault detection and signal verification, particularly where signal to broadband noise problems exist, the human ear and brain can easily decode an audible signal rapidly and economically.

A current-sensitive circuit was devised to identify open transmitter driver circuits. It uses a toroid choke converted into a current transformer to provide current verification via an LED indicator.

In addition, means were provided for introducing controlled signals into the processing system. This was done to allow circuit function verification. The verification was provided by appropriate displays on the CRT, the Versatec hard copy unit, or an external oscilloscope.

Several system software innovations were introduced which allowed the intensity, skew, and spread parameters to be selectively weighted by appropriate keyboard entries.

Tracking capabilities were significantly improved by development of a spatial averaging technique. The value of each beam and range discriminant was coverted to a weighted spatial average over 1, 3, or 5 range gates, or 1 or 3 beams. An exclusion zone was added around the highest peak value to eliminate the possibility of two different position estimates for the same vortex. Other software techniques, including frame-to-frame integration, were used to reject noise bursts.

A patch panel was designed to allow receiver beam selection. It permitted selection of various beam-to-beam angles and beamwidths.

An improvement was made to allow frequency calibration of the 144 comb filters in the system. The filters may be excited by the internal system generators under computer control in such a way that they are offset specifically known frequencies away from the transmit frequency. The frequency offset for each filter may be set via a variable resistor added to the system. In all, 144 such resistors were added. The relative amplitude response of each filter for each frequency offset can also be displayed on the CRT or the hard copy unit. An array of adjustable resistors may be used to provide individual filter amplitude settings for uniform or weighted response.

It is the opinion of the author that the above innovations, while clever, are not patentable since they use combinations of well-known techniques.

200 Copies